

**NONLINEAR FINITE ELEMENT ANALYSIS OF
BEAM-COLUMN SUBASSEMBLIES**

by

Gulsah Sagbas

A Thesis submitted in conformity with the requirements
for the Degree of Master of Applied Science
Graduate Department of Civil Engineering
University of Toronto

© Copyright by Gulsah Sagbas 2007

CHAPTER 1

Introduction

The accurate seismic assessment of beam-column subassemblies has been an important objective for many research groups over the years. Experimental and analytical research on different aspects of these members by various research groups has provided numerous design and assessment techniques with little consensus amongst these research groups. The need to understand the seismic performance of non-seismically designed beam-column subassemblies is another aspect of this challenging problem. The overall failure mechanisms under gravity and seismic loads have been identified, but the relative contribution of each member to these failure mechanisms is still being discussed. The most challenging aspect of reinforced concrete structures is the combination of two different materials to resist applied loading conditions effectively and efficiently. The difficulty of reinforced concrete design is best described by Paulay (1994) as a "... skilful combination of two materials; one inherently brittle, the other very ductile".

While research on the structural behaviour of reinforced concrete structures is continuing, the connection details for moment-resisting framed buildings are known to be crucial for the survival of the building. As observed by earthquake reconnaissance teams during site visits of disaster areas, the local failures of these members most likely lead to global failure mechanisms. In spite of the ductility requirements of the seismic codes around the world, these structures fail in brittle failure mechanisms. Insufficient reinforcement anchorage lengths, unconfined member connections against counteracting forces, and material quality deficiencies of the concrete and of the reinforcement are mainly the reasons for these failures.

There is an ongoing effort in modelling reinforced concrete structures, either to assess their seismic performance or to understand the effects of new rehabilitation techniques applied to upgrade their response. Advanced and more applicable structural

modelling techniques are needed for the seismic assessment of existing buildings, and for the development of new rehabilitation techniques.

The research in this study is focused on the modelling of beam-column subassemblies, a crucial connection mechanism for load transfer in moment-resisting framed structures. Through the years, various behaviour models to explain the load transfer mechanisms within the joint panel region have been proposed and adopted by reinforced concrete design codes around the world. The analytical studies were mostly limited to specific types or failure mechanisms of beam-column subassemblies. Since these members are subject to various failure mechanisms depending on material quality, reinforcement detailing and connection types; engineers tended to focus on one aspect of the problem to simplify the analysis procedure. However, the flexural and shear deformations within the joint contribute to different failure mechanisms, and this makes it difficult to develop a global model. Although, there are many models suggested in previous studies, there is no scientific consensus on a model or a modelling tool that is applicable to all conditions of beam-column subassemblies. The models that are available to designers involve tedious data input and output procedures, and are mostly dependent on empirical parameters or on the failure mechanism of the specimen analyzed.

In this study, a nonlinear finite element program, VecTor2, is used for modelling beam-column subassemblies. The beam-column subassemblies modelled here are chosen to represent various challenging aspects of the problem, such as:

- Beam longitudinal reinforcement comprised of smooth (plain round) reinforcement rather than deformed bars,
- Non-seismically designed beam-column subassemblies with unconfined joint panels,
- Different failure mechanisms,
- Different types of connections; exterior and interior beam-column subassemblies

A diverse range of specimens was selected to investigate whether VecTor2 provides a reliable and applicable tool for modelling beam-column subassemblies.

The details of the nonlinear finite element models for beam-column subassemblies will be discussed. A new rehabilitation technique for non-seismically designed beam-column subassemblies, proposed by Pampanin and Christopoulos (2003) and tested at the University of Canterbury, is also investigated numerically. The analytical results for all specimens are presented and discussed in comparison to experimental results in this thesis.

NONLINEAR FINITE ELEMENT PROGRAM, VecTor2

The nonlinear finite element modelling of beam-column subassemblies are carried out using VecTor2, a two-dimensional nonlinear finite element analysis program for reinforced concrete (NLFEARC) structures developed at the University of Toronto over the past 20 years. VecTor2 is based on the Modified Compression Field Theory (MCFT) by Vecchio and Collins (1986), and the Disturbed Stress Field Model (DSFM) by Vecchio (2000).

The use of VecTor2 for the numerical analysis of two-dimensional reinforced concrete membrane structures is facilitated by the pre-processor FormWorks (Wong, 2002). Augustus, the post-processor for VecTor2, (©Bentz, 1996-2007), is used to observe the analysis results. VecTor2 is singled out as a user-friendly among other finite element programs with the addition of these processors.

VecTor2 is capable of modelling two-dimensional reinforced concrete membrane structures under monotonic, cyclic and reversed cyclic loading conditions. The behavioural models for concrete, and for reinforcing or prestressed steel, are based on models that are widely accepted by the scientific community. The post-cracking influences on concrete, such as compression softening, tension stiffening, hysteretic effects, dowel action of steel reinforcement, and bond mechanisms representing the

interaction between concrete and reinforcement, are some of the behaviour mechanisms that are considered by VecTor2.

Most of the finite element modelling tools available for nonlinear analysis of reinforced concrete structures require definition of the failure mechanism or are dependent on empirical values obtained through similar experimental tests. VecTor2, on the contrary, performs an analysis using only the sectional, material and loading system details of the specimens necessary to define the structure. Additional information on VecTor2 is given in the last section of Chapter 2, and further information about the program is given in “VecTor2 & FormWorks User’s Manual” by Wong and Vecchio (2002).

OBJECTIVE OF RESEARCH

The main focus of this study was to understand the modelling capabilities of VecTor2 under reversed cyclic loading conditions for beam-column subassemblies. Therefore, a variety in the types of connections, material properties and connection details examined was crucial for confirming the applicability of the program or identifying its limitations. The specimens consisted of exterior and interior, and seismically and non-seismically designed, beam-column subassemblies that were analyzed under simulated seismic loading conditions similar to those followed during the experimental tests. The modelling efforts were utilized using the default behavioural or constitutive model options in order to prove that the program successfully captures the necessary response parameters without any modifications to the structure details.

The study of the bond material behaviour at the interface between reinforcement and concrete was another focus of this research. Specimens with deformed and smooth (plain round) reinforcement were specifically selected to assess the applicability of the tools for modelling bond behaviour in reinforced concrete structures. The bond elements and bond material behaviour models adopted by VecTor2 have been verified for monotonic loading conditions, but needed to be assessed for cases where reversed cyclic loading is applied. The details of modelling smooth reinforcement with VecTor2, and

improvements made to the program for future modelling purposes, are also described in Chapter 2.

VecTor2, compared to other alternatives, is a user-friendly finite element analysis program that successfully captures the response of different types of reinforced concrete structures under different loading conditions. An important goal of this study was to show the success of the program using only the default material constitutive models in modelling the specimens. The results of this study will allow VecTor2 to be used as a modelling tool for beam-column subassemblies, and will provide useful data for the designer. A reliable and efficient finite element program is much needed at the initial design stage for expensive experimental studies, and can provide seismic assessment data for the structures before and after retrofitting techniques are applied.

OUTLINE OF CHAPTERS

Previous research on the modelling of beam-column subassemblies are presented, and detailed information on the VecTor2 program are given in Chapter 2. The models developed so far, and the capability of these models, is briefly explained.

The finite element modelling techniques and results are presented in two chapters according to the reinforcement used in these specimens. Information and analysis results on beam-column subassemblies designed with deformed reinforcement are given in Chapter 3, while those for smooth reinforcement are given in Chapter 4. The comparative results of the observed and predicted response of these specimens are also given in these chapters for further discussion on the results of this analytical research. The seismic response in terms of story shear force versus story displacement, sequence of nonlinear events, failure mechanism and crack formation, energy dissipation capacity, ductility and stiffness values are presented for comparison purposes.

General guidelines for modelling beam-column subassemblies with VecTor2 are described in detail in Chapter 5. The focus of this chapter is on the interaction between the concrete and the reinforcement; bond element modelling of beam-column

subassemblies with different reinforcement configurations in the joint panel zone is also discussed.

Finally, the capabilities of the nonlinear finite element program VecTor2 are summarized, and the ability of the program to adequately simulate the cyclic response of beam-column subassemblies is discussed, in Chapter 6.

CHAPTER 2

Previous Research on the Modelling of Beam-Column Subassemblies

Experimental and analytical studies on the seismic behaviour of beam-column subassemblies have provided extensive data for structural engineers over the years. However, there is still an ongoing discussion on the contribution of different behaviour mechanisms to the global performance of these structural members. In addition, there is a need for an applicable and reliable seismic assessment tool for non-seismically designed beam-column subassemblies. An advanced finite element program, which can perform a nonlinear analysis on these structures before and after they are retrofitted, will be very useful towards ongoing rehabilitation efforts.

The seismic behaviour of beam-column subassemblies involves the effects of different load transfer and deformation mechanisms. The local behaviour parameters, such as the bond-slip effects of the beam longitudinal reinforcement, and the shear deformation mechanisms in the joint should be well integrated. These are the most challenging aspects of finite element modelling of beam-column subassemblies. So far, most of the modelling efforts on beam-column subassemblies have focused on one single aspect of the problem, which resulted in models that were developed accordingly.

Analytical studies on both seismically and non-seismically designed beam-column subassemblies are discussed in this chapter. The constitutive and behavioural models used for finite element modelling, and the recently developed options for modelling the bond-slip effects in VecTor2, are also explained in the last section of this chapter.

2.1. ANALYTICAL RESEARCH ON BEAM-COLUMN SUBASSEMBLIES

The shear resistance mechanisms developed in beam-column subassemblies under seismic forces were initially suggested by Park and Paulay (1975). It was suggested that the diagonal compression strut and truss mechanism occurred consecutively under seismic loading effects. Briefly, compressive forces acting on a joint are carried by the equilibrium of concrete compressive forces and the bond forces on the reinforcement through a single diagonal strut. The beam-column subassembly follows this mechanism until the stress transfer mechanism at the joint is destroyed. This stress transfer mechanism is dependent on the bond strength. Later, the truss mechanism is active in the shear resistance. The diagonal concrete compression field and the reinforcement in the orthogonal directions are needed to satisfy equilibrium in the joint as illustrated in Fig. 2.1. The force transfer mechanisms on an exterior and an interior beam-column subassembly suggested by Park (2002) are shown in Fig. 2.2.

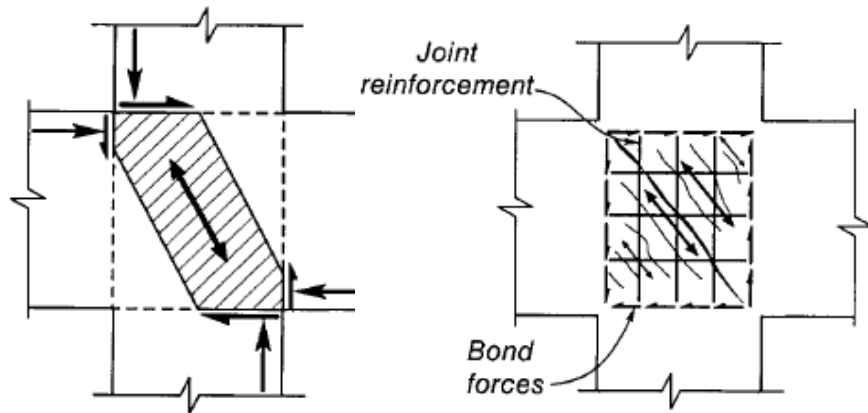


Fig. 2.1 Diagonal Strut and Truss Mechanisms (Park and Paulay, 1975)

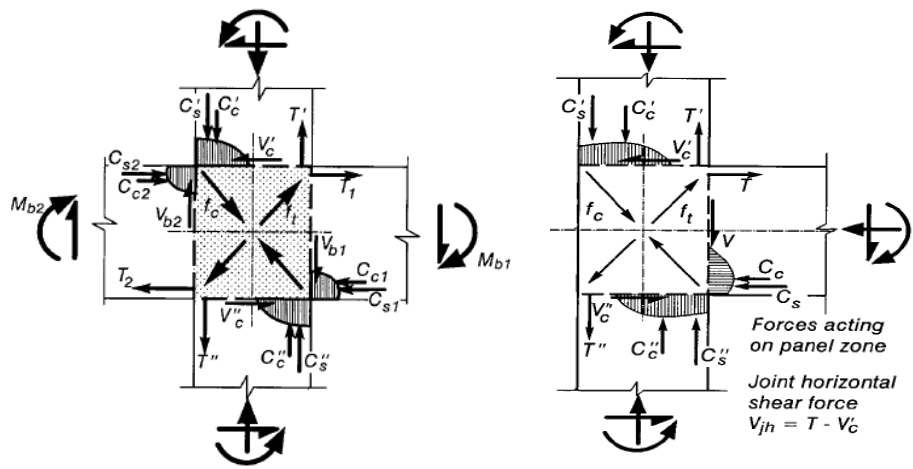


Fig. 2.2 Exterior and Interior Joints under Seismic Loading (Park, 2002)

This model is highly accurate in estimating the strength and the failure mechanisms of beam-column subassemblies. However, it was found by Shiohara (2004) to be inadequate in considering the effects of axial load applied to columns and the flexural strengths of the adjoining members to the joint. As for non-seismically designed or gravity load designed beam-column subassemblies, there is still no consensus on a theory or a model that can be used for the seismic assessment of these structures.

Most of the modelling efforts concentrate on the shear deformation and neglect the bond-slip effects in the joint. The assumption of perfect bond of the reinforcement in the joint region was shown to be inaccurate by Shiohara (2001), Hakuto et al. (1999) and Fleury et al. (2000). These members are subjected to high deformations at the joint panel regions; therefore an integration of a bond-slip model is essential. However, this bond-slip effect is completely different for deformed and smooth (plain round) reinforcing bars. The bond-slip effect is further described in Sections 2.1.2, and 2.2.3. The discussion on previous modelling studies is categorized as seismically, and non-seismically designed members in this chapter.

2.1.1. SEISMICALLY DESIGNED MEMBERS

Experimental and analytical research on beam-column subassemblies first began in the late 1970s to better understand the seismic performance of these members and their contribution to the global behaviour mechanism of reinforced concrete moment resisting framed buildings, (e.g., Bertero and Popov, 1977; Filippou et al., 1983; Soroushian et al., 1988). Some research groups with the knowledge of these failure mechanisms also undertook extensive research on the bond-slip behaviour of deformed reinforcement in the joints, (e.g., Viathanatepa et al., 1979; Eligehausen et al., 1983; Soroushian et al., 1991), and used the results of these material models in their analytical research.

Elmorsi et al. (2000) proposed a beam-column joint model which consisted of a 12-node inelastic plane stress element to represent the joint. This element was connected to the beams and columns with 10-node inelastic plane stress transition elements as shown in Fig. 2.3. The beams and columns were modelled with elastic beam line-elements, and inelastic truss elements. The contact elements were also used on the beam longitudinal reinforcement at the joint to represent the bond-slip effects.

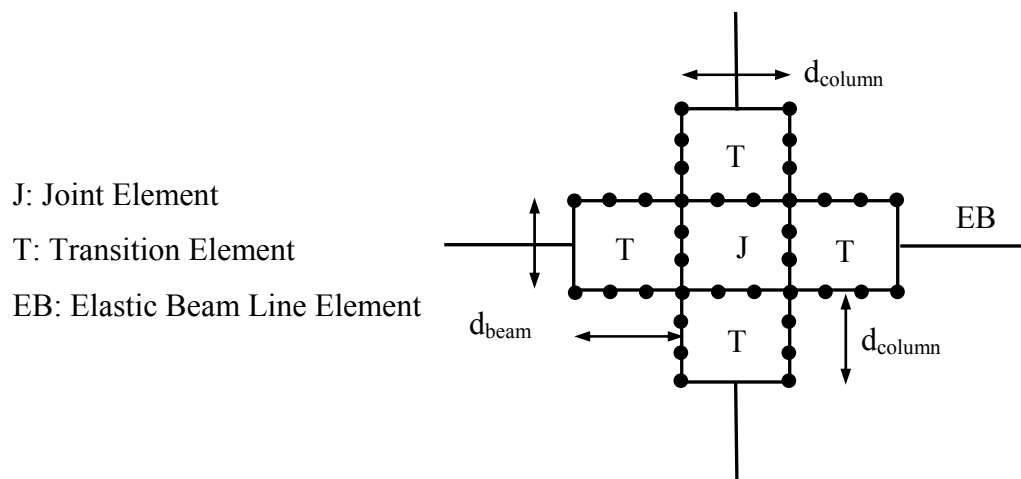


Fig. 2.3 Elmorsi's Model for Beam-Column Joint (Elmorsi et al., 2000)

A smeared crack approach was used for the concrete model, and the hysteretic models were further developed to account for the shear deformations in the joint. The

bilinear stress-strain curve proposed by Menegotto and Pinto (1973) was used for the reinforcement material behaviour. A bond-slip model was developed based on modifications applied to the model by Eligehausen et al. (1983). The only difference in the proposed bond-slip model by Elmorsi et al. (2000) was the gradual increase path on the friction branch of the cyclic curve. A gradual increase in the bond stress at the friction curve was also suggested by Soroushian et al. (1991) and Filippou et al. (1983) to Eligehausen's cyclic bond stress-slip behaviour. A comparison of these bond-slip models is given in Fig. 2.4. This model successfully considered both bond-slip and shear deformation effect on beam-column subassemblies.

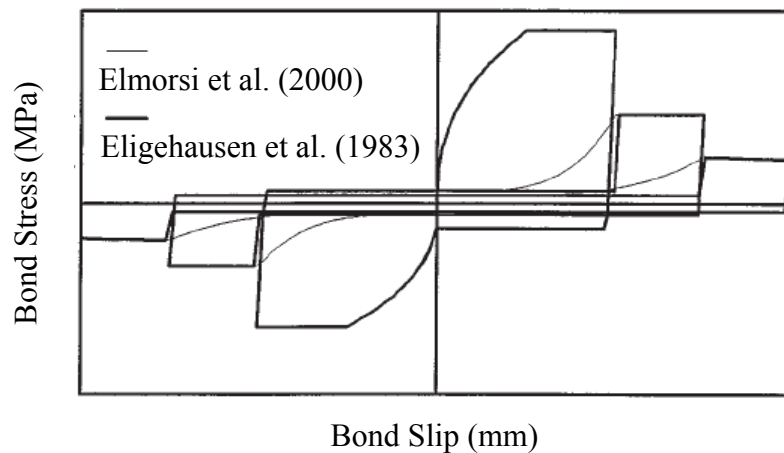


Fig. 2.4 Comparison of Bond-Slip Models (Elmorsi et al., 2000)

Limkatanyu and Spacone (2003) also studied the modelling of beam-column subassemblies. The contributions of each member to the joint were modelled separately and members were connected with rigid links. Failure mechanisms involving shear deformations of the joint panel were neglected and only cases with bond-slip loss within the joint were considered in this study. However, excessive shear deformations in the joint panel region were observed by Dhakal et al. (2005) during an experimental study on the seismic performance of gravity-load designed beam-column subassemblies under different frequency excitations. This study suggested that both shear deformations and bond-slip effects should be considered specifically for medium- or low-confined joints or gravity-load designed beam-column subassemblies.

Lowes and Altoontash (2003) considered these effects on a two-dimensional beam-column joint model. This model was designed to consider inelastic response mechanisms, such as the shear failure of the joint core, the loss of shear load transfer due to cracking at the beam column interfaces, and the failure of the bond on the longitudinal reinforcement. Behaviour models for the hysteretic response, shear-panel component, and bond-slip component were used to develop the beam-column joint element. Each behaviour model was calibrated with the experimental data on beam-column joints through tests. The proposed hysteretic load-deformation response model specific to the possible failure modes within the joint was calibrated using the Park and Ang (1985) hysteretic damage index, while the shear-panel component of the model was formulated according to the Modified Compression Field Theory (MCFT) (Vecchio and Collins, 1986), and calibrated against experimental data by Stevens et al (1991). As for the bond-slip component model, a combination of various models on the bond stress-slip relation for deformed reinforcement was adapted to the model. The interior reinforced concrete beam-column subassemblies with moderate shear reinforcement in the joints were used for the application of this model at the global level (Lowes and Altoontash, 2003).

Later, based on the results of their previous study, Mitra and Lowes (2004) revised the bond-slip material and geometric behaviour of this joint model. Force-based lumped plasticity elements were added to the model for beams and columns. These revisions increased the application area of this model for beam-column subassemblies with moderate shear reinforcement. The results of this study showed that the model needs additional improvement in terms of bond-slip strength, and for joint shear response of members with a ratio of shear reinforcement to the total shear demand of the joint lower than 0.15 (Mitra and Lowes, 2004).

Shiohara (2004) proposed a new model to assess the resistance mechanisms of beam-column subassemblies under seismic loading, based on a series of tests on seismically designed members according to the AIJ Guidelines. This model simulated the moment effects of the beams and the columns with four triangular segments. As observed during tests, the joint shear deformations were mainly due to the diagonal cracking of the joint in the opposite directions. The model considered two deformation

modes; Joint Shear Mode (J-Mode) and Beam Flexural Mode (B-Mode). The theory was not based on the common flexural theory of “plane sections remain plane” to consider the local adhesion effects of reinforcement which were critical in the seismic performance of these members. The strength and failure mode of the beam-column subassemblies were estimated using the equilibrium conditions for each failure mode and failure criteria for concrete, reinforcement and bond strength separately. The failure mode and the shear strength were found from the combination of these parameters (Shiohara, 2004). This model was proven to be successful for both exterior and interior beam-column subassemblies, but not applicable to non-seismically designed beam-column subassemblies.

2.1.2. NON-SEISMICALLY DESIGNED MEMBERS

The seismic behaviour of non-seismically designed beam-column subassemblies are affected by various additional parameters. These members are prone to severe brittle failure mechanisms due to the confinement problems at the beam-column joint, arising from insufficient anchorage for beam and column reinforcement and the use of low strength materials (smooth reinforcement and/or low strength concrete) (Pampanin et al., 2006).

Non-seismically designed beam-column subassemblies are mostly designed with hooked-end smooth beam bars. The bond-slip behaviour of smooth bars is significantly different than that of deformed bars under seismic loading. The bond behaviour of deformed bars is based on two parameters as stated by Abrams (1913): chemical adhesion or “adhesive resistance”, and mechanical adhesion or “sliding resistance”. The former is mainly based on the chemical interaction between mortar and concrete. Mechanical adhesion, commonly referred to as mechanical interlock, occurs as a result of the imperfections on the surface of the reinforcing bar. These imperfections are mostly the lugs on the surface of deformed bars, which aren't present on smooth bar surfaces (Abrams, 1913). Therefore this mechanical adhesion isn't available for smooth bars; here, the only resistance mechanism against bond-slip effects is the chemical adhesion.

The seismic performance of beam-column subassemblies is highly affected by the application of these smooth bars. The behaviour is similar to that of deformed bars until the adhesive bond is lost under seismic loading. After that, smooth bars tend to push-pull freely under cyclic loading conditions. This was also observed during an experimental investigation by Feldman and Bartlett (2005); contrary to deformed bar behaviour, upon cracking, smooth reinforcement lost its grip to the concrete and the adhesion between concrete and reinforcement was lost due to local slip of the bar. As a result, “concrete wedge” mechanisms are usually observed in exterior beam-column subassemblies with hooked-end smooth reinforcement applications, as was observed by Pampanin et al. (2002). The formation of this mechanism is given in Fig. 2.5. According to Park (2002), interior beam-column subassemblies designed with large diameter smooth beam bars also lead to bar slips due to high bond stresses on these bars.

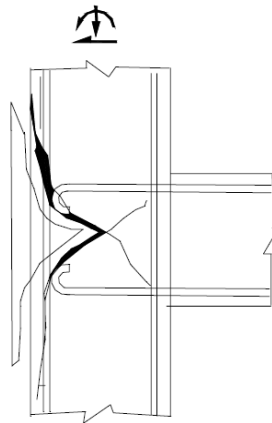


Fig. 2.5 Concrete Wedge Mechanism for Exterior Beam-Column Subassembly
(Pampanin et al., 2002)

Various other studies provided data on the behaviour of smooth bars, (e.g., Abrams, 1913; Kankam, 1997), but none of these results are applicable for use in the global modelling of non-seismically designed beam-column subassemblies.

An experimental research on the behaviour of hooked-end and straight-end smooth bars by Fabbrocino et al. (2002) provided useful results on the bond-slip behaviour. This study was mainly focused on the bond-slip effects of smooth bars used in non-seismically designed beam-column subassemblies. The study consisted of a series

of monotonic and cyclic pull-out and beam tests on straight and 180° circular hooked-end 12 mm and 16 mm smooth bars. The results of the bond stress-slip curve showed an initial adhesion phase and a residual strength phase for these bars. No maximum plateau after reaching maximum stress was observed for smooth bars. The same behaviour was also seen by Feldman and Barlett (2005) during their experimental research on bond strength of smooth (plain) round and square bars. Fabbrocino et al. (2002) also compared the monotonic bond-slip behaviour of straight-shaped smooth bars to the theoretical bond stress-slip behaviour suggested by CEB-FIB MC90 (1993), as illustrated in Fig. 2.6.

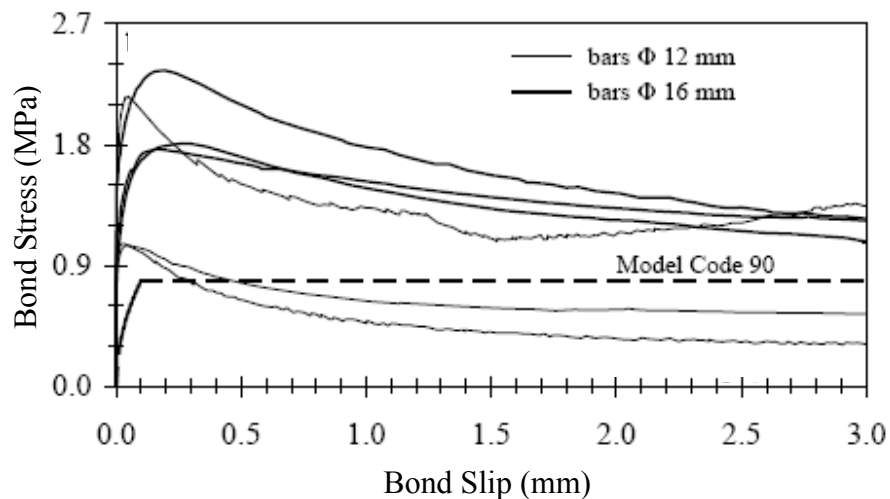


Fig. 2.6 Experimental Results and CEB-FIB MC90 (1993) Provisions on Smooth Bars (Fabbrocino et al., 2002)

The peak bond stress was higher than the peak bond stress suggested by the CEB-FIB MC90 (1993), but the residual stress was similar to the CEB-FIB MC90 (1993) theoretical values, especially for 16 mm diameter bars. Later, another study by Fabbrocino et al. (2004) on 12 mm diameter smooth bars bond-slip behaviour suggested that the CEB-FIB MC90 (1993) formulations for “good bond” and “poor bond” can be used for determining the peak and residual bond stress values. A comparison of this study with the Model Code 90 formulations is given in Fig. 2.7. The results of this research were later used for modelling non-seismically designed beam-column

subassemblies in this current study. Unfortunately, the derivation of a smooth bar bond model based on this limited information wasn't possible.

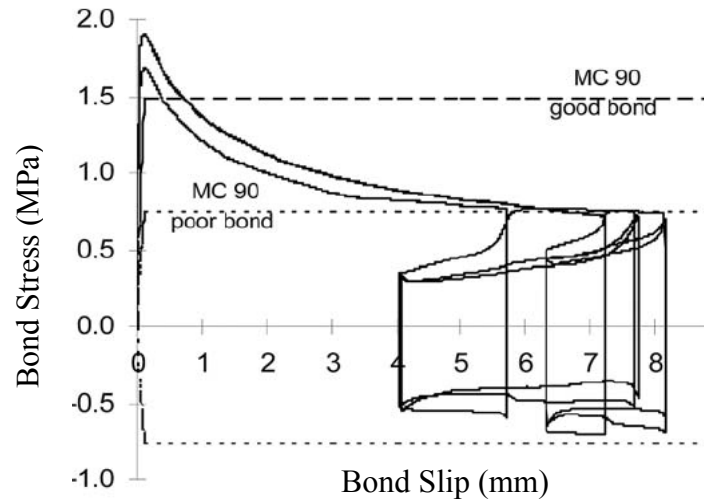


Fig. 2.7 Experimental Results and CEB-FIB MC90 (1993) Provisions on 12 mm Smooth Bars (Fabbrocino et al., 2004)

Another modelling effort on non-seismically designed beam-column subassemblies was a section-based model accounting for the inelastic behaviour mechanisms of the joints proposed by Pampanin et al. (2003). This model was used for exterior and interior beam-column subassemblies. Later, the hysteretic response models were refined and used for modelling a series of non-seismically designed exterior beam-column subassemblies (Chen, 2006). As shown in Fig. 2.8, one-dimensional frame elements were used for structural members, and an equivalent moment rotational spring for the joint panel. The joint panel model was developed considering the elastic and inelastic mechanisms of the joint, and the beam and column elements were connected to the joint panel with concentrated inelasticity at the critical section interface. The values were defined through appropriate moment-curvature graphs based on the section analysis. The cyclic behaviour of these specimens was adopted from the experimental research to account for the pinching effect, and the joint panel hysteresis was calibrated

using values from the experimental data. This study was successful in modelling the non-seismically designed beam-column subassemblies that were considered.

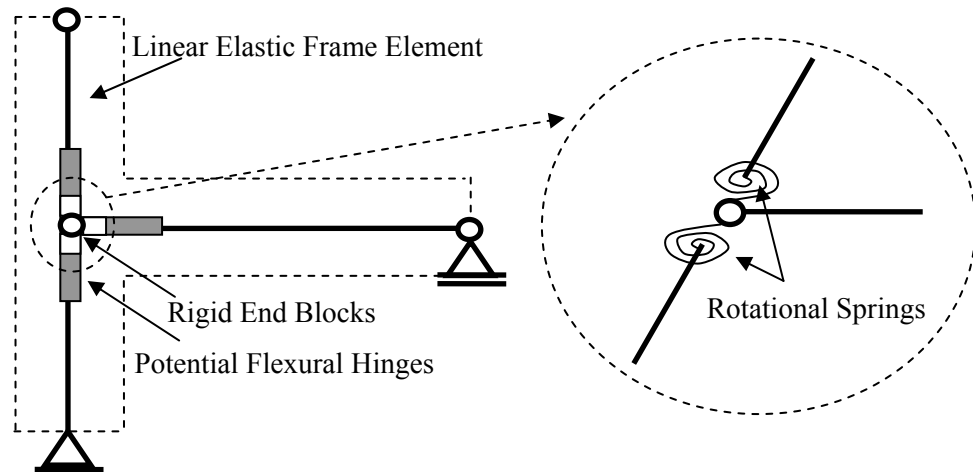


Fig. 2.8 Pampanin's Analytical Model for Beam-Column Subassemblies
(Pampanin and Christopoulos, 2003)

2.2. VecTor2 - FINITE ELEMENT MODELLING

The nonlinear analysis of beam-column subassemblies was carried out using VecTor2 in this study. As stated in Chapter 1, VecTor2 is a two-dimensional nonlinear finite element analysis program developed at the University of Toronto for reinforced concrete structures. Before proceeding to the analytical study, the material behaviour models and the elements that are used in modelling the beam-column subassemblies are described in this section. The detailed information on other elements or models is given in the "VecTor2 & FormWorks User's Manual" by Wong and Vecchio (2002).

VecTor2 is a nonlinear finite element analysis program with a user friendly pre-processor FormWorks, (Wong and Vecchio, 2002), and post-processor Augustus,

(©Bentz, 1996-2007) also developed at the University of Toronto. Any reinforced concrete structure can be modelled either manually using ASCII text files or the FormWorks program. The modelling of a structure starts with the selection of loading conditions and material behaviour models. Then the regional properties, meshing options and restraint conditions of the structure are described to simulate the actual loading system. The element properties for concrete, reinforcement and bond regions are individually assigned to the model. The finite elements that are available in the VecTor2 library are simple and low-powered elements which have linear displacement functions leading to fewer suspicious and faulty behaviour results. Once the model is ready for analysis, VecTor2 starts an iterative secant stiffness procedure for the nonlinear analysis of the reinforced concrete structure under designated loading and restraint conditions. The results of an analysis by VecTor2 can either be obtained from the ASCII result files or simply by using the post-processor, Augustus. Most of the local and global member behaviour can be observed using Augustus, however there are still some results that can only be examined through the result text files.

2.2.1. CONCRETE

Plain or uniformly reinforced concrete regions can be modelled with three different elements and various material behaviour models in VecTor2.

Elements:

The concrete element that has been used in this study is a four-node rectangular element, as shown in Fig. 2.9. This is a plane stress rectangle with uniform thickness in the out-of-plane direction. The element, having eight degrees of freedom, allows translation at each node in x- and y-directions, and should be defined by a counter clockwise sequence.

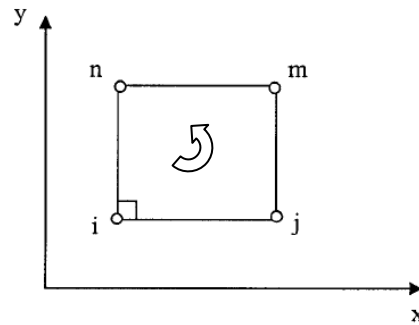


Fig. 2.9 Rectangular Concrete Element (Wong and Vecchio, 2002)

Reinforced concrete elements with smeared reinforcement can also be modelled in this step. If the reinforcement is to be modelled as discrete reinforcement bars, then this information should be given in the definition of reinforcement material and region.

The meshing of each model is at the user's discretion while respecting the necessary limitations of each element available for the concrete regions. The aspect ratio of the element is advised not to be more than 3:2. There is also a feature that allows the user to assign voids and nodes that are different than the assigned mesh parameters; this is especially useful for restraint and force application nodes.

Behaviour Models:

Different constitutive and behavioural models are available in VecTor2. The nonlinear behaviour of the structure changes according to the model that has been selected. Therefore, it is extremely important for the user to have knowledge of all the models that are available and the effects of these models on the behaviour of the structure. The material models assigned to the beam-column subassemblies examined in this study are discussed below.

The Concrete Pre-Peak Response was modelled using the default option. This is a simple compression curve model for concrete regions, and can be observed in Fig. 2.10. The Hognestad Parabola can be used for concrete regions having a compressive strength value less than 40 MPa. This model option computes the principal compressive concrete stress before the compressive strain reaches the peak compressive strain value, ϵ_p .

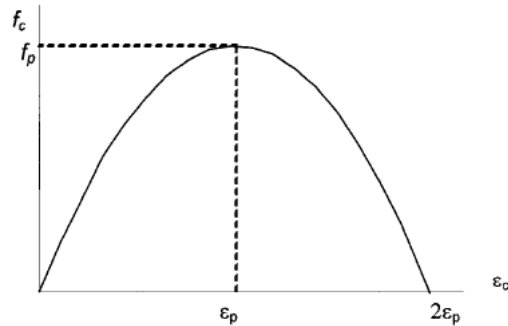


Fig. 2.10 Hognestad Parabola for Concrete Pre-Peak Response
(Wong and Vecchio, 2002)

The Concrete Post-Peak Response was modelled using the “Modified Park-Kent” option, as illustrated in Fig. 2.11. This is a modified “Park and Kent” model that accounts for the improved concrete compressive strength and ductility due to confinement.

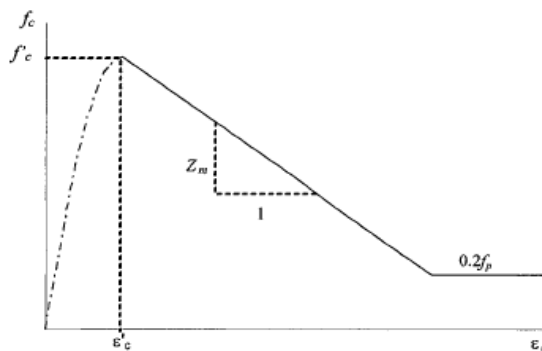


Fig. 2.11 Modified Park-Kent for Concrete Post-Peak Response
(Wong and Vecchio, 2002)

This option computes the principal compressive concrete stress after the compressive strain surpasses the peak compressive strain value, ϵ_p . The descending linear branch after the peak strain is followed by a plateau at a value of $0.2 f_p$.

The Concrete Compression Softening models that are available in VecTor2 were developed from a series of panel and shell elements tested at the University of Toronto (Vecchio and Collins, 1992). The effect of concrete cracking on the compression strength and stiffness are taken into account by either strength-and-strain softened or strength-only softened models. From the four different models available in VecTor2, the default model, “Vecchio 1992-A(e1/e2-Form)” was assigned to the concrete material properties. Briefly, this is a strength-and-strain softened model in which both uniaxial compressive strength and strain values are softened.

Concrete Tension Stiffening is the tensile resistance of cracked concrete arising from the bond with the reinforcement within the cracked regions. This phenomenon is especially important in finite element modelling. The coarseness of the element mesh has an important effect on simulating this behaviour. The “Modified Bentz 2003” model, which is a rigorous adaptation of previous Bentz (2000) model, was selected to represent this behaviour. This model incorporates the bond actions to the tension stiffening behaviour, and accounts for two-dimensional stress conditions and for the placement of each type of reinforcement.

The Concrete Tension Softening model considers the post-cracking behaviour of concrete that has been described in many fracture mechanics approaches of concrete behaviour after cracking. This is an important behaviour to model especially for lightly reinforced concrete members. The default “Linear” model, in which the concrete tensile stresses represented by a linearly descending branch, was selected for the specimens modelled in this study. The fracture energy used in this model is independent of element size, and is assigned a value of 75 N/m.

Concrete Tension Splitting refers to the formation of splitting cracks parallel to the reinforcement in tension due to the deformations occurring in the reinforcement. As selected by default in VecTor2, this effect was not considered in any of the analyses.

Concrete Confinement is an option that is used to simulate the enhanced strength and ductility effect of confined concrete under compression. The default “Kupfer/Richard” model, utilized in this study, is a combination of a biaxial compression model by Kupfer et al. (1969) and a model that considers the effect of spiral reinforcement in columns by Richard et al. (1928).

Concrete Dilatation refers to the lateral expansion of concrete under compression and the slight increase in strength and ductility of the member. The selected model, “Variable Kupfer”, determines the Poisson’s ratio in relation to ascending compressive strains. The Poisson’s ratio increases nonlinearly with the compressive strains.

The Concrete Cracking Criterion was modelled with the “Mohr-Coulomb (Stress)” option. The cracking strength is a property that changes in relation to the stress states. This effect is also taken into account to represent the tension and compression dominant failure conditions in modelling with VecTor2. The Mohr-Coulomb criterion is a two-parameter model that estimates the failure shear stress and failure plane in frictional materials.

Concrete Crack Slip Check is an option in VecTor2 that limits the local stresses at a crack to the maximum shear stress value. The “Vecchio-Collins 1986” model, which is based on Walraven (1981) and Vecchio and Collins (1986), limits the local shear stress at the crack depending on the concrete compressive strength, crack spacing, and aggregate size. It should be noted that for the Disturbed Stress Field Model (DSFM) analyses, the crack slip check is not utilized.

The Concrete Crack Width Check is specifically designed for shear-critical reinforced concrete members having little or no shear reinforcement. The crack width can be limited to one-quarter or one-half the aggregate size, or 1 mm, 2 mm, 5 mm and

10 mm widths. This option can also be neglected by choosing the “Stability Check Omitted” option. The default option in VecTor2 for this parameter is “Agg/5 mm Max Crack Width”. Other options of this parameter have been studied in modelling during the course of this study.

The Concrete Hysteretic Response can be modelled with linear, nonlinear, or nonlinear decay options. The default option in VecTor2, “Nonlinear with Plastic Offsets” is found to be inadequate in modelling the reversed cyclic behaviour of beam-column subassemblies. Another option, the “Palermo – Nonlinear with Cyclic Decay” proposed by Palermo and Vecchio (2002), was assigned to model the hysteretic behaviour of concrete in the beam-column subassemblies in this study. This model is different in the way that it models the damage mechanisms in the reloading phases, and in its consideration of partial loading and unloading phases. For the shape of the unloading curves and the calculation of the instantaneous plastic offset strains in the compression and tension domains, the model uses a different approach. The hysteretic response figures in compression and tension for this model option are given in Fig. 2.12 and Fig. 2.13.

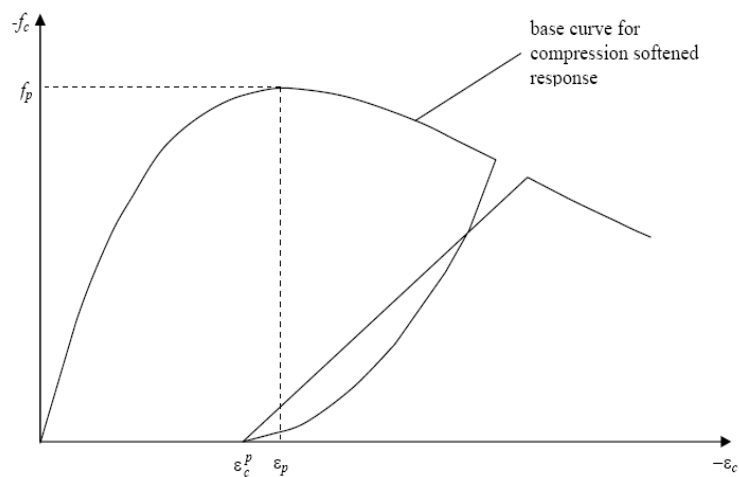


Fig. 2.12 Palermo Model for Concrete Hysteretic Response in Compression
(Wong and Vecchio, 2002)

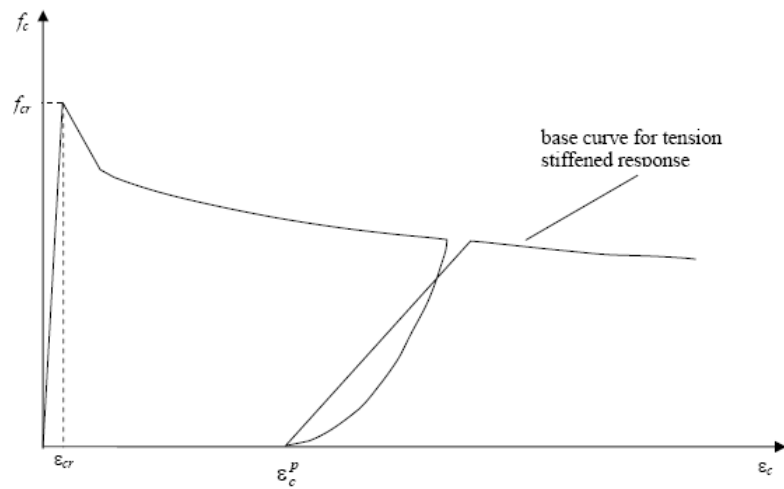


Fig. 2.13 Palermo Model for Concrete Hysteretic Response in Tension
(Wong and Vecchio, 2002)

As explained above, the default models were chosen for most of the parameters. The other available options were also selected to observe the effects on the nonlinear behaviour of the specimens. The behavioural models that were used for the concrete in this thesis are given in Table 2.1.

Table 2.1 Material Behaviour Models for Concrete

Material Property	Model
Concrete Compression Pre-Peak Response	Hognestad Parabola
Concrete Compression Post-Peak Response	Modified Park-Kent
Concrete Compression Softening	Vecchio 1992-A (e1/e2-Form)
Concrete Tension Stiffening	Modified Bentz 2003
Concrete Tension Softening	Linear
Concrete Tension Splitting	Not Considered
Concrete Confined Strength	Kupfer/Richard Model
Concrete Dilation	Variable Kupfer
Concrete Cracking Criterion	Mohr-Coulomb (Stress)
Concrete Crack Slip Check	Vecchio-Collins 1986
Concrete Crack Width Check	Agg/5 Max Crack Width/ Stability Check Omitted*/ 10 mm Max Crack Width*
Concrete Hysteretic Response	Palermo 2002 (w/ Decay)*
* non-default model	

2.2.2. REINFORCEMENT

All reinforcement was modelled using discrete bar elements. This option of modelling is useful when the area of interest is the local stress-strain or the bond-slip response in the reinforcement. It is advised to use the smeared reinforcement option for uniformly distributed reinforced concrete regions (e.g., stirrup reinforcement in beams and ties in columns), while the discrete reinforcement option is best for other types of reinforcement (e.g., longitudinal reinforcement in beams and columns and all reinforcement in joint regions).

Elements:

Reinforcement bars can be discretely represented with two-node truss elements which have nodal displacements in two directions and four degrees of freedom, as illustrated in Fig. 2.14.

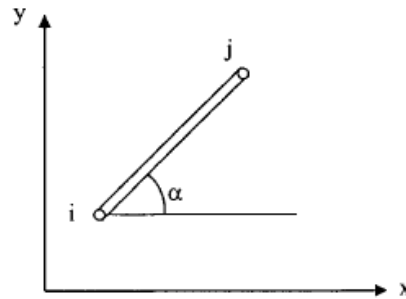


Fig. 2.14 Truss Element (Wong and Vecchio, 2002)

The monotonic stress-strain response is modelled with a trilinear stress-strain behaviour. The strain hardening effect of reinforcement until rupture is considered in VecTor2. The stress-strain response of reinforcement is shown in Fig. 2.15.

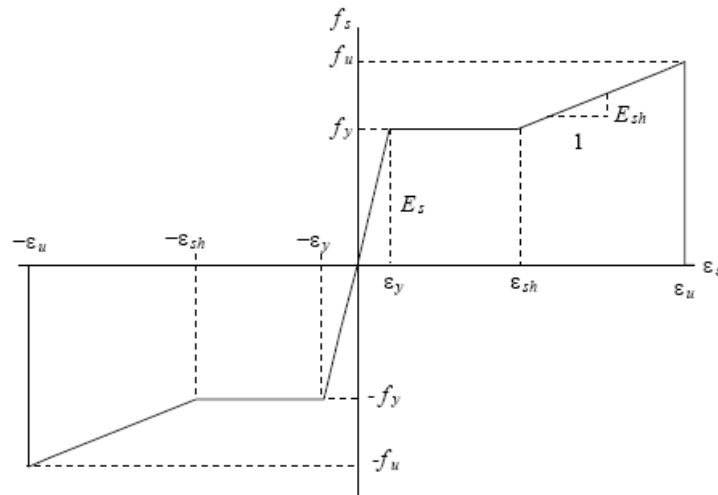


Fig. 2.15 Stress-Strain Response for Reinforcement (Wong and Vecchio, 2002)

Behaviour Models:

The different constitutive and behavioural models used for modelling the reinforcement in this study are briefly described in this section.

The Reinforcement Hysteretic Response is important specifically in reversed cyclic loading conditions. Using the monotonic stress-strain behaviour as a backbone, the hysteretic response models define unloading and reloading curves depending on the model selected from the VecTor2 library. The model described in this section is the default option, “Seckin w/ Bauschinger Effect”, used for modelling purposes in this study. This is a formulation developed by Seckin (1981) for the hysteretic response of reinforcement which includes the Bauschinger effect. After the plastic prestraining, the local stress changes upon load reversal result in premature yielding of reinforcement. As shown in Fig. 2.16., the monotonic stress-strain curve is followed by a linear unloading curve. The reloading curve is defined with a Ramsberg-Osgood formulation including the Bauschinger effect.

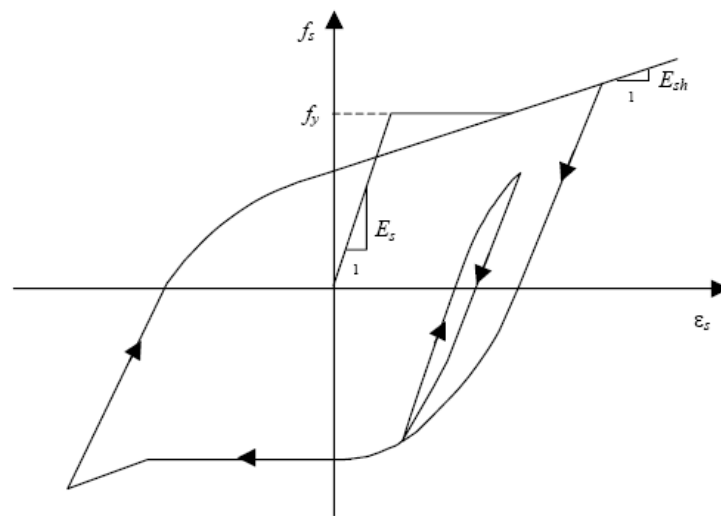


Fig. 2.16 Seckin Model for Hysteretic Response of Reinforcement
(Wong and Vecchio, 2002)

The Reinforcement Dowel Action, which is the contribution to the shear resistance provided by the reinforcement crossing cracks, is considered with this

parameter. Dowel action is important for the shear strength and post-peak ductility of reinforced structures with low shear reinforcement ratios. The ‘Tassios (Strength)’ and ‘Tassios (Crack Slip)’ options are available for modelling the dowel action in VecTor2. The shear resistance is estimated as a function of the shear slip at a crack, and the amount of shear slip is reduced by subtracting this shear resistance from the local shear stress value on the crack. The dowel action mechanism is shown in Fig. 2.17.

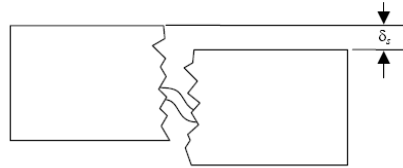


Fig. 2.17 Reinforcement Dowel Action (Wong and Vecchio, 2002)

Reinforcement Buckling model is considered effective in the analysis procedure when discrete reinforcement (truss bar elements) are attached to concrete with bond elements. In cases of buckling failure mechanisms due to high compressive stresses, there is no contribution to the flexure and shear resistance of the structure by the concrete cover and reinforcement. The ‘Asatsu Model’ option is considered when the reinforcement is under excessive compressive stresses and the bond deterioration is severe with a cumulative energy exceeding the fracture energy.

The constitutive and behavioural models that are used for the reinforcement in this thesis are summarized in Table 2.2.

Table 2.2 Material Behaviour Models for Reinforcement

Material Property	Model
Reinforcement Hysteretic Response	Seckin Model (Bauschinger)
Reinforcement Dowel Action	Tassios Model (Crack Slip) Tassios Model (Crack Strength)*
Reinforcement Buckling	Asatsu Model
* non-default model	

2.2.3. BOND

The performance of the beam-column subassemblies in shear are highly affected by the bond-slip behaviour of the beam longitudinal reinforcement. It is certain that the nature of this bond behaviour between the concrete and the reinforcement needs to be considered as an important parameter in modelling the seismic behaviour. Another part of this research was to understand the effectiveness of this option under reversed cyclic loading conditions. The reinforcement bond behaviour was modelled using the “Embedded Deformed” or “Embedded Smooth Rebar” options in VecTor2.

Elements:

Two bond element types are available in VecTor2: i) Link Elements, and ii) Contact Elements. The link elements (Ngo and Scordelis, 1967) were used to simulate the behaviour between concrete and reinforcement in this study. The connections details of these elements can be seen in Fig. 2.18. The link elements are two-node non-dimensional elements which consist of two orthogonal springs that link the concrete and discrete reinforcement. These two nodes can displace independently from each other simulating the relative displacement effect between concrete and reinforcement elements. The connection details of these link elements allow these two nodes to be able to deform in both the x- and y- direction.

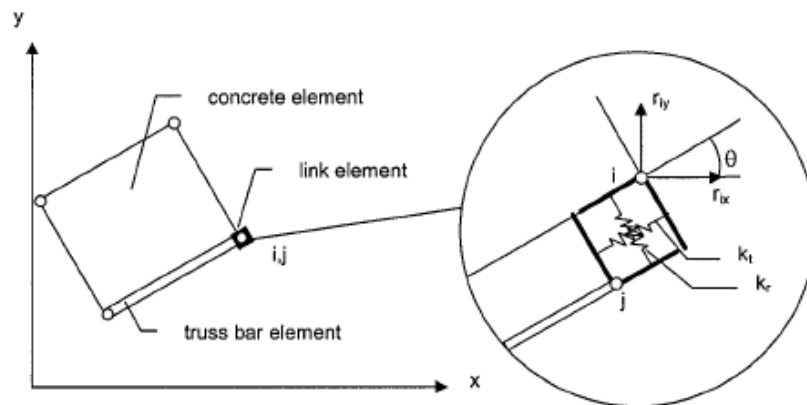


Fig. 2.18 Link Element (Wong and Vecchio, 2002), after Ngo and Scordelis (1967)

Behaviour Models:

The general parameters used in all bond models will be explained for both deformed and smooth reinforcement, before each model is discussed individually. Deformed and smooth reinforcement are modelled with the Embedded Rebar option. The bond material property for embedded reinforcement is specified by either the confinement pressure index (β) or by a user-defined bond stress-slip relationship. Eligehausen et al. (1983) and CEB-FIB MC90 (1993) agreed on two bond regions based on the failure mechanisms. Eligehausen et al. (1983) observed two distinct failure mechanisms; i) Pull-out Failure and ii) Splitting Failure, and suggested that they are mostly related to the transverse reinforcement provided and the clear distance between the bars. For intermediate values of transverse reinforcement, the CEB-FIB MC90 (1993) suggests using a linear interpolation between these two cases. The values of confinement pressure index for these two distinct cases are:

- $\beta = 0$ Unconfined Concrete - Splitting Failure Mechanism
- $\beta = 1$ Confined Concrete - Pull-out Failure Mechanism

The CEB-FIB MC90 (1993), mostly based on Eligehausen's bond slip model, defines the region as a confined region when the transverse pressure is high ($p \geq 7.5$ MPa) or transverse reinforcement is closely spaced satisfying conditions of $\Sigma A_{sw} \geq n A_s$. The confinement pressure index (β) is a unitless parameter which is estimated by using the ratio of the transverse reinforcement in sections. The transverse reinforcement ratio within the bond region, ρ_v , is multiplied by the yield stress of the reinforcement then divided by the high confinement pressure value of 7.5 MPa accepted by CEB-FIB MC90 (1993). The values assigned for minimum concrete cover and reinforcement layers through depth of the member are other important parameters for each bond model. The minimum concrete cover is estimated through the concrete cover values around the reinforcement and the minimum value of all the parameters are used for definition, as illustrated in Fig. 2.19. The number of reinforcement layers through depth of a structure is estimated as shown in Fig. 2.20.

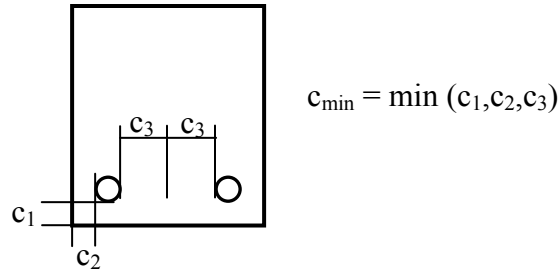


Fig. 2.19 Minimum Concrete Cover

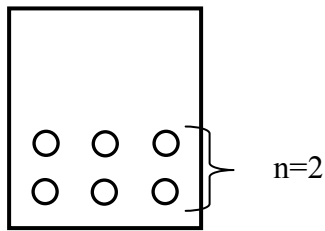


Fig. 2.20 Number of Reinforcement Layers through the Depth

The hooked bar option is another parameter that is described later in this chapter. This option activates a bond-slip model specific to hooked end bars, and is given on the bond property window (see Fig. 2.21).

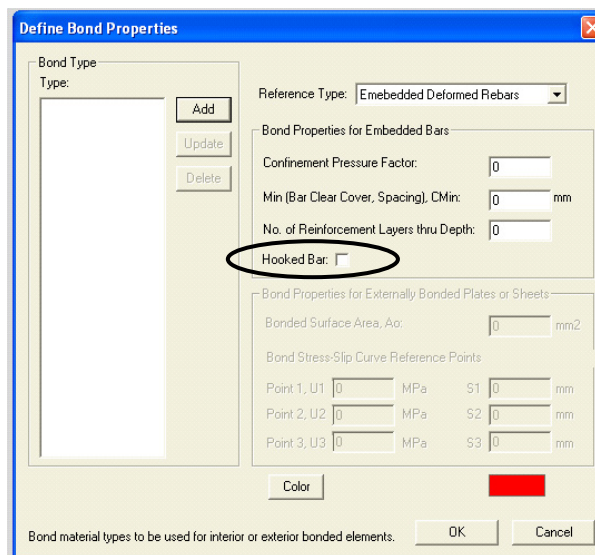


Fig. 2.21 Bond Properties - Deformed Reinforcement Option

The reinforcement size related effects are considered by not only the diameter of the reinforcement, but also the lug spacing, S, and lug height, H. The values of these two parameters for deformed reinforcement are given in Table 2.3. The value of lug spacing remains the same for smooth reinforcement, but the lug height is estimated as $H=S/75$.

Table 2.3 Reinforcement Properties of Embedded Deformed Bars

d_b (mm)	S(mm)	H(mm)
≥ 55	39.4	2.55
43-55	30.6	2.2
35-43	25	1.79
29-35	20.9	1.48
25-29	17.6	1.26
19-25	13.6	0.98
15-19	11.2	0.72
11-15	7.9	0.45
0-11	0.70d _b	0.04d _b

Currently, the only distinction between deformed and smooth reinforcement in VecTor2, is the value of the lug height. However, it was observed that this causes an overestimation in the bond-stress behaviour for smooth reinforcement. Therefore, a user defined embedded bar option was added for improved modelling of smooth reinforcement in VecTor2. This option allows the user to assign a selected bond stress-slip curve for the bond-slip behaviour of the elements. The bond stress-slip relation is assigned with three nodes to represent the stress-slip curve as shown in Fig. 2.22. The bonded surface area input is left as zero.

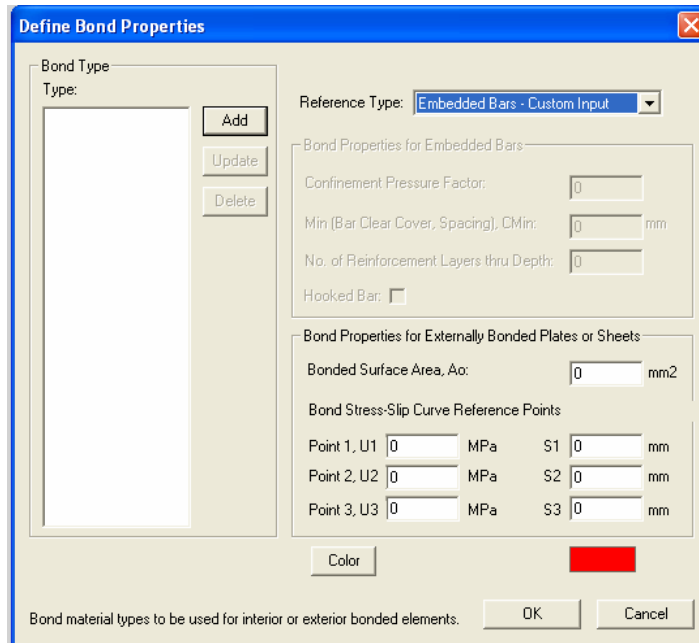


Fig. 2.22 Bond Properties - Custom Input Option

There are five different bond models that are available for deformed bars in VecTor2: Perfect Bond, Eligehausen, Gan, Harjili and Fujii Models. The Perfect Bond, Eligehausen and Gan Model are described in this study. Further details on other models are given in Wong and Vecchio (2002).

Perfect Bond:

A “Perfect Bond” connection between reinforcement and concrete is assumed in this model. The bond-slip behaviour is characterized by very large stiffness and strength values so that no slip action occurs in the reinforcement. The bond stress-slip values are the same for the confined and unconfined concrete cases. The formulation and the bond stress-slip curve are given below in Fig 2.23.

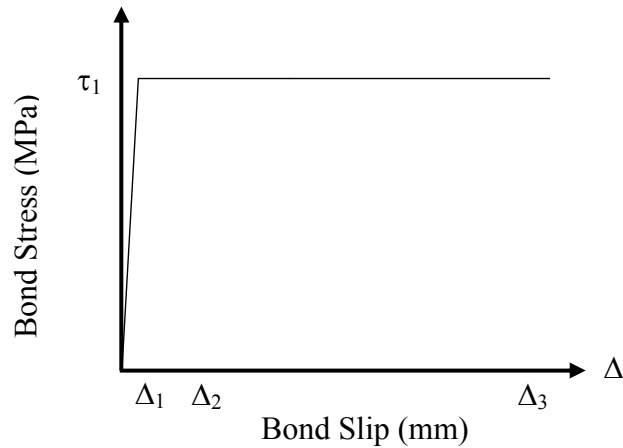


Fig. 2.23 Perfect Bond Model (Wong and Vecchio, 2002)

$$\tau_1 = \tau_2 = \tau_f = 250 \text{ MPa} \quad (2.1)$$

$$\Delta_1 = 0.1 \text{ mm} \quad (2.2)$$

$$\Delta_2 = 3.0 \text{ mm} \quad (2.3)$$

$$\Delta_3 = 10.0 \text{ mm} \quad (2.4)$$

Eligehausen Model:

As previously described in Section 2.1.1., this is a model proposed by Eligehausen et al (1983). Experimental research on the seismic performance of beam-column subassemblies by Viwathanetpa et al. (1979), Eligehausen et al (1983), and Filippou et al. (1983) suggested that the bond-slip behaviour of these members consisted of two distinct regions: i) Confined and ii) Unconfined. These definitions were adopted by the CEB-FIB MC90 (1993) based on previous research on bond-slip behaviour of reinforcing bars. Later, similar studies by Soroushian et al. (1989), and Pochanart et al. (1989) provided enough data to define the formulation based on Eligehausen et al. (1983). In the Eligehausen Model, these two distinct cases are computed as:

- For unconfined regions where $\beta = 0$, the bond stress-slip values of the monotonic curve are calculated as:

$$\tau = \tau_{s1} (\Delta_s / \Delta_{s1})^\alpha \quad \Delta \leq \Delta_{s1} \quad (2.5)$$

$$\tau = \tau_{s2} \quad \Delta_{s1} < \Delta \leq \Delta_{s2} \quad (2.6)$$

$$\tau = \tau_{s2} - \left[\frac{(\Delta - \Delta_{s2})}{(\Delta_{s3} - \Delta_{s2})} (\tau_{s2} - \tau_{sf}) \right] \quad \Delta_{s2} < \Delta \leq \Delta_{s3} \quad (2.7)$$

$$\tau = \tau_{sf} \quad \Delta_{s3} < \Delta \quad (2.8)$$

where:

$$\tau_{s1} = 0.748 \sqrt{\frac{f'_c c}{d_b}} \leq \tau_{p1} \quad (2.9)$$

$$\tau_{s1} = \tau_{s2} \quad (2.10)$$

$$\tau_{sf} = 0.234 \sqrt{\frac{f'_c c}{d_b}} \leq \tau_{pf} \quad (2.11)$$

$$\Delta_{s1} = \Delta_{p1} \exp \left[\frac{1}{\alpha} \ln \left(\frac{\tau_{s1}}{\tau_{p1}} \right) \right] \quad (2.12)$$

$$\Delta_{s2} = \Delta_{p2} \quad (2.13)$$

$$\Delta_{s3} = \Delta_{p3} \quad (2.14)$$

$$\alpha = 0.4 \quad (2.15)$$

τ_{p1} and τ_{pf} are the confined region bond stress values, defined in Equations 2.20 and 2.22.

- In confined regions where $\beta = 1$, bond stress-slip values of the monotonic curve are:

$$\tau = \tau_{p1} = \left(\Delta/\Delta_{p1}\right)^\alpha \quad \Delta \leq \Delta_{p1} \quad (2.16)$$

$$\tau = \tau_{p2} \quad \Delta_{p1} < \Delta \leq \Delta_{p2} \quad (2.17)$$

$$\tau = \tau_{p2} - \left[\frac{(\Delta - \Delta_{p2})}{(\Delta_{p3} - \Delta_{p2})} (\tau_{p2} - \tau_{pf}) \right] \quad \Delta_{p2} < \Delta \leq \Delta_{p3} \quad (2.18)$$

$$\tau = \tau_{pf} \quad \Delta_{p3} < \Delta \quad (2.19)$$

where:

$$\tau_{p1} = \left(20 - \frac{d_b}{4}\right) \sqrt{\frac{f'_c}{30}} \quad (2.20)$$

$$\tau_{p1} = \tau_{p2} \quad (2.21)$$

$$\tau_{pf} = \left(5.5 - 0.07 \frac{S}{H}\right) \sqrt{\frac{f'_c}{27.6}} \quad (2.22)$$

$$\Delta_{p1} = \sqrt{\frac{f'_c}{30}} \quad (2.23)$$

$$\Delta_{p2} = 3.0 \text{ mm} \quad (2.24)$$

$$\Delta_{p3} = S \quad (2.25)$$

$$\alpha = 0.4 \quad (2.26)$$

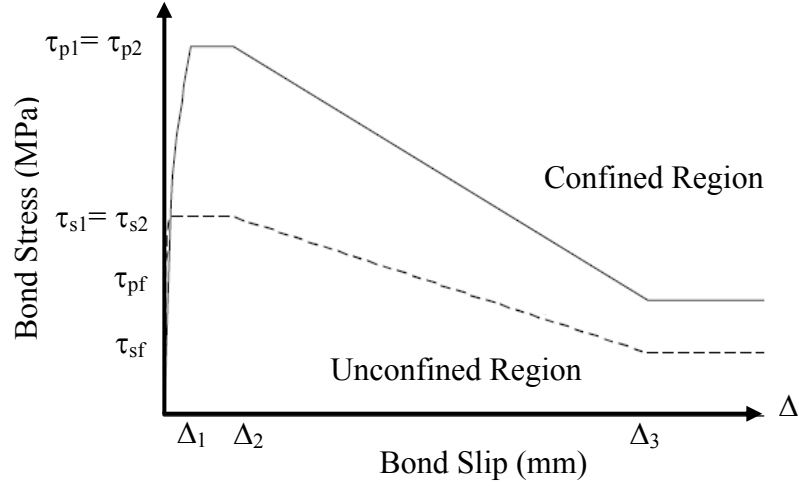


Fig. 2.24 Eligehausen Confined and Unconfined Bond Stress-Slip Model

- If the confinement pressure index is between 0 and 1, the behaviour of the bond model is computed for the Eligehausen Model as:

$$\tau = \tau_{sp1} \left(\frac{\Delta}{\Delta_{sp1}} \right)^\alpha \quad \Delta \leq \Delta_{sp1} \quad (2.27)$$

$$\tau = \tau_{sp1} - \left[\frac{(\Delta - \Delta_{sp1})}{(\Delta_{sp3} - \Delta_{sp2})} (\tau_{sp2} - \tau_{spf}) \right] \quad \Delta_{sp1} < \Delta \leq \Delta_{sp2} \quad (2.28)$$

$$\tau = \tau_{sp2} - \left[\frac{(\Delta - \Delta_{sp2})}{(\Delta_{sp3} - \Delta_{sp2})} (\tau_{sp2} - \tau_{spf}) \right] \quad \Delta_{sp2} < \Delta \leq \Delta_{sp3} \quad (2.29)$$

$$\tau = \tau_{spf} \quad \Delta_{sp3} < \Delta \quad (2.30)$$

where:

$$\tau_{sp1} = \tau_{s1} + \beta(\tau_{p1} - \tau_{s1}) \quad (2.31)$$

$$\tau_{sp1} = \tau_{sp2} \quad (2.32)$$

$$\tau_{spf} = \tau_{s1} + \beta(\tau_{pf} - \tau_{sf}) \quad (2.33)$$

$$\Delta_{sp1} = \Delta_{s1} + \beta(\Delta_{p1} - \Delta_{s1}) \geq \Delta_{s1} \quad (2.34)$$

$$\Delta_{sp2} = \Delta_{p2} \quad (2.35)$$

$$\Delta_{sp3} = \Delta_{p3} \quad (2.36)$$

Gan Model:

This model describes the same behaviour for confined regions as the Eligehausen Model, but a slightly different response for unconfined regions where splitting failure mechanisms are significant.

- In unconfined regions, bond stress-slip values of the monotonic curve are:

$$\tau = \tau_{s1} \left(\Delta_s / \Delta_{s1} \right)^\alpha \quad \Delta \leq \Delta_{s1} \quad (2.37)$$

$$\tau = \tau_{s1} - \left[\frac{(\Delta - \Delta_{s1})}{(\Delta_{s2} - \Delta_{s1})} (\tau_{s1} - \tau_{sf}) \right] \quad \Delta_{s1} < \Delta \leq \Delta_{s2} \quad (2.38)$$

$$\tau = \tau_{sf} \quad \Delta_{s2} < \Delta \quad (2.39)$$

where:

$$\tau_{s1} = 0.748 \sqrt{\frac{f'_c c}{d_b}} \leq \tau_{p1} \quad (2.40)$$

$$\tau_{s2} = 0.15 \tau_{s1} \quad (2.41)$$

$$\tau_{sf} = \tau_{s2} \quad (2.42)$$

$$\Delta_{s1} = \Delta_{p1} \exp \left[\frac{1}{\alpha} \ln \left(\frac{\tau_{s1}}{\tau_{p1}} \right) \right] \quad (2.43)$$

$$\Delta_{s2} = 2 \text{ mm} \quad (2.44)$$

$$\Delta_{s3} = \Delta_{p3} \quad (2.45)$$

τ_{p1} , Δ_{p1} and Δ_{p3} are the confined region bond stress-slip values, previously defined in Equations 2.20, 2.23, and 2.25.

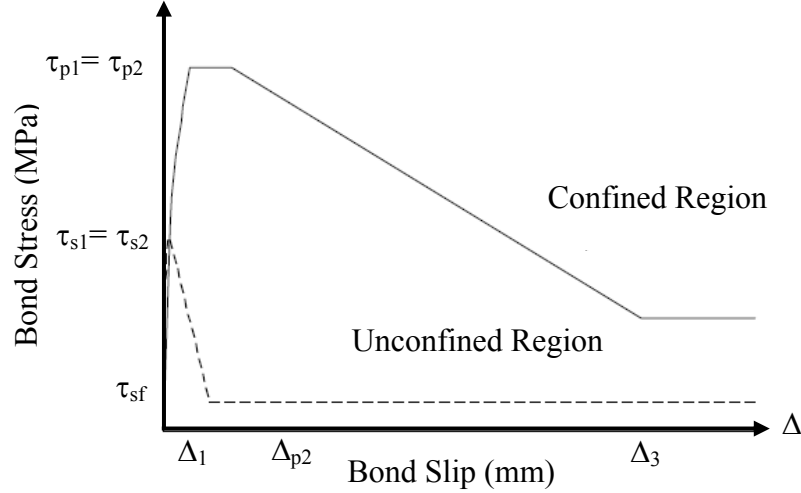


Fig. 2.25 Gan Confined and Unconfined Bond Stress-Slip Model

- If the confinement pressure index is between 0 and 1, the behaviour of the bond model is computed for the Gan Model as follows;

$$\tau_{sp1} = \tau_{s1} + \beta(\tau_{p1} - \tau_{s1}) \quad (2.46)$$

$$\tau_{sp2} = \tau_{s2} + \beta(\tau_{p2} - \tau_{s2}) \quad (2.47)$$

$$\tau_{spf} = \tau_{s1} + \beta(\tau_{pf} - \tau_{sf}) < \tau_{sf} \quad (2.48)$$

$$\Delta_{sp1} = \Delta_{s1} + \beta(\Delta_{p1} - \Delta_{s1}) \geq \Delta_{s1} \quad (2.49)$$

$$\Delta_{sp2} = \begin{cases} 2.0 & \text{if } \beta = 0 \\ \Delta_{p2} & \text{if } 0 < \beta \end{cases} \quad (2.50)$$

Hooked Bar Model:

The formulation of this model was implemented into VecTor2 by Gan (2000) based on the research results by Eligehausen et al. (1983). They conducted tests on a confined

concrete member with #8 (25 mm) deformed bar and average bond stress-slip values for hooks confined in concrete were proposed. The bond stress-slip values used for this model can be observed in Table 2.4 and in Fig. 2.26.

Table 2.4 Bond Stress-Slip Parameters of Hooked Bars (Eligehausen et al., 1983)

Parameter	Hooks in Confined Concrete
Δ_1	1.0
Δ_2	3.0
Δ_3	100.0
τ_1	22.0
τ_2	4.0
α	0.20

The formulation in VecTor2 for this model is as follows:

$$\tau = 22\left(\Delta/\Delta_{p1}\right)^\alpha \quad \text{MPa} \quad \Delta \leq \Delta_1 \quad (2.51)$$

$$\tau = 22 \quad \text{MPa} \quad \Delta_1 < \Delta \quad (2.52)$$

α and Δ_{p1} is computed according to the model selected.

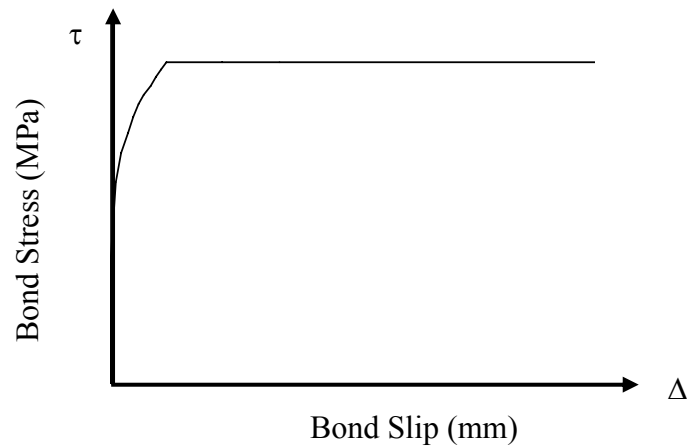


Fig. 2.26 Bond Stress-Slip Model for Hooked End Bars

Bond Models in VecTor2 under Reversed Cyclic Loading:

The cyclic curve proposed by Eligehausen et al. (1983) is used for both the Eligehausen and Gan models with regards to the bond stress-slip cyclic behaviour. The cyclic curve for Eligehausen's bond-slip model is given in Fig. 2.27. A preliminary investigation on concrete blocks with embedded deformed bars was carried out to better understand the bond-slip behaviour. After a careful investigation of the monotonic and cyclic bond-slip behaviour in VecTor2, a difference between the Eligehausen and VecTor2 cyclic behaviour was observed. Eligehausen's model follows an unloading branch up to a frictional bond stress, which was defined as a quarter of the maximum bond stress value of the previous loading cycle. The bond stress remains constant under further slippage in the negative direction, and increases following the backbone curve of the monotonic bond slip curve.

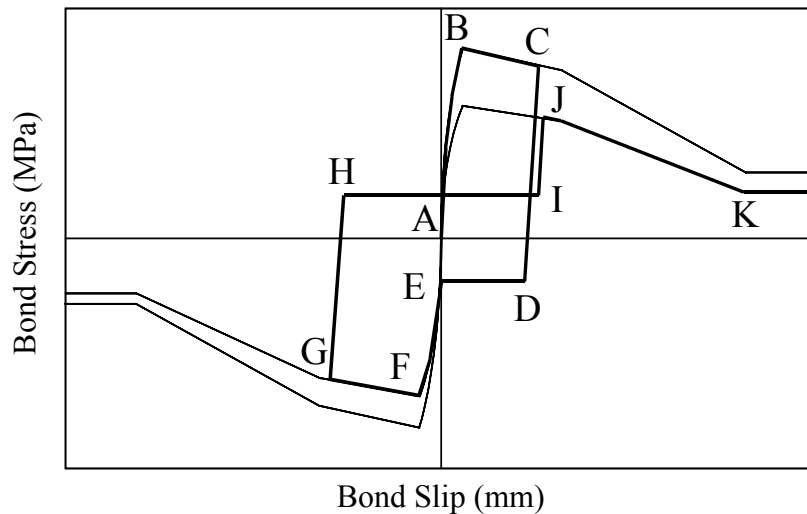


Fig. 2.27 Cyclic Bond Stress-Slip Model by Eligehausen et al. (1983)

The bond stress-slip values are reduced compared to the actual monotonic behaviour. The bond stress-slip behaviour displays a reduction in the bond resistance to represent the additional loading, and the slip effects are computed by a reduction factor denoted as the damage index parameter, D . The damage index is defined between zero and one. The value is equal to 1 for full damage with a resulting zero bond stress value, and represents the case where the bond is completely destroyed. If the damage index

parameter is zero, then the reduced curve will follow a similar behaviour to the monotonic bond-slip curve. The damage index and the reduction of the bond stress value are estimated using the Equations 2.60 to 2.64.

The reduced envelope that is followed in reversed cyclic loading conditions is explained here. First, the stiffness parameters attained at the i^{th} cycle, and then the bond stress-slip values for unloading and reloading branches are given in the following section.

During the i^{th} cycle stiffness parameters are computed as follows:

$$E_i = 0 \quad (2.53)$$

$$E_i = E_{i-1} + \Delta E_i \quad (2.54)$$

(D1) for $\Delta_{im} \leq \Delta_{0.8max}$;

$$\Delta E_i = 0 \quad (2.55)$$

(D2) for $\Delta_{0.8max} < \Delta_{im} \leq \Delta_{1s}$;

$$\Delta E_i = \tau_{im} \Delta_1 (\Delta_{im} / \Delta_1)^{(1+\alpha)} / (1+\alpha) + 0.5 * 0.25 \tau_{im} \Delta_{im} \quad (2.56)$$

(D3) for $\Delta_{1s} < \Delta_{im} \leq \Delta_{2s}$;

$$\Delta E_i = \tau_{1i} \Delta_{1s} / (1+\alpha) + 0.5(\tau_{1i} + \tau_{im})(\Delta_{im} - \Delta_1) + 0.5 * 0.25 \tau_{im} \Delta_{im} \quad (2.57)$$

(D4) for $\Delta_{2s} < \Delta_{im} \leq \Delta_{3s}$;

$$\Delta E_i = \tau_{1i} \Delta_1 / (1+\alpha) + 0.5(\tau_{1i} + \tau_{2i})(\Delta_3 - \Delta_1) + 0.5(\tau_{2i} + \tau_{im})(\Delta_{im} - \Delta_2) + 0.5 * 0.25 \tau_{im} \Delta_{im} \quad (2.58)$$

(D5) for $\Delta_{im} > \Delta_{3s}$;

$$\begin{aligned} \Delta E_i = & \tau_{1i} \Delta_1 / (1+\alpha) + 0.5(\tau_{1i} + \tau_{2i})(\Delta_3 - \Delta_1) + 0.5(\tau_{2i} + \tau_{fi})(\Delta_3 - \Delta_2) + \tau_{fi}(\Delta_{im} - \Delta_3) + \dots \\ & \dots + 0.5 * 0.25 \tau_{im} \Delta_{im} \end{aligned} \quad (2.59)$$

where,

E_i = energy consumption index at i^{th} cycle;

$\Delta_{0.8max}$ = slip corresponding to 80% stress of τ_{1s} ;

τ_{1i} , τ_{2i} , and τ_{fi} = bond stresses corresponding to slips Δ_1 , Δ_2 , and Δ_3 ;

These bond stress values are estimated using damage index which is described later;

$$\tau_{1i} = \tau_{1s} (1 - D_i) \quad (2.60)$$

$$\tau_{2i} = \tau_{2s} (1 - D_i) \quad (2.61)$$

$$\tau_{fi} = \tau_{fs} (1 - D_i) \quad (2.62)$$

The damage index at i^{th} cycle is computed by;

$$D_i = 1 - e^a \quad (2.63)$$

$$a = -1.2(E_i/E_0)^{1.1} \quad (2.64)$$

In this formula, E_0 is different for confined and unconfined cases, and is computed from the area enveloped by bond stress-slip curve limited by Δ_3 ;

For unconfined cases:

$$E_0 = \tau_1 \Delta_1 / (1 + \alpha) + \tau_1 (\Delta_3 - \Delta_1) + 0.5(\tau_1 + \tau_f)(\Delta_3 - \Delta_2), \quad (2.65)$$

For confined cases:

$$E_0 = \tau_{1s} \Delta_{1s} / (1 + \alpha) + 0.5(\tau_{1s} + \tau_{2s})(\Delta_{2s} - \Delta_{1s}) + 0.5(\tau_{1s} + \tau_{fs})(\Delta_{3s} - \Delta_{2s}) \quad (2.66)$$

The bond stresses at the unloading and reloading branches are as follows:

- The i^{th} unloading cycle is given by,

$$\tau_i = 0.25 \tau_{im} \quad 0 \leq |\Delta_i| < |\Delta_i^p| \quad (2.67)$$

$$\tau_i = (\Delta_i - \Delta_i^p) \tau_{im} / (\Delta_{im} - \Delta_i^p) \quad |\Delta_i^p| \leq |\Delta_i| < |\Delta_{im}| \quad (2.68)$$

$$\tau_i = f(\Delta_i) \quad |\Delta_{im}| \leq |\Delta_i| \quad (2.69)$$

where

$$\Delta_i^p = \Delta_{im} - \tau_{im} / G_0 \quad 0 \leq |\Delta_i| < |\Delta_i^p| \quad (2.70)$$

$$G_0 = \tau_1 \alpha 100^{(1-\alpha)} \quad (2.71)$$

Δ_i^p is the plastic bond slip value that is attained at bond slip Δ_{im} , whereas Δ_{im} is the

maximum slip attained at the positive half cycle (for i^{th} negative loading) or the maximum slip attained at the negative half cycle (for i^{th} positive loading). τ_{im} is the absolute value of bond stress corresponding to this slip value, Δ_{im} .

- The i^{th} reloading cycle is given by

$$\tau_i = f(\Delta_i) \geq -0.25 \tau_{im} \quad \text{for } \tau_i \geq 0 \quad (2.72)$$

$$\tau_i = f(\Delta_i) \leq -0.25 \tau_{im} \quad \text{for } \tau_i < 0 \quad (2.73)$$

where

$f(\Delta_i)$ in equations above is computed from the bond stress obtained from the base curve reduced by the bond degradation at the current cycle.

The cyclic behaviour of the bond-slip model in VecTor2 is shown in Fig. 2.28. As shown in this figure, this model doesn't involve the frictional bond resistance in Eligehausen's model. The bond-slip behaviour decreases to the zero bond stress-slip value and then increases in the negative loading branch following the monotonic behaviour. The reduced envelope approach under reversed cyclic loading conditions is applied similar to the Eligehausen's model, but some of the energy dissipation capacity of the specimens is lost between the unloading and reloading cycles as a result.

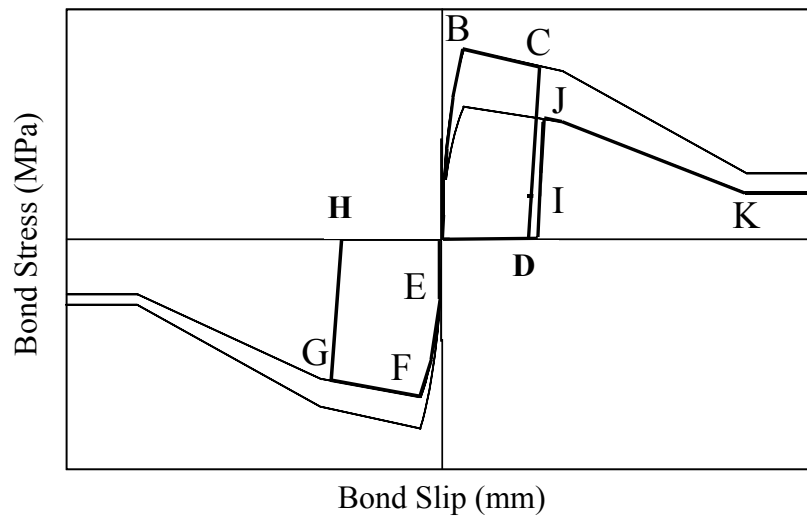


Fig. 2.28 Cyclic Bond Stress-Slip Model in VecTor2

CHAPTER 3

Analysis of Deformed Reinforcement Beam-Column Subassemblies

VecTor2, a two-dimensional nonlinear finite element analysis program, was used for modelling the reinforced concrete beam-column subassemblies. In the search for an applicable and reliable beam-column subassembly model, specimens were selected from beam-column subassemblies which were different in type of connection, material properties, reinforcement detailing, test set-up and loading system. All specimens were modelled with the same material, geometric, and loading conditions applied during the experimental testing program.

The specimens used for modelling purposes with VecTor2 are briefly described here while additional information on these specimens can be found in the experimental study reports and journal papers that are referenced in this thesis. The finite element models of the specimens, and the results of the analytical studies in comparison to experimental results, are also given for each test specimen following the specimen details. Information on the beam-column subassemblies designed with deformed reinforcement is given in this chapter; specimens with smooth (plain round) reinforcement are treated in the next chapter, Chapter 4. The specimens in each chapter are described in two sub-sections: exterior and interior beam-column subassemblies.

3.1. EXTERIOR BEAM-COLUMN SUBASSEMBLIES

3.1.1 SPECIMEN ED1

The beam-column subassemblies considered here were full-scale models from a multi-storey moment resisting frame building with a 20 ft span and 10 ft storey height. The beam-column subassemblies were designed according to the seismic requirements of ACI 318-77 (Bond, 1969; Goyal, 1969). The specimen selected for this study was a beam-column subassembly designed with deformed reinforcement and the joint panel region was unconfined against shear deformations in the joint.

3.1.1.1. TEST SPECIMENS

Sectional and Material Properties:

The column was 15 by 15 inches (381 mm x 381 mm) with eight #8 longitudinal bars, and the beam was 12 by 20 inches (305 mm x 508 mm) with five #9 bars. The sectional details and reinforcement layout of the specimen are given in Fig 3.1.

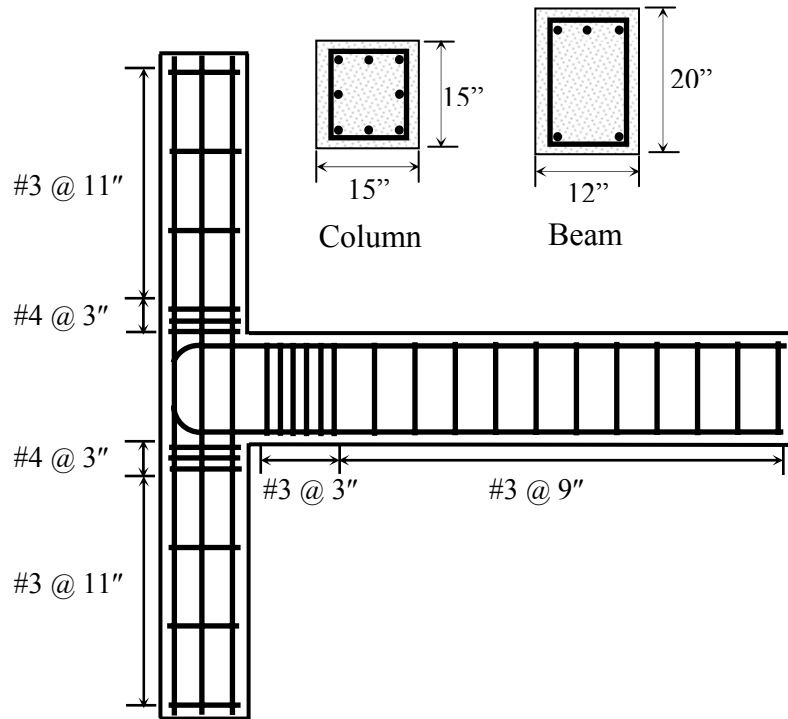


Fig. 3.1 Reinforcement Layout for Specimen ED1

The concrete castings of the specimens were completed in three stages; lower column, beam and upper column. The material properties of concrete and reinforcement are given in Table 3.1 and 3.2.

Table 3.1 Material Properties of Concrete for Specimen ED1

Parameter	Beam	Joint	Column
f_c' (ksi (MPa))	4.51 (31.1)	4.51 (31.1)	5.58 (38.5)

Table 3.2 Material Properties of Reinforcement for Specimen ED1

Type	Area in ² (mm ²)	f _y ksi (MPa)	E _s ksi (MPa)	f _u ksi (MPa)
# 9	1.00 (645)	50.6 (349)	29000 (200000)	90 (620)
# 8	0.79 (510)	48.6 (335)		80 (552)
# 4	0.20 (129)	55 (379)		90 (620)
# 3	0.11 (71)	62 (428)		110 (758)

Test Set-Up and Loading:

Simulation of the seismic and gravity load conditions was accomplished by applying a constant axial load to the center of the column with a Universal Hydraulic Machine. The reversed vertical cyclic loading was applied to the tip of the beam with a hydraulic jack. The hydraulic jack, connected to the reaction floor, was capable of moving in each direction with a capacity of 16 tons. The lower column end was restrained by a reinforced concrete pedestal mounted on the reaction floor, and the upper column top was loaded through the head of the testing machine restricting the movement of the column in the horizontal direction.

The axial load applied to the top of the column was kept constant during testing at 500 kips (2225 kN). The hydraulic jack at the beam tip was connected at a distance of 10 ft (3050 mm) from the column centerline, and moved in the vertical direction to simulate seismic loading of the beam-column subassembly. A detailed figure of the test set-up is shown in Fig. 3.2. The loading protocol was defined during the testing based on the failure status of the specimen.

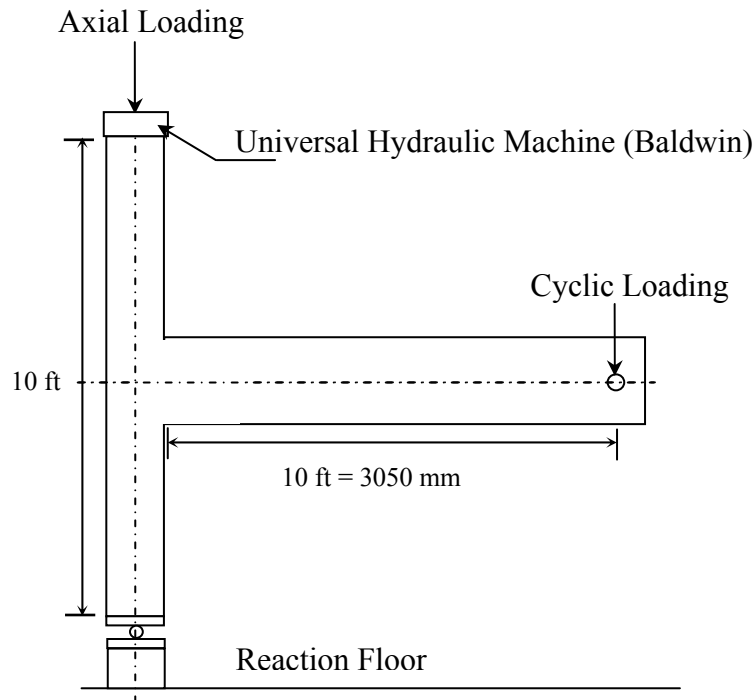


Fig. 3.2 Test Set-up and Loading System for Specimen ED1

3.1.1.2. FINITE ELEMENT MODELLING

This specimen had no challenging aspects for modelling with VecTor2 in terms of specimen geometry, material properties, test set-up or loading conditions. Details of the concrete regions, and reinforcement and bond elements used for the non-linear analysis of this specimen are given in this section.

Material and Regional Properties:

The material properties of the concrete and reinforcement were modelled as described in the experimental test reports. The concrete regions were modelled with rectangular elements, and truss elements were assigned to the reinforcement together with bond-link elements. Smearred reinforcement was also assigned to the concrete regions to represent the confinement effect of transverse bars. This effect was utilized in

VecTor2 as the ratio of reinforcement in the out-of-plane direction, ρ_z . As all reinforcement was modelled as discrete truss elements, the selection of a proper mesh size was affected by the size of the connecting members and reinforcement layouts. The coarseness of the mesh was gradually changed for a better representation of the model during the course of this numerical investigation. The final model shown in Fig. 3.3 was the final result of this process.

In the analysis, the specimen was modelled with 1787 rectangular concrete elements by using a 35 by 65 mm mesh configuration. Six concrete regions were utilized within the model, and are briefly described in Table 3.3. The first region was a fictitious load bearing concrete region assigned to the sections where the supports or loads were applied. These regions were used to avoid unrealistic local failures in the model. Three regions were assigned to the column, and one to the beam. Detailed information on the concrete regions is given in Fig. 3.3 and in Table 3.3.

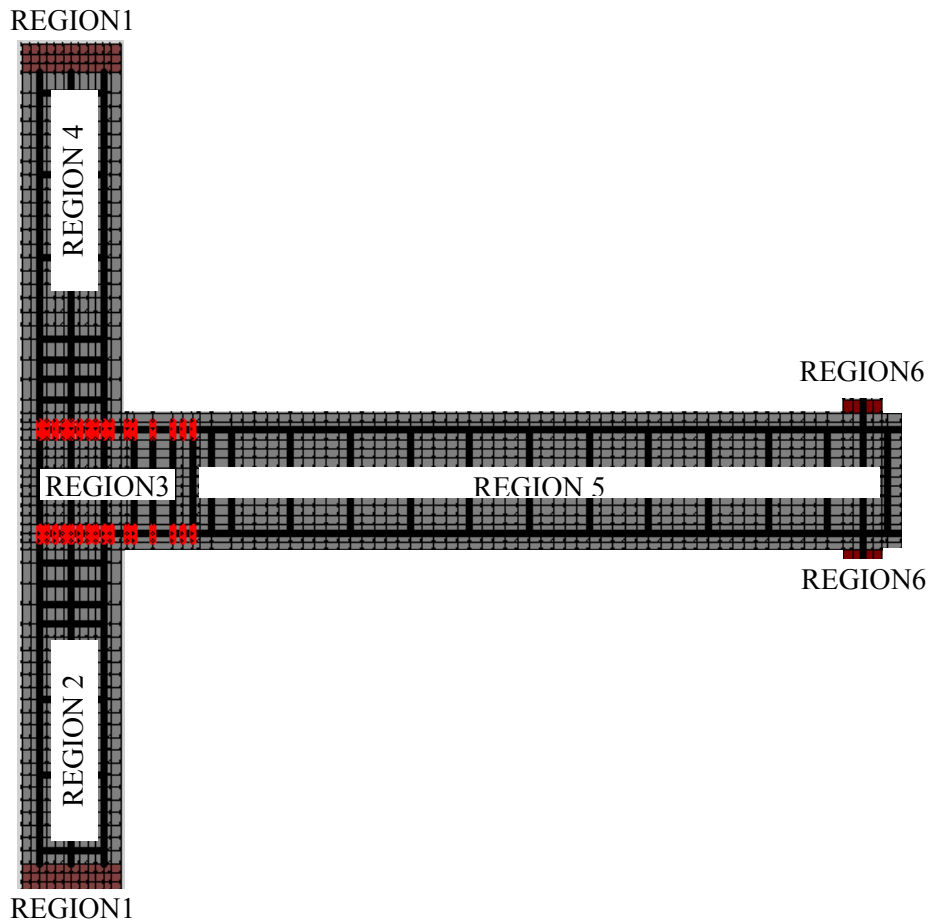


Fig. 3.3 Material Regions for Specimen ED1

Table 3.3 Concrete Regions for Specimen ED1

Concrete Regions	# 1	# 2	# 3	# 4	# 5	#6
Thickness (mm)	380				305	
Mesh Size (mm)	35 x 65	35 x 65	35 x 35	35 x 65	65 x 35	65 x 65
Purpose	Bearing	Lower Column	Joint	Upper Column	Beam	Bearing
Reinforcement	None	# 3	None	# 3	# 3	None
ρ_z (%)		0.13		0.13	0.20	

A total of 649 truss elements and 30 bond-link elements were used to represent the reinforcement and bond details of the specimen. The representation of the reinforcement and bond element configuration is shown in Fig. 3.4, and detailed information about these properties is given in Table 3.4 and Table 3.5.

Table 3.4 Reinforcement Elements for Specimen ED1

Reinforcement	Type	Location
# 1	3 #8	Column Longitudinal Outer Reinforcement
# 2	2 #8	Column Longitudinal Center Reinforcement
# 3	3 # 9	Beam Top Layer Longitudinal Reinforcement
# 4	2 # 9	Beam Bottom Layer Longitudinal Reinforcement
# 5	1 # 4	Transverse Reinforcement on Columns
# 6	1 # 3	Transverse Reinforcement on Beams

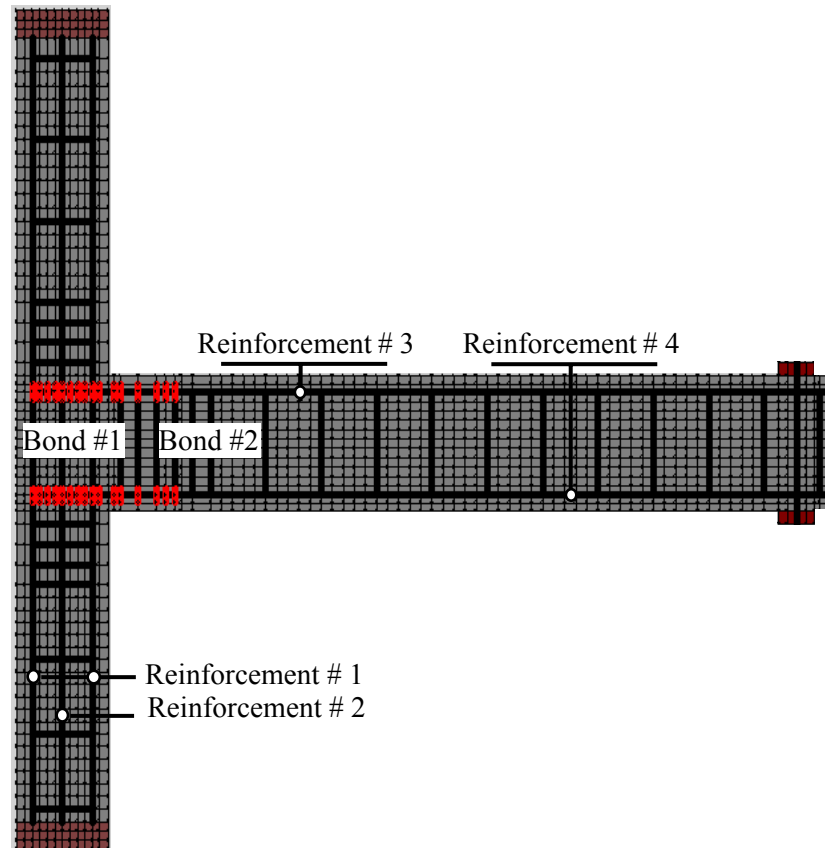


Fig. 3.4 Reinforcement Regions for Specimen ED1

The bond elements were introduced in two regions. Soroushian et al. (1988) suggested modeling these hooked bars with a stiff spring connected to the bond-slip elements on the straight section of the reinforcement. As this beam-column joint was unconfined and the beam longitudinal reinforcement was anchored into the joint with 180° hooks not extending into the column, this specimen was modelled with two bond materials. The first utilized the perfect bond behaviour to represent the hook section of the reinforcement. The perfect model is a bond-slip model where a larger stiffness property was assigned to the bond elements to limit the slip of the reinforcement. The second was the imperfect bond material for the straight section of the beam reinforcement. The configuration of the bond-link elements and confinement pressure

index values selected for each bond-link element are given in Fig. 3.4 and in Table 3.5. The confinement pressure values were estimated based on the definition given in the CEB-FIB MC90 (1993). As explained in Chapter 2, the ratio of the transverse reinforcement along the beam longitudinal bars is used for the definition of the confinement pressure value. The concrete cover and number of reinforcement layers through depth was another parameter as these are also effective values in determination of failure mechanism in the bond-slip models.

Table 3.5 Bond Elements for Specimen ED1

Type	Bond # 1	Bond # 2
Reinforcement	Hooked End	Straight Section
Bond Model	Perfect	Imperfect
Confinement Pressure (MPa)	N/A	2.66

Loading and Restraint Conditions:

The loading protocol used during testing was followed exactly in the analysis, including the small cycle intervals, as shown in Fig. 3.5. Load Case 1 was the horizontally applied displacement-based reversed cyclic loading, and Load Case 2 was the constant axial load applied to the top of the column. The restraint conditions consisted of a pinned support at the end of lower column, and a pinned roller support at the top of the upper column to limit the lateral movement of the column.

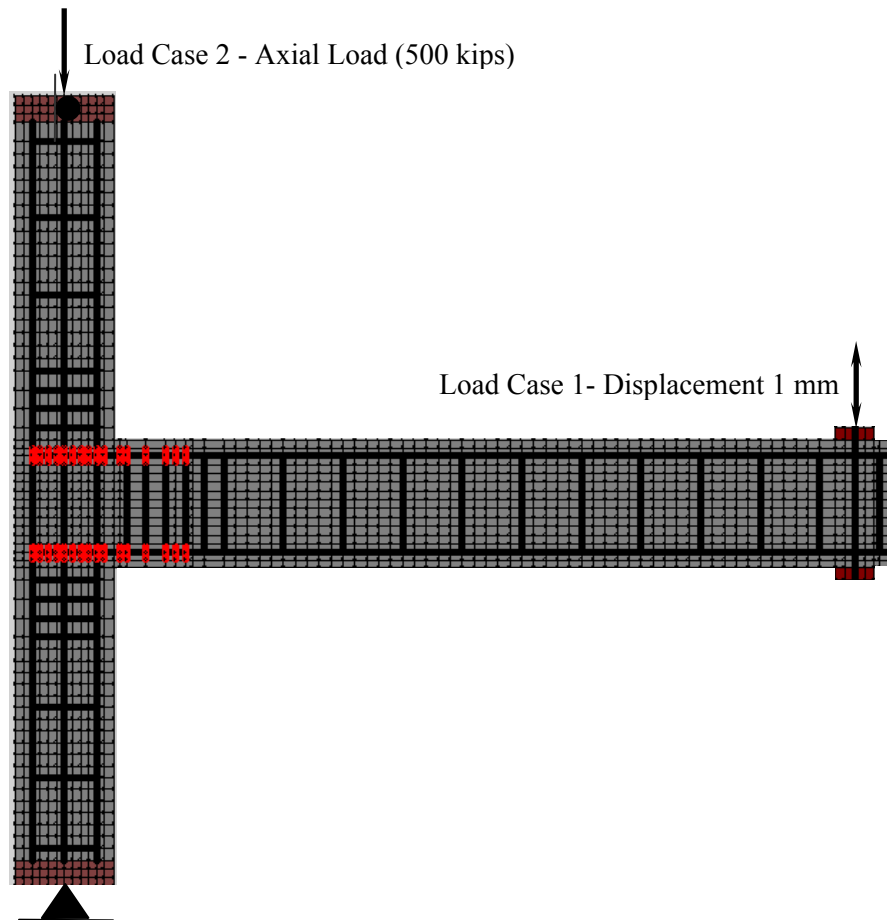


Fig. 3.5 Loading and Restraint Conditions for Specimen ED1

3.1.1.3. RESULTS OF EXPERIMENTAL AND ANALYTICAL STUDY

The failure of this specimen was caused by extensive shear cracking at the beam-column joint. The load versus displacement results and the final failure mechanism of the experimental study are given in comparison to the VecTor2 analytical results in Fig. 3.6 and Fig. 3.8. The first shear cracking was reported to have been seen at the 2nd cycle in the positive loading direction. These cracks propagated through the upper and lower column gradually, and the specimen failed with extensive cracking and concrete cover spalling in the joint (Bond, 1969; Goyal, 1969). Limited information about the sequence of events was obtained from the test results, and a comparison between the analytical

and experimental results is given in Table 3.6. The ductility ratios in of the specimen the positive and negative loading directions were estimated, and are given in Fig. 3.6 for further comparison between the analytical and experimental results. The total energy dissipation capacities obtained from the predicted and observed response of the specimen are also compared in Fig. 3.7.

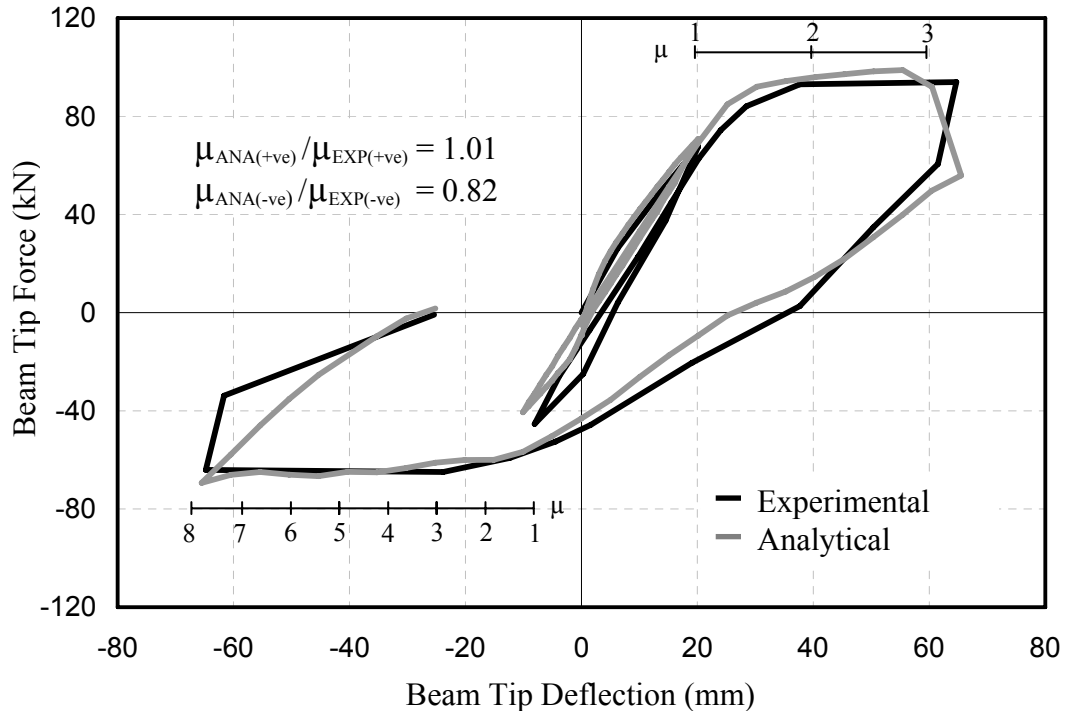


Fig. 3.6 Comparison of Story Shear vs. Story Displacement of Specimen ED1

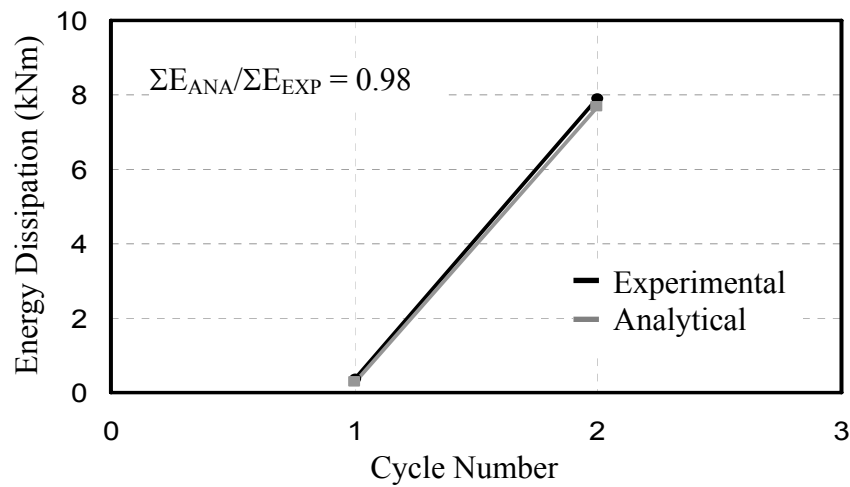


Fig. 3.7 Comparison of Energy Dissipation of Specimen ED1

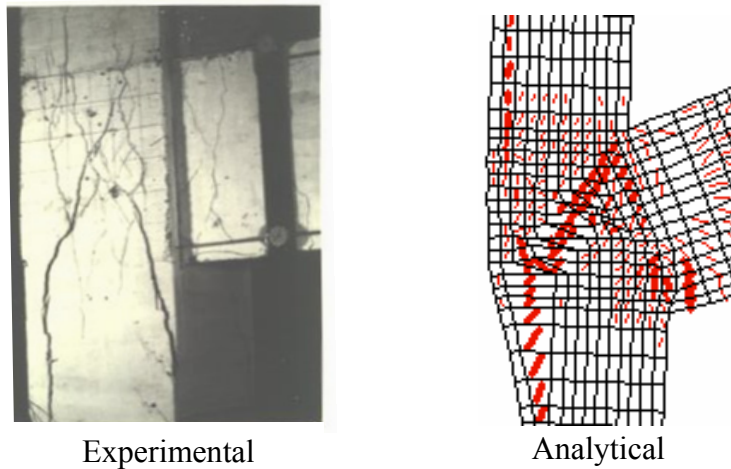


Fig. 3.8 Comparison of Final Failure of Specimen ED1

Table 3.6 Sequence of Events for Specimen ED1

Event	Experimental		Analytical	
	Story Shear (kN)	Displacement (mm)	Story Shear (kN)	Displacement (mm)
Positive Loading Direction				
2nd Cycle	First Joint Shear Cracking			
Max Story Shear	94.00	58.00	98.00	62.00
Negative Loading Direction				
Max Story Shear	64.90	62.00	69.30	62.00
End of Testing	Failure by Extensive Cracking in Joint Panel Region & Concrete Cover Spalling			

In the analytical results, the first shear cracking at the joint was also observed at the 2nd cycle of the positive loading. Later, the diagonal crack openings at the joint gradually increased, and a concrete wedge mechanism appeared and was similar to the experimental results. The expansion of the joint and column with extensive diagonal

cracking in opposite directions were also predicted in the final failure figures of the VecTor2 analysis.

The ratio of the predicted and observed ductility ratios for this specimen was 1.01 in the positive loading direction, and 0.82 in the negative loading direction. The predicted energy dissipation capacity for this specimen was compared to the observed value, and a ratio of 0.98 was obtained. As can be seen from the results above, the VecTor2 analysis was successful in capturing not only the hysteretic behaviour of the specimen, but the failure mechanism as well.

3.1.2 SPECIMEN ED2

The second specimen modelled is from a Benchmark Study (Shiohara and Kusuhara, 2006) which consisted of seismically designed, interior and exterior beam-column subassemblies. These specimens were seismically designed according to the AIJ 1999 code revisions. The specimen described in this section represents a 1/2-scale exterior beam-column subassembly of a typical moment resisting reinforced concrete framed building, tested by Shiohara and Kusuhara (2006) at the University of Tokyo, Japan. There were four other interior beam-column subassemblies tested in the same study, and these are discussed later in Section 3.2 of this chapter.

3.1.2.1. TEST SPECIMENS

Sectional and Material Properties:

Symmetric sectional details were chosen for both the columns and beams by the research group in order to exclude dimensional effects. The beam and column were both 300 by 300 mm. The average compressive strength, Young's modulus, and tensile splitting strength were 28.3 MPa, 25900 MPa and 2.67 MPa, respectively. The sectional details of this specimen can be observed in Fig. 3.9.

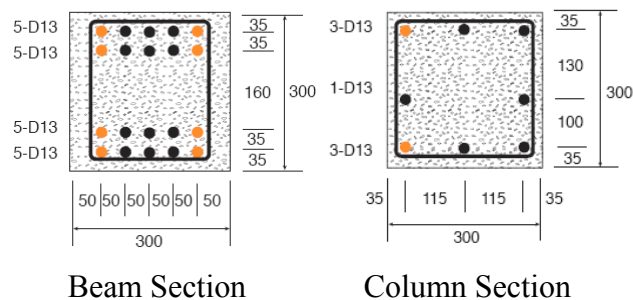


Fig. 3.9 Sectional Details of Specimen ED2 (Shiohara and Kusuhara, 2006)

Twenty D13 reinforcing bars were used for the longitudinal reinforcement of the beams. A state-of-the-art data acquisition technique was used to observe the post-yielding stress and strains on the reinforcement. The sections of the longitudinal bars were reduced in some sections of beams and columns for this purpose. The reinforcing bars represented in lighter colour in Fig. 3.9 were these grooved bars. Eight of the longitudinal reinforcing bars in the beam, and two of the reinforcing bars in the column was grooved in section. The sections of these bars were reduced by 29%. Detailed information about the sectional details can be found in the Benchmark Test Report by Shiohara and Kusuhara (2006). The transverse reinforcement was provided with a 50 mm spacing in all sections of the beam, column and joint. The material properties of the reinforcement are given in Table 3.7.

Table 3.7 Reinforcement Details for Specimen ED2

Type	Grade	Diameter (mm)	Area (mm ²)	f _y (MPa)	E _s (MPa)	f _u (MPa)
D13	SD390	14	127	456	176000	582
D13	SD345	14	127	357	176300	493
D6	SD295	6	32	326	151300	488
Grooved Longitudinal Reinforcing Bars						
D13	SD390	12.1	96	440	167000	566
D13	SD345	11.4	90	356	164000	460

Test Set-Up and Loading:

The beam-column subassemblies were tested under displacement-based reversed cyclic loading conditions. The displacement-based horizontal loading, and a constant axial load of 216 kN, were applied to the specimen. It was reported by Shiohara and Kusuhara (2006) that the axial load was applied to the specimen before the horizontal displacement loading started, and it was maintained at the same level during the testing.

The horizontal and axial loads were applied to the top of the column. The movement of the free tip of the beam was limited in the vertical direction. The test set-up is shown in Fig. 3.10.

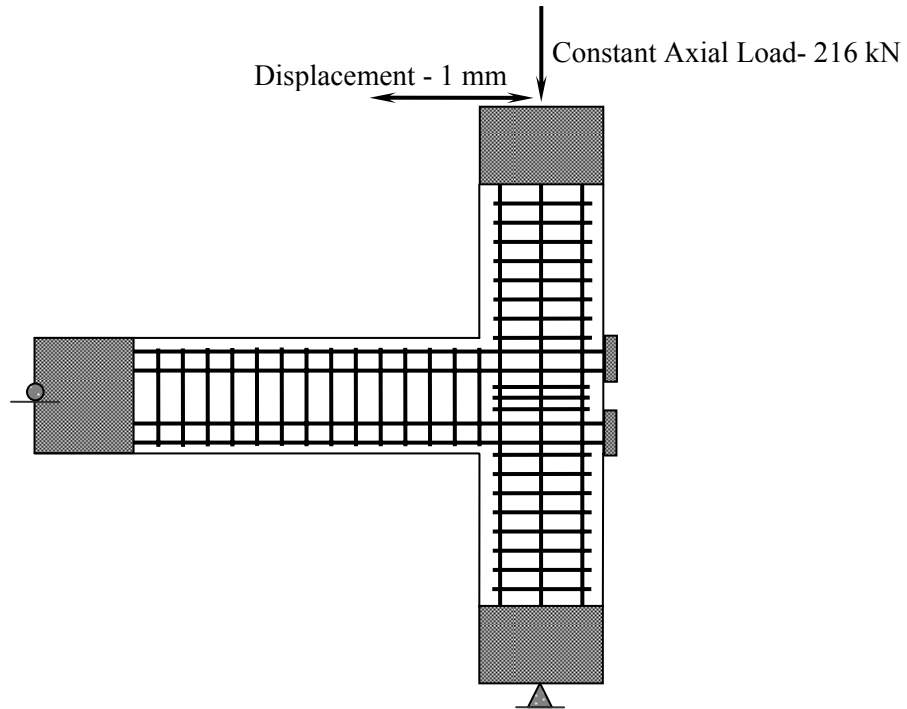


Fig. 3.10 Test Set-up and Loading System for Specimen ED2

As stated by Shiohara and Kusuhara (2006), the reversed cyclic loading was applied with increasing displacement amplitudes. The intervals started with 0.0625% drift and were gradually increased to 1% drift ratio. After the 1% reversed cycle was finalized, a 0.5% small drift was applied at the end of each 1% drift ratio. At the end of the 4% drift cycle, the specimens were loaded monotonically until failure occurred. The unit story drift value corresponded to 1470 mm for this specimen. The loading protocol followed during testing is given in Fig. 3.11

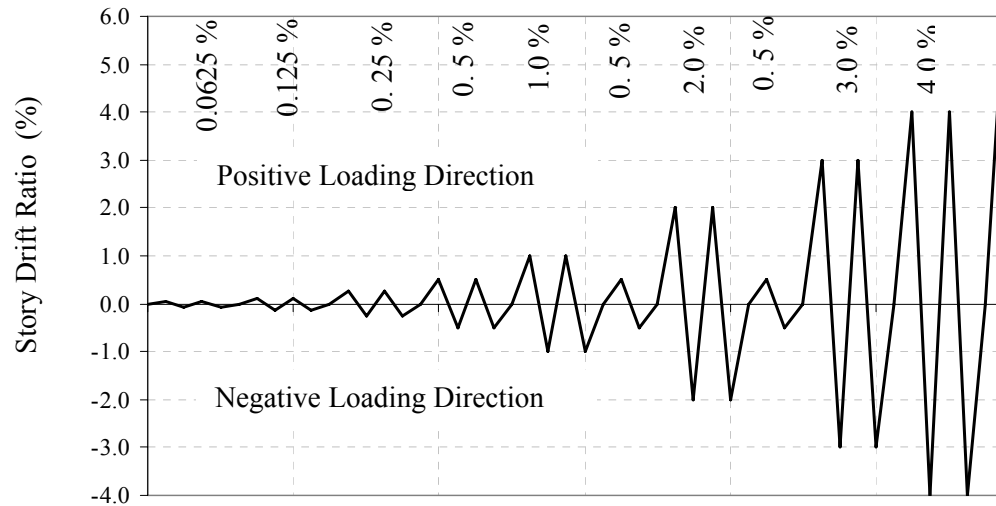


Fig. 3.11 Loading Protocol for Specimen ED2

3.1.2.2. FINITE ELEMENT MODELLING

Material and Regional Properties:

The material properties of concrete and reinforcement were modelled using an approach similar to the one used for Specimen ED1. Three concrete regions were assigned to represent this beam-column subassembly. The specimen was modelled with 1308 rectangular concrete elements, with a 25 by 25 mm mesh configuration. As illustrated in Fig. 3.12 and in Table 3.8, the first region is a fictitious concrete zone added to the model for the reasons described earlier for Specimen ED1. The second and third regions were assigned to the beams and columns as actual member sections.

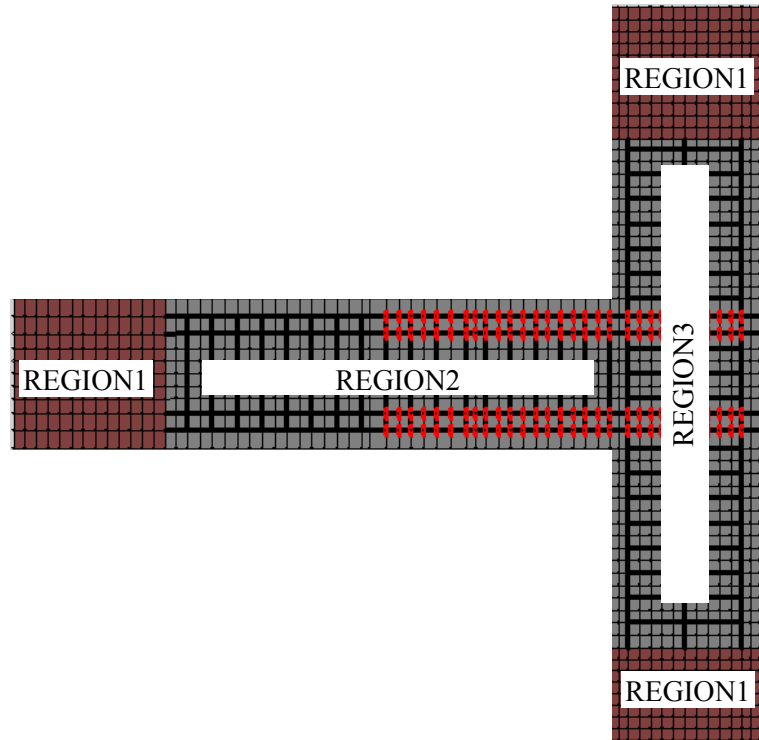


Fig. 3.12 Material Regions for Specimen ED2

Table 3.8 Concrete Regions for Specimen ED2

Concrete Regions	# 1	#2	# 3
Thickness (mm)	300		
Mesh Size (mm)	25 x 25		
Purpose	Bearing	Beam	Column and Joint
Reinforcement	None	D6	
ρ_z (%)		0.43	

All in-plane reinforcement was modelled with discrete truss elements, and additional smeared reinforcement was used to represent for out-of-plane confinement effect. The bond elements were also assigned to represent the interaction between

concrete and reinforcement. A total of 655 truss elements and 120 bond-link elements were used for this specimen. The reinforcement and bond element configuration is shown in Fig. 3.13, and detailed information about the reinforcement regions is given in Table 3.9.

Table 3.9 Reinforcement Elements for Specimen ED2

Reinforcement	Type	Location
# 1	5 D13 (Full Section)	Beam Longitudinal
# 2	5 D13 (25% Reduced Section)	
# 3	3 D13 (29% Reduced Section)	Column Longitudinal
# 4	3 D13 (Full Section)	
# 5	2 D13 (Full Section)	
# 6	1 D6 (Full Section)	Transverse Reinforcement



Fig. 3.13 Reinforcement and Bond Regions for Specimen ED2

The bond elements were introduced into the model in two regions. As the beam reinforcement was welded to steel plates, and the transverse reinforcement along the beam provided moderate confinement for this structure, this section was modelled as a confined region. The bond-slip effect of the reinforcement was modelled by Bond #2 in the joint. The section, which represented the interface between the longitudinal reinforcement in beams outside the joint, was modelled as an unconfined region, and defined by Bond #1. The confined and unconfined regions were assigned according to the CEB-FIB MC90 (1993) definitions. The configuration of bond-link elements and confinement pressure index values selected for each bond-link element is given in Fig. 3.12 and Table 3.10.

Table 3.10 Bond Elements for Specimen ED2

Type	Bond # 1	Bond # 2
Reinforcement	Beam Top and Bottom Layer Longitudinal	
Confinement Pressure (MPa)	1.4	7.5

Loading and Restraint Conditions:

As described previously, the loading protocol employed during testing (see Fig. 3.11) was followed in the analysis including the small cycle intervals. Load Case 1 was the horizontally applied displacement-based reversed cyclic loading, and Load Case 2 was the constant axial load applied to the top of the column. The lower end of the column was restrained with a pinned support, and a pinned roller support was used at the end of the beam allowing only lateral movement of the beam.

3.1.2.3. RESULTS OF EXPERIMENTAL AND ANALYTICAL STUDY

Specimen ED2 experienced flexural cracking at the beam-column interface, and shear cracking in the joint. A comparison of the story shear versus story drift ratios from the experimental and the VecTor2 analytical results given in Fig. 3.14, show very similar behaviour. The sequence of events in positive and negative loading directions of the specimen were also reported, and these are compared to the VecTor2 analytical results in Table 3.11 and Table 3.12.

In the experiment, the first flexural and shear cracking was reported at the end of the 1.0% drift ratio cycle. The yielding of beam longitudinal reinforcement occurred between 1.0% and 2.0 % drift ratios. At the 2.0% drift cycle, flexural cracks were reported observed at the upper and lower column ends. Horizontal cracks were reported between the two steel anchorage plates at the end of the 3.0% drift ratio. The anchorage plates were also reported to be pushed off from the concrete at the end of the test. The

alignment of the upper and lower column was gradually disturbed during testing. Later these cracks propagated and joined the shear cracks at the center of the joint, accompanied by the concrete cover spalling and the anchorage plate pushing off the concrete (Shiohara and Kusuhara, 2006).

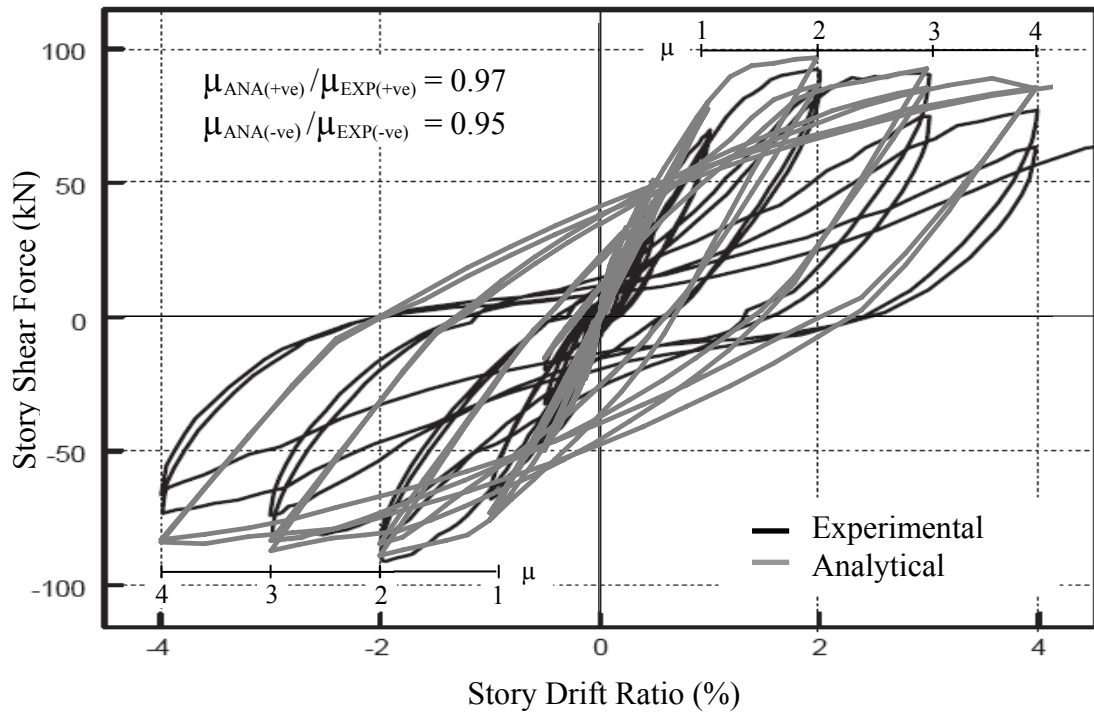


Fig. 3.14 Comparison of Story Shear vs. Story Drift Ratio of Specimen ED2

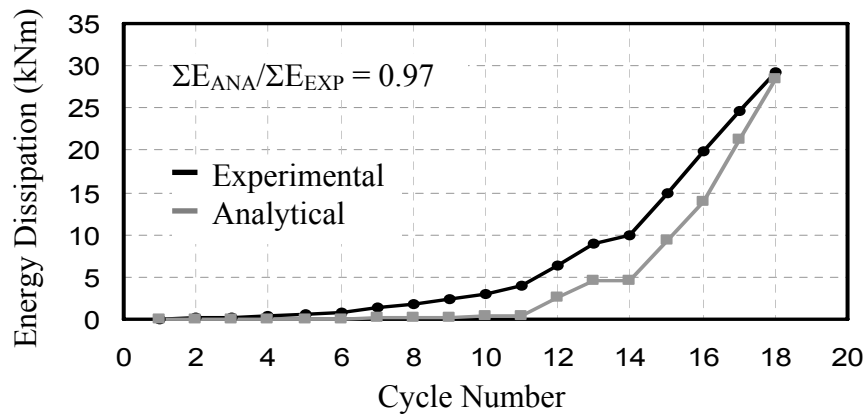


Fig. 3.15 Comparison of Energy Dissipation of Specimen ED2

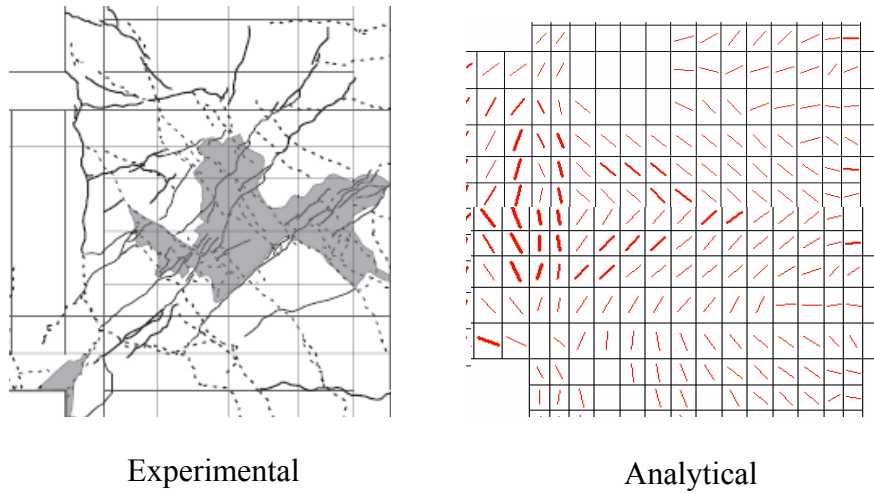


Fig. 3.16 Comparison of Final Failure of Specimen ED2

Table 3.11 Sequence of Events at the Positive Loading Direction

Event	Experimental		Analytical	
	Story Shear (kN)	Story Drift (%)	Story Shear (kN)	Story Drift (%)
Beam Reinforcement-1 st Layer Yielding	74.50	1.15	88.80	1.18
Beam Reinforcement-2 nd Layer Yielding	83.40	1.40	92.00	1.38
Column Reinforcement-Yielding	87.20	2.20	85.10	2.00
Max Story Shear	92.20	1.96	95.90	1.98

Table 3.12 Sequence of Events at the Negative Loading Direction

Event	Experimental		Analytical	
	Story Shear (kN)	Story Drift (%)	Story Shear (kN)	Story Drift (%)
Beam Reinforcement-1 st Layer Yielding	63.70	0.98	68.10	0.79
Beam Reinforcement-2 nd Layer Yielding	79.30	1.38	81.20	1.19
Column Reinforcement-Yielding	87.20	1.55	85.00	1.58
Max Story Shear	91.10	1.95	88.90	1.98

The experimental results for the formation of cracks at 1.0%, 2.0% and 3.0% drift ratios are also compared to the analytical results in Fig. 3.17, Fig. 3.18, and Fig. 3.19.

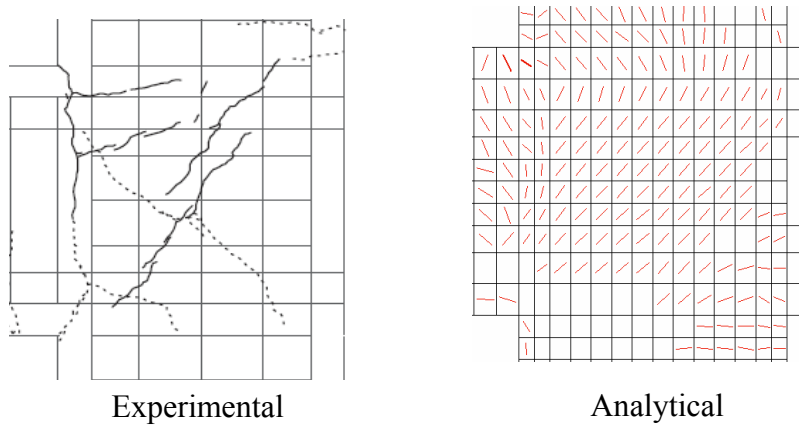


Fig. 3.17 Failure at the 1% Drift Ratio

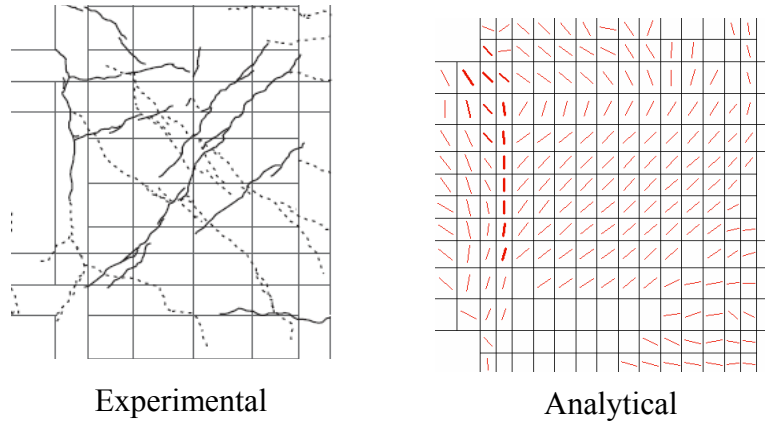


Fig. 3.18 Failure at the 2% Drift Ratio

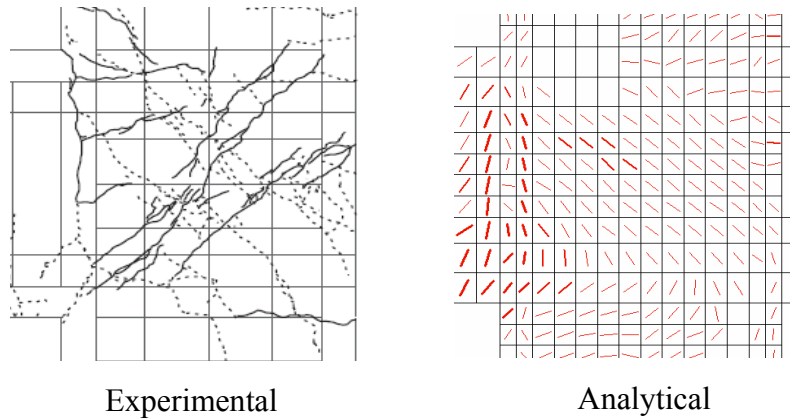


Fig. 3.19 Failure at the 3% Drift Ratio

According to the crack formation figure that is given in Fig. 3.17, the shear cracks at the joint and the flexural cracks at the beam-column interface were observed similar to experimental results at the 1.0% drift cycle. Later at the 2.0% drift cycle, analytical results showed the propagation of these flexural cracks in the beam, as shown in Fig. 3.18. The flexural cracks between the anchorage plates were also observed at the 3.0% drift ratio which increased in the last cycle. The joint and the alignment of the column were gradually disturbed with the formation of these cracks. However, the specimen maintained its strength at the final loading cycle in both loading directions contrary to the experimental hysteretic response.

The ratio of the predicted and observed ductility ratios for this specimen was 0.97 in the positive loading direction, and 0.95 in the negative loading direction. The predicted energy dissipation capacity for this specimen was also compared to the observed value, and a ratio of 0.97 was obtained.

A comparison of the results for this specimen suggests a reasonably good correlation between the predicted and observed behaviour. Similar failure mechanisms were captured with the VecTor2 analysis of this specimen. The crack formations and crack widths were also predicted quite similar to the experimental results. As can be seen in Table 3.12 and 3.13, the comparisons of the sequence of events at the positive and negative loading directions were also a good match to the actual behaviour of the specimen.

3.1.3 SPECIMEN ED3

Non-seismically designed beam-column subassemblies were also modelled using VecTor2 in this thesis. These specimens were tested by Chen (2006) at the University of Canterbury, New Zealand to obtain seismic assessment information for pre-1970s reinforced concrete moment resisting frame buildings. The two specimens in this group were $2/3$ -scale exterior beam-column subassemblies which were tested under simulated gravity and seismic loading conditions. There are two subsets of specimens in this group; i) beam-column subassemblies reinforced with deformed reinforcement and ii) ones with smooth reinforcement. In this section, the deformed reinforcement specimens are discussed. The smooth reinforcement specimens are examined in Chapter 4.

The specimens in this group were designed with structural deficiencies such as unconfined beam-column joints and low quality concrete. Also, they did not adhere to the weak beam-strong column design philosophy for ductile failure mechanism, reflecting typical pre-1970s non-seismically designed structural members. Two of the exterior beam-column subassemblies were identical in geometry, loading conditions, and material properties. However, the reinforcement detailing was slightly different from one group to the other.

3.1.3.1. TEST SPECIMENS

Sectional and Material Properties:

The specimens were designed using beams that were deep relative to the columns. The beams were 200 by 330 mm, and the columns were 230 by 230 mm. The material properties of the concrete were similar for each specimen, and can be seen in Table 3.13.

All specimens were designed with the same column capacity and beam-column joint detailing. The longitudinal reinforcement used for these specimens was D10 deformed reinforcing bars. Smooth reinforcing bars were used for the transverse

reinforcement with a 100 mm spacing in the columns and a 133 mm spacing in the beams. The joint was reinforced with only one transverse R6 reinforcing bar, to address the unconfined joint deficiency in non-seismically designed beam-column subassemblies. The material properties of the reinforcement are given in Table 3.14.

Table 3.13 Material Properties of Concrete for Specimen ED3 (Chen, 2006)

Specimen	f_c (MPa)	E_c (MPa)
TDD1	23.3	28700
TDD2	24.7	28700

Table 3.14 Material Properties of Reinforcement for Specimen ED3 (Chen, 2006)

Type	Grade	Diameter (mm)	Area (mm ²)	f_y (MPa)	E_s (MPa)	f_u (MPa)
D10	300	10	127	357	176300	493
R6	300	6	32	326	151300	488

Detailed information on the reinforcement layout is given in Fig. 3.20 and Table 3.15. The longitudinal reinforcement of the beam was different for the deformed and smooth reinforcement specimens. The longitudinal reinforcement in the beam was partially anchored into the joint, but the anchorage that was provided was insufficient to supply enough confinement in the joint.

Table 3.15 Reinforcement Detailing for Specimen ED3 (Chen, 2006)

Specimen	Beam		Column		Joint
	Longitudinal	Transverse	Longitudinal	Transverse	
TDD1	4 D10 2 D10	R6 @	3 D10 3 D10	R6 @	1-R6
TDD2	6 D10 4 D10	133 mm	3 D10 3 D10	100 mm	

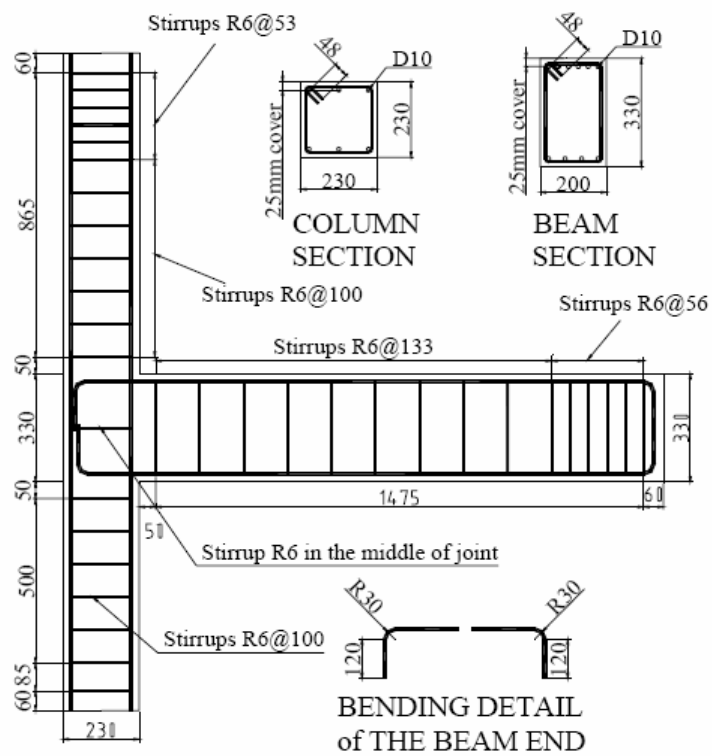


Fig. 3.20 Reinforcement Detailing for Specimen ED3 (Chen, 2006)

Test Set-Up and Loading:

The test set-up was designed to simulate the behaviour of an exterior beam-column subassembly under seismic loading conditions (see Fig. 3.21). A displacement-controlled loading system was used to apply the horizontal force to the top of the column

until the lateral drift of the column reached a particular level. As reported by Chen (2006), three different loads were applied to the top of the column in these specimens: horizontal reversed cyclic loading, constant axial loading, and varying axial loading based on the story shear force. The axial loading consisted of the constant 75 kN axial load and the varying axial load equal to 1.8 times the shear force. The direction of this second axial load changed based on the loading direction during testing. The test set-up was designed to allow for a free rotation of the column and a horizontal rotation of the beam end with pin roller restraints. A graphical representation of the linear relation between shear force and axial load is given in Fig. 3.22.

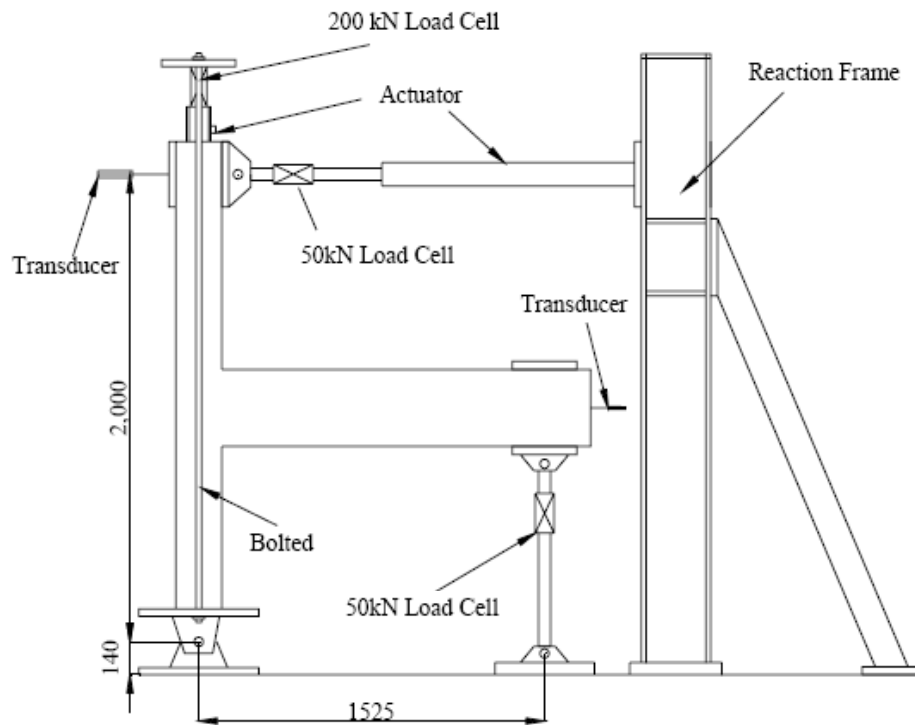


Fig. 3.21 Test Set-up for Specimen ED3 (Pampanin et al, 2006)

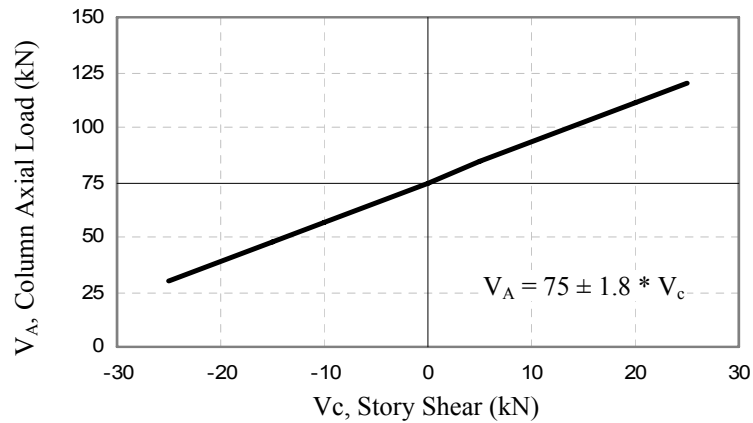


Fig. 3.22 Axial Load vs. Story Shear for Specimen ED3

The loading protocol followed for these specimens is given in Fig. 3.23. They were subjected to two consecutive cycles of drift ratios ranging from 0.1% to 4%. After the 0.5% drift level (first shear cracking in the joint region), a small cycle of 0.25% drift following each main drift level was applied to the specimens (Chen, 2006).

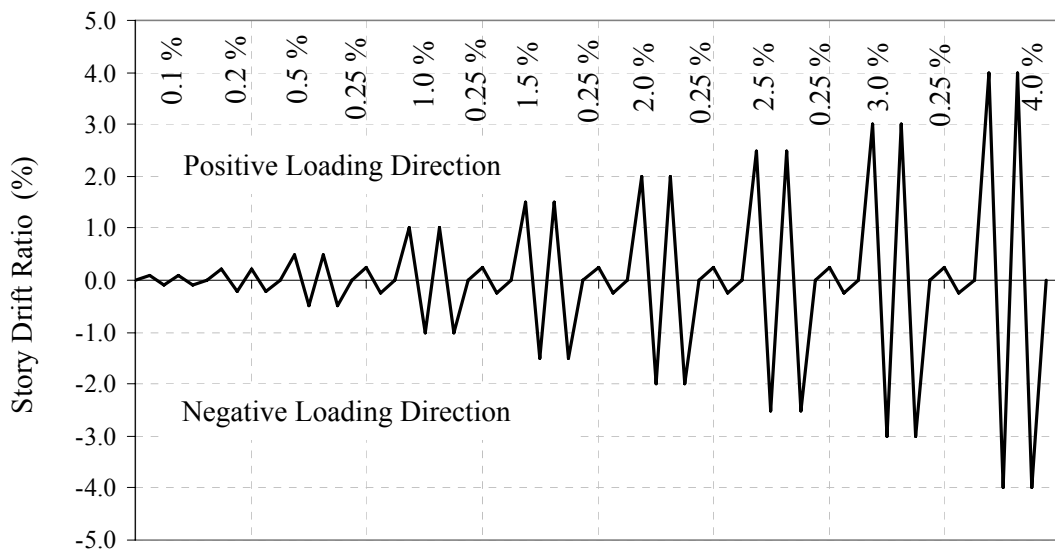


Fig. 3.23 Loading Protocol for Specimen ED3

3.2.2.2. FINITE ELEMENT MODELLING

Material and Regional Properties:

Seven concrete regions were defined in modelling these specimens. A total of 1796 rectangular concrete elements, with a 25 by 25 mm mesh configuration, were used to represent these beam-column subassemblies. Due to different transverse reinforcement configurations, additional regions were assigned to the specimen. Detailed information about the concrete regions is given in Fig. 3.24 and Table 3.16.

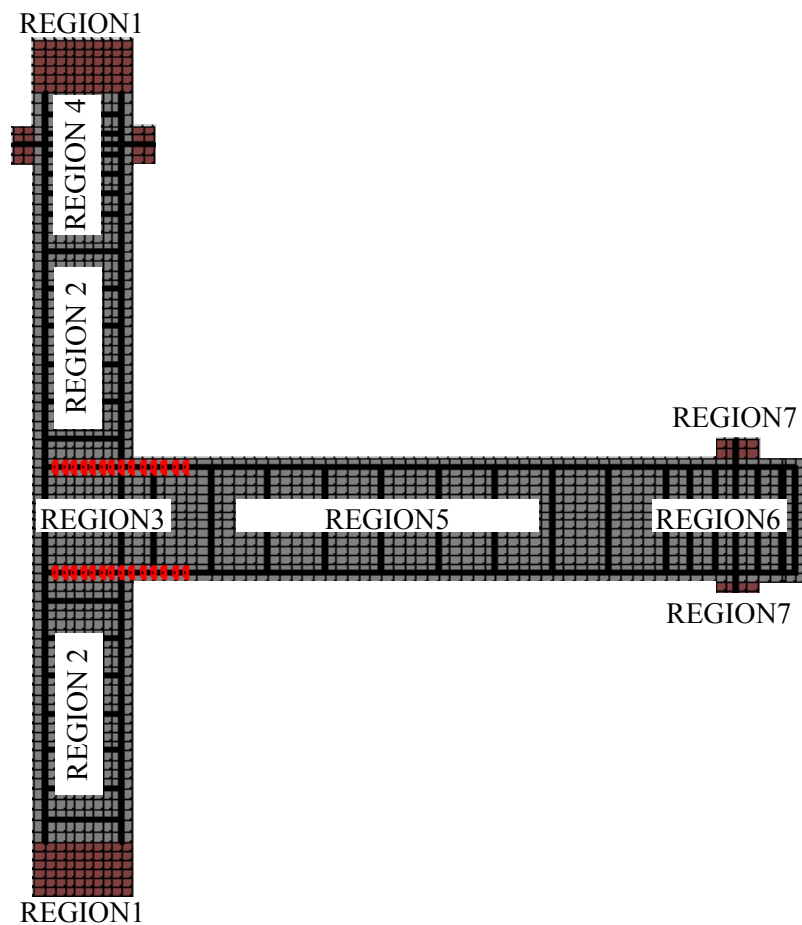


Fig. 3.24 Material Regions for Specimen ED3

Table 3.16 Concrete Regions for Specimen ED3

Concrete Regions	#1 (#7)	# 2	# 3	# 4	# 5	# 6
Thickness (mm)	230 (200)	230			200	
Mesh Size (mm)	25 x 25					
Purpose	Bearing	Column	Joint	Column	Beam1	Beam2
ρ_z (%)	None	0.267	0.074	0.464	0.129	0.305

In addition, 678 truss elements and 28 bond-link elements were used to represent the reinforcement and bond representations within the model. The reinforcement elements were modelled similar to the previous exterior specimens. A representation of the reinforcement and bond element configuration is given in Fig.3.25 and Table 3.17.

Table 3.17 Reinforcement Elements for Specimen ED3

Reinforcement	Type	Location
# 1	3 D10	Column Longitudinal Reinforcement
# 2	4 D10 (6 D10)	Beam Top Layer Longitudinal Reinforcement
# 3	2 D10 (4 D10)	Beam Bottom Layer Longitudinal Reinforcement
# 4	1 R6	Transverse Reinforcement
# 5	D 20	Strengthening Rebar for Test Set-Up

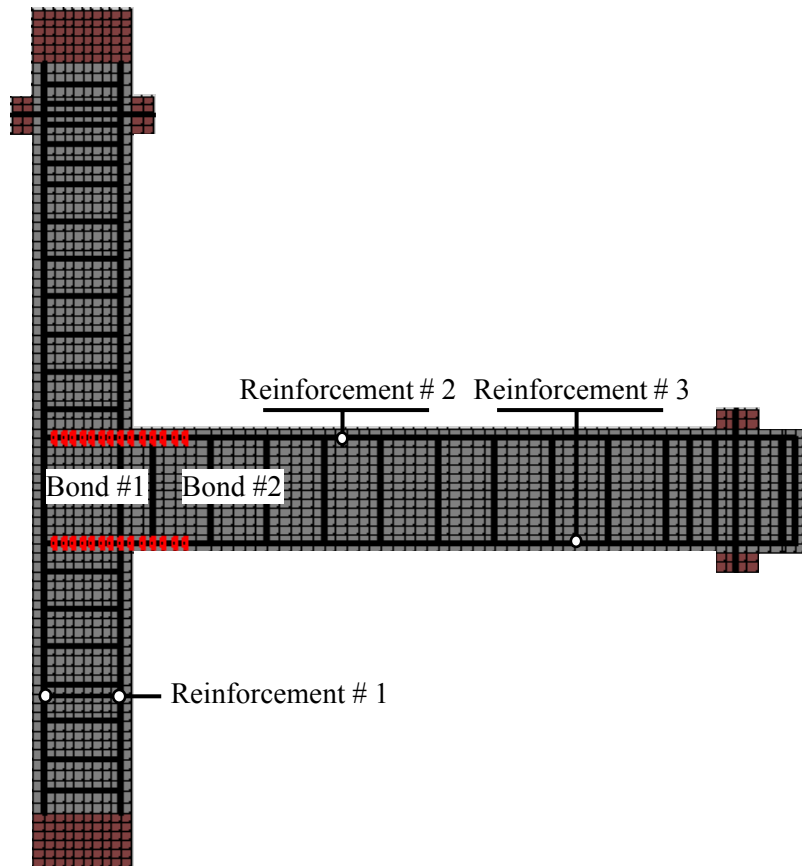


Fig. 3.25 Reinforcement Regions for Specimen ED3

The bond at the interface between the reinforcement and concrete was modelled in a similar way to Specimen ED1 in this chapter. Perfect bond was specified for the hooked end, and an unconfined concrete region was used for the rest of the beam longitudinal reinforcement based on the CEB-FIB MC90 (1993) definitions. The configuration of the bond-link elements, and the confinement pressure index values selected for each bond-link element, are given in Fig. 3.25 and in Table 3.18.

Table 3.18 Bond Elements for Specimen ED3

Type	Bond # 1	Bond # 2
Reinforcement	Hook End	Straight Section
Bond Model	Perfect	Imperfect
Confinement Pressure (MPa)	N/A	0.50

Loading and Restraint Conditions:

The loading protocol used during testing (see Fig. 3.23) was followed exactly in the analyses including the small cycle intervals. Load Case 1 was the horizontally applied displacement-based reversed cyclic loading, Load Case 2 had a constant axial load applied to the top of the column, and Load Case 3 included the changing component of the vertical column load which was a function of the storey shear force experienced by the member. The simulated loading and the restraint conditions are shown below in Fig. 3.26.

The loading for this type of testing was a challenge to model with VecTor2. It could only be modelled approximately. Firstly, a reversed cyclic analysis was performed only with the first and second load case, and then the lateral load values were obtained at each cycle and were introduced in the third load case. As the number of load stages was defined by the first load case, the changing axial load applied as the third load case was implemented based on the loading procedure of the first load case. The restraints included a pinned support on the lower end of the column, and two pinned roller supports on the beam 1525 mm away from the centerline of the column.

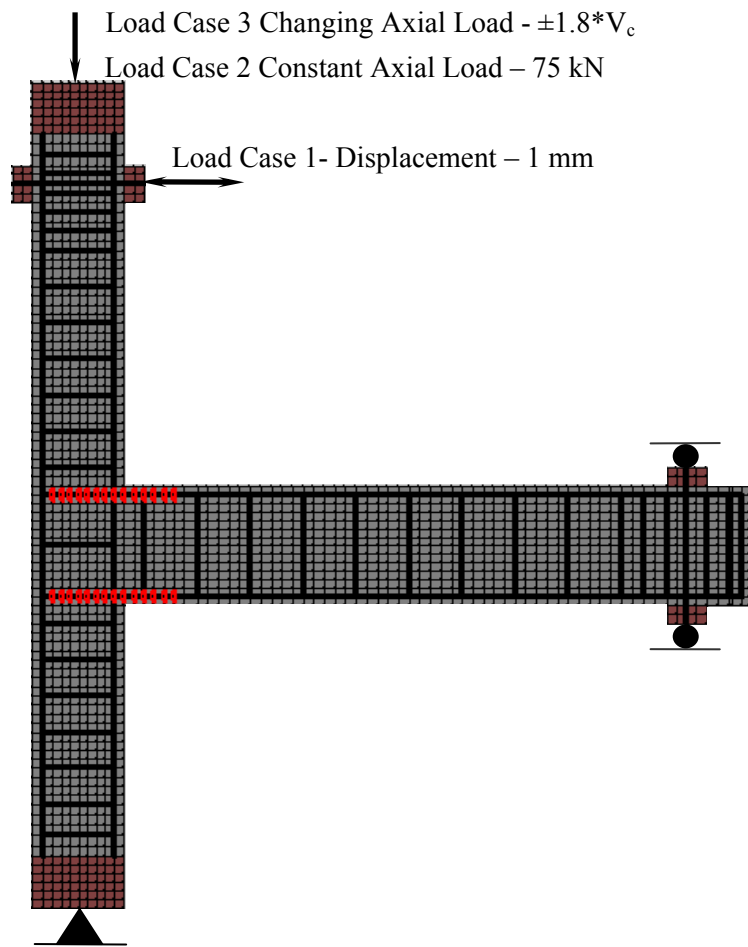


Fig. 3.26 Loading and Restraint Conditions for Specimen ED3

3.1.2.3. RESULTS OF EXPERIMENTAL AND ANALYTICAL STUDY

Specimen TDD1

This specimen was reported to experience large flexural cracking at the beam-column interface and concrete spalling from the back of the column at the joint. The story shear force versus lateral displacement behaviour is given above in Fig. 3.27 in comparison to VecTor2 analytical results. The observed and predicted response showed very good correlation in terms of capturing the different peak story shear force and ultimate displacement values. As the beam longitudinal reinforcement arrangements in

the top and bottom layer were at a ratio of 2:1, the shear force response of the specimen followed a similar ratio, 16 kN and 8 kN, respectively.

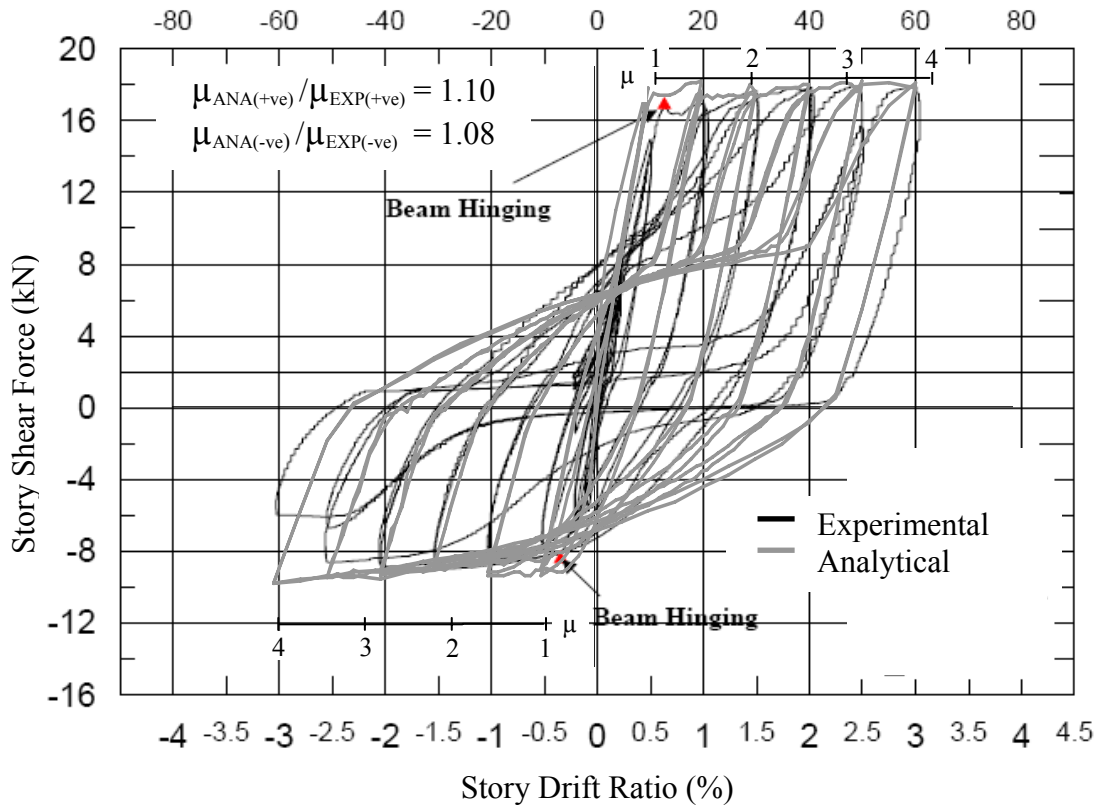


Fig. 3.27 Comparison of Story Shear vs. Story Drift Ratio for Specimen TDD1

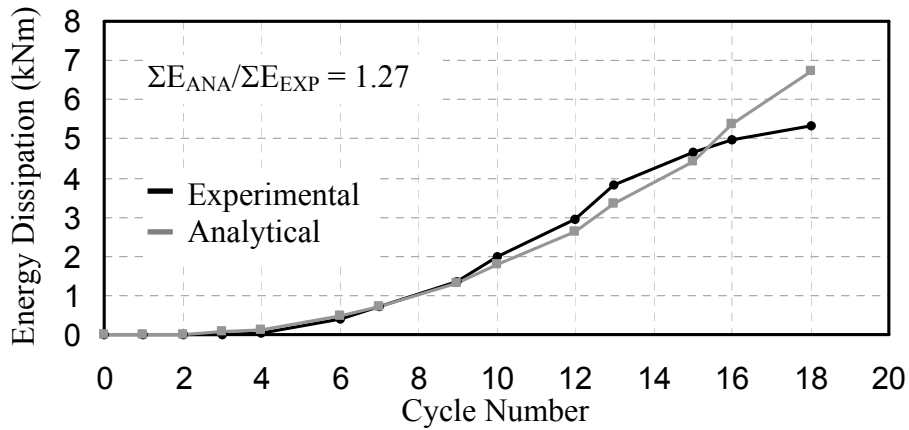


Fig. 3.28 Comparison of Energy Dissipation of Specimen TDD1

The ratio of the predicted to the observed ductility ratio for this specimen was 1.10 in the positive loading direction, and 1.08 in the negative loading direction. The

predicted energy dissipation capacity for this specimen was also compared to the observed value, and a ratio of 1.27 was obtained.

The flexural cracking failure mechanism at the beam-column interface was successfully captured in the analytical study (see Fig. 3.29). However, the crack formation and failure mechanism figure obtained from Augustus represented a flexural-shear cracking zone at the beam-column face. This was the combination of separate but close flexural cracks similar to the behaviour observed during the tests in Fig. 3.29. The flexural cracking was observed extensively on the bottom surface of the beam similar to the test results, but the crack formation shown in Fig. 3.29 was probably taken when zero loading was applied to the specimen. The cracks on the top surface of the beam can be seen in a picture from the back side of the specimen in Fig. 3.30. The shear cracks in the joint that occurred at the column left lower side and right upper side during testing were also observed in the predicted response. Although a wide area of shear crack formation that might possibly form a concrete wedge was observed, the flexural cracking at the beam-column face limited this formation and defined the failure mechanism of this specimen. The sequence of events observed during the test and computed during the analysis showed good correlation, as seen in Table 3.19.

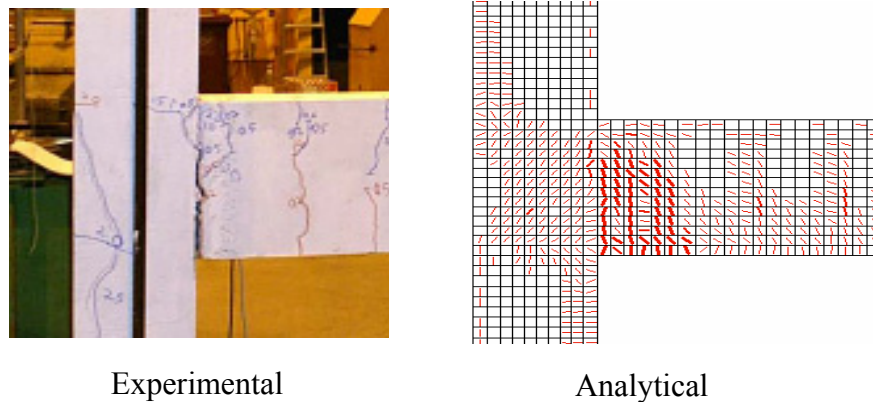


Fig. 3.27 Comparison of Final Failure for Specimen 1BB1



Fig. 3.30 Final Failure at the back side of Specimen TDD1 (from Chen, 2006)

Table 3.19 Sequence of Events for Specimen TDD1

Event	Experimental		Analytical	
	Story Shear (kN)	Story Drift (%)	Story Shear (kN)	Story Drift (%)
Positive Loading Direction				
Beam Hinging	16.00	0.50	17.30	0.50
Max Story Shear	18.00	3.00	18.00	3.00
Negative Loading Direction				
Beam Hinging	8.00	0.50	9.20	0.50
Max Story Shear	10.00	2.00	9.80	3.00

Overall, the predicted response for this specimen was a good match to the observed response. The only difference between observed and predicted response was the story shear force at the final loading stage, which was approximately 60%. The strength degradation at this final stage couldn't be captured due to the lack of concrete wedge effect at the column. As the shear cracking wasn't captured in the analytical

response, the shear force versus displacement curve did not experience any pinching effect at this final stage.

Specimen TDD2

A brittle joint failure mechanism was observed at the end of the testing. According to the experimental results, the first shear crack within the joint was observed at the 0.65% drift ratio in both loading directions. Later, a concrete wedge mechanism was formed with the propagation of individual shear cracks at the 3.0% drift ratio. The story shear force versus story drift ratio for his specimen is given in Fig. 3.31.

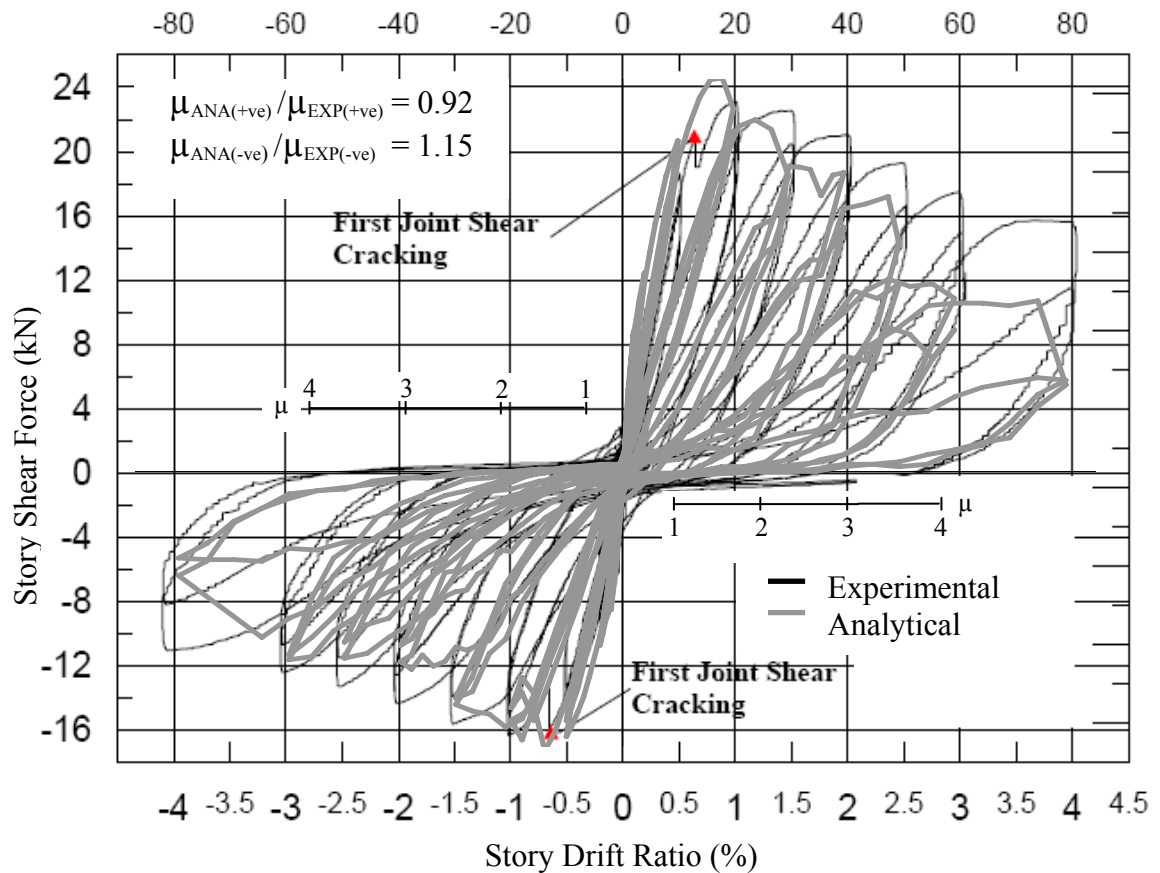


Fig. 3.31 Comparison of Story Shear vs. Story Drift Ratio for Specimen TDD2

The brittle joint failure was also observed in the VecTor2 analytical results, and a comparison of the experimental and analytical results for the crack formation and failure mode of this specimen is shown in Fig. 3.33. The VecTor2 analysis was also successful in capturing the sequence of events, which is also given in comparison to the experimental results in Table 3.20.

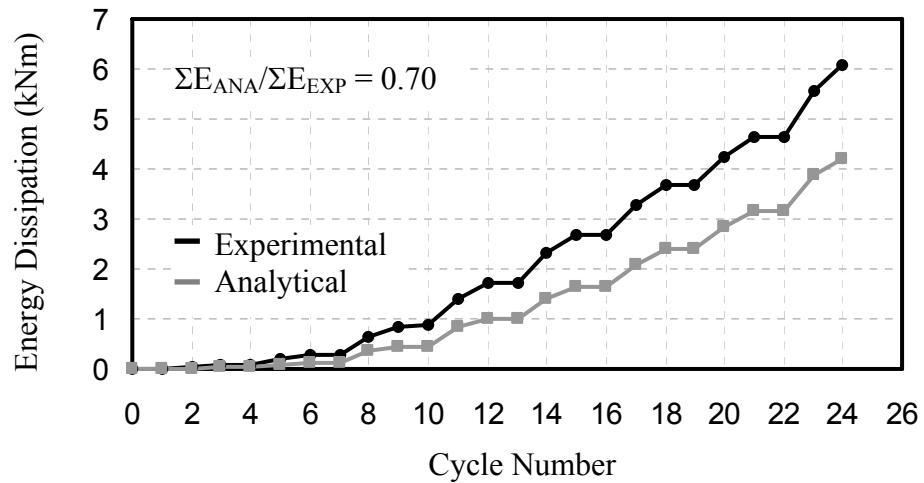


Fig. 3.32 Comparison of Energy Dissipation of Specimen TDD2

The ratio of the predicted and observed ductility ratios for this specimen was 0.92 in the positive loading direction, and 1.15 in the negative loading direction. The predicted energy dissipation capacity for this specimen was also compared to the observed value, and a ratio of 0.70 was obtained.

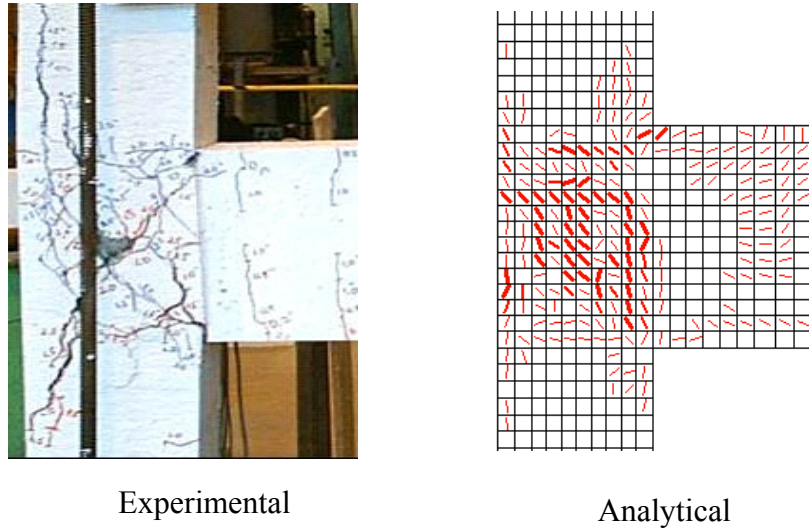


Fig. 3.33 Comparison of Final Failure for Specimen TDD2

Table 3.20 Sequence of Events for Specimen TDD2

Event	Experimental		Analytical	
	Story Shear (kN)	Story Drift (%)	Story Shear (kN)	Story Drift (%)
Positive Loading Direction				
First Joint Shear Cracking	21.00	0.65	23.30	0.75
Concrete Wedge Mechanism	12.00	3.00	10.80	2.75
Max Story Shear	23.00	1.00	24.50	0.80
Negative Loading Direction				
First Joint Shear Cracking	16.00	0.65	17.00	0.75
Concrete Wedge Mechanism	12.00	3.00	11.00	2.85
Max Story Shear	16.00	1.00	17.00	0.60

Different crack formations and failure mechanisms successfully matched the experimental results for both specimens. The excessive flexural cracking at the beam-column interface observed at the Specimen TDD1, and the concrete wedge at the joint due to extensive shear cracking at the Specimen TDD2, were also successfully captured within the analytical results. The sequence of events were also compared in Table 3.19 and Table 3.20. Based on these comparisons, the first crack formation, and the propagation of the cracks at each loading directions were close to the actual behaviour of the specimen. The maximum story shear force was also estimated at similar drift ratios by the VecTor2 analysis.

3.1.4. DISCUSSION ON EXTERIOR BEAM-COLUMN SUBASSEMBLIES

The VecTor2 analysis of the exterior beam-column subassemblies described in the previous sections provided accurate simulations of the load-deformation responses. The predicted peak shear force values for all exterior specimens designed with deformed reinforcement are compared to the observed shear force values, in the positive and negative loading directions, are given in Table 3.21 and Table 3.22.

A total of four exterior specimens were modelled, and the peak shear force results suggest a mean of 1.04 and a coefficient of variation of 2.26 % for the positive loading direction. The ultimate displacement results suggest a mean of 1.03 and a coefficient of variation of 4.00 % in the same loading direction. As for the same comparison at the negative loading direction, the ratio of the predicted to the observed shear force capacity had a mean of 1.02, and a coefficient of variation of 4.28%. The ultimate displacement results suggest a mean of 0.99 and a coefficient of variation of 1.21 %.

There is a better correlation in the positive loading direction. The possible reason for that is the difference in the actual bond-slip behaviour and the model that is currently used in VecTor2 under cyclic loading conditions. The changing bond-slip effects after the loading direction was changed couldn't be captured instantaneous as it was in the actual behaviour. This might be the reason for slight overestimations in the strength in

the negative loading direction. This difference was further explained in Chapter 2. Overall the predicted response of the exterior specimens designed with deformed reinforcement was successful in estimating the crack formations, load-deformation characteristics and energy dissipation capacity.

Table 3.21 Comparison of Peak Shear Force at the Positive Loading Direction

Specimen	V_{\max} (EXP) (kN)	V_{\max} (VT2) (kN)	V_{\max} (VT2)/ V_{\max} (EXP)
ED1	94.0	98.0	1.04
ED2	92.2	95.6	1.04
ED31 (TDD1)	18.0	18.0	1.00
ED32 (TDD2)	23.0	24.5	1.07
Mean			1.04
St. Dev			0.02
COV (%)			2.26

Table 3.22 Comparison of Peak Shear Force at the Negative Loading Direction

Specimen	V_{\max} (EXP) (kN)	V_{\max} (VT2) (kN)	V_{\max} (VT2)/ V_{\max} (EXP)
ED1	64.9	69.3	1.07
ED2	91.1	88.9	0.98
ED31 (TDD1)	10.0	9.8	0.98
ED32 (TDD2)	16.0	17.0	1.06
Mean			1.02
St. Dev			0.04
COV (%)			4.28

Table 3.23 Comparison of Ultimate Displacement at the Positive Loading Direction

Specimen	Δ_{\max} (EXP) (mm)	Δ_{\max} (VT2) (mm)	Δ_{\max} (VT2)/ Δ_{\max} (EXP)
ED1	58.0	62.0	1.07
ED2	74.0	79.0	1.08
ED31 (TDD1)	60.0	59.6	0.99
ED32 (TDD2)	80.0	79.3	0.99
		Mean	1.03
		St. Dev	0.04
		COV (%)	4.00

Table 3.24 Comparison of Ultimate Displacement at the Negative Loading Direction

Specimen	Δ_{\max} (EXP) (mm)	Δ_{\max} (VT2) (mm)	Δ_{\max} (VT2)/ Δ_{\max} (EXP)
ED1	62.0	62.0	1.00
ED2	59.0	58.0	0.99
ED31 (TDD1)	60.0	59.6	0.99
ED32 (TDD2)	82.0	79.4	0.97
		Mean	0.99
		St. Dev	0.01
		COV (%)	1.21

3.2. INTERIOR BEAM-COLUMN SUBASSEMBLIES

3.2.1. SPECIMEN ID1

The four interior beam-column subassemblies described in this section were also from a Benchmark Study by Shiohara and Kusuhara (2006). These specimens were seismically designed according to the AIJ 1999 code revisions. One-half scale interior and exterior beam-column subassemblies were tested under displacement-controlled reversed cyclic loading conditions. The modelling of the exterior beam-column subassembly from this group has already been discussed in this thesis in Section 3.2. The specimens were divided into two main subsets, A and B, according to the reinforcement detailing, and three subsets, A1, A2, A3 and B1, according to the applied loading type.

3.2.1.1. TEST SPECIMENS

Sectional and Material Properties:

The sectional and material properties for these specimens were similar to those of the exterior beam-column subassembly examined in Section 3.1.2. (i.e., Specimen ED2). All beams and columns were 300 by 300 mm. The average compressive strength, Young's modulus, and tensile splitting strength were 28.3 MPa, 25900 MPa and 2.67 MPa, respectively.

The reinforcement detailing for all the specimens are given in Fig. 3.34 and in Fig. 3.35. Specimens A1, A2 and A3 were designed with sixteen D13 reinforcing bars for the longitudinal reinforcement of the beams. Eight of these bars had their section reduced by 25% for data acquisition purposes. The reinforcing bars represented in lighter colour in Fig. 3.34 and Fig. 3.35 were these grooved bars. All columns were reinforced with sixteen D13 reinforcing bars. There was no reduction on the sections of column longitudinal bars. Specimen B1 was designed with twenty D13 longitudinal reinforcing bars. Eight of the beam longitudinal bars had their section reduced by 25%,

and six of the longitudinal bars had their section reduced by 29%. As for the transverse reinforcing bars, D6 reinforcing bars were used with a 50 mm spacing in the beams, columns and joints. The material properties of reinforcing steel are given in Table 3.25.

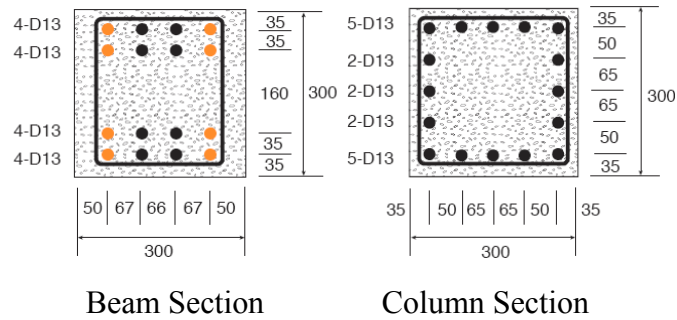


Fig. 3.34 Sectional Details for Specimens A1, A2, A3 (Shiohara and Kusuhara, 2006)

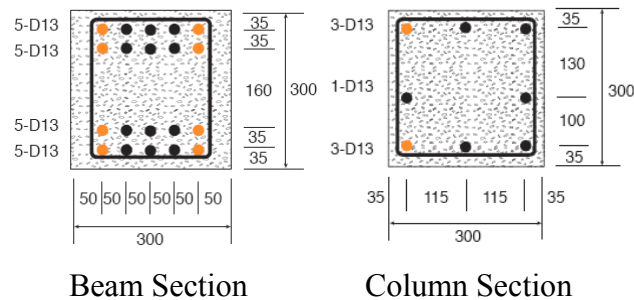


Fig. 3.35 Sectional Details for Specimen B1 (Shiohara and Kusuhara, 2006)

Table 3.25 Material Properties of Reinforcement (Shiohara and Kusuhara, 2006)

Type	Grade	Diameter (mm)	Area (mm ²)	f _y (MPa)	E _s (MPa)	f _u (MPa)
D13	SD390	14	127	456	176000	582
D13	SD345	14	127	357	176300	493
D6	SD295	6	32	326	151300	488
Grooved Longitudinal Reinforcing Bars						
D13	SD390	12.1	96	440	167000	566
D13	SD345	11.4	90	460	163000	460

Test Set-Up and Loading:

The beam-column subassemblies were tested under displacement-controlled reversed cyclic loading conditions. The displacement-based load was applied horizontally at different amplitudes, and the axial load was constant, 216 kN, at all times. Three different loading types were reported by Shiohara and Kusuhara (2006). The horizontal load and axial load were applied to the top of the upper column for the Loading Type I case. The beam ends were restrained with pinned roller supports, and the column with a pinned support. The test set-up for Loading Type I is shown in Fig. 3.36.

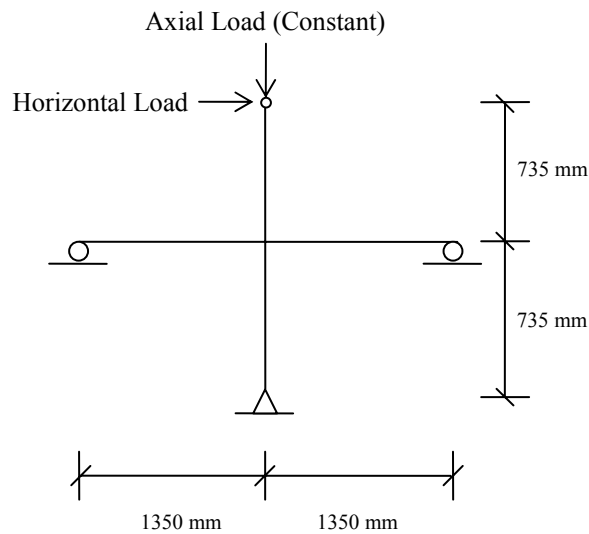


Fig. 3.36 Loading Type I

In the Loading Type II case, the loading system remained the same, but the restraint conditions were changed slightly. The pinned roller support at the right beam end was removed, and the rest of the restraint conditions were kept the same as illustrated in Fig. 3.37.

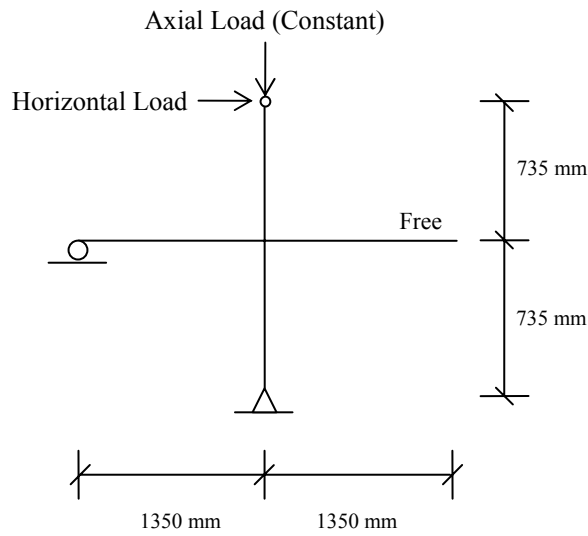


Fig. 3.37 Loading Type II

For the Loading Type III case, both the restraint conditions, and the loading system were changed. The lateral load was applied to the end of the left beam, and the pinned roller support at the end of this beam was kept. The end of the left beam however was completely free to move in each direction. The pinned support at the end of the lower column was also kept the same in this loading system (see Fig. 3.38).

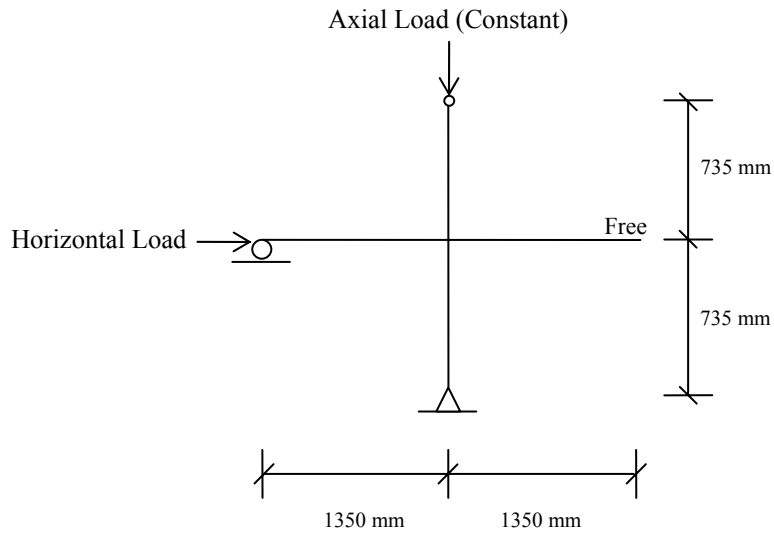


Fig. 3.38 Loading Type III

As stated in the report by Shiohara and Kusuhara (2006), the loading protocol employed during testing for all of these specimens is given in Fig. 3.39.

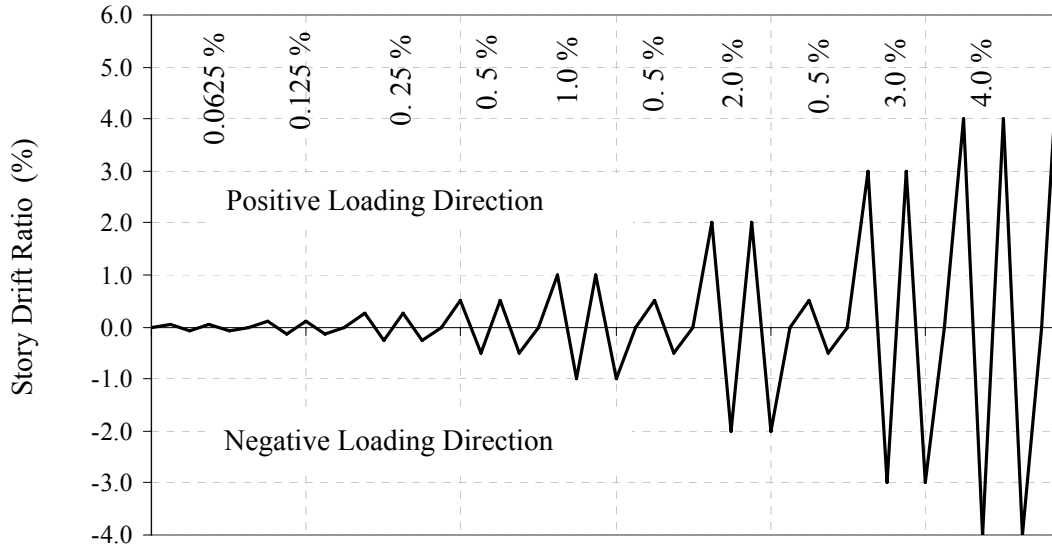


Fig. 3.39 Loading Protocol for Specimen ID1 (Shiohara and Kusuhara, 2006)

3.2.1.2. FINITE ELEMENT MODELLING

Material and Regional Properties:

The specimens were all modelled with three concrete regions, and with a total of 1782 concrete elements using a 25 by 25 mm mesh configuration. As shown in Fig. 3.40 and Table 3.26, the first region was the fictitious concrete region. The second and third regions were assigned to the beams and columns of these specimens. The smeared reinforcement ratio, ρ_z , was estimated using the transverse reinforcement ratio in the out-of-plane direction in all sections of the specimens.

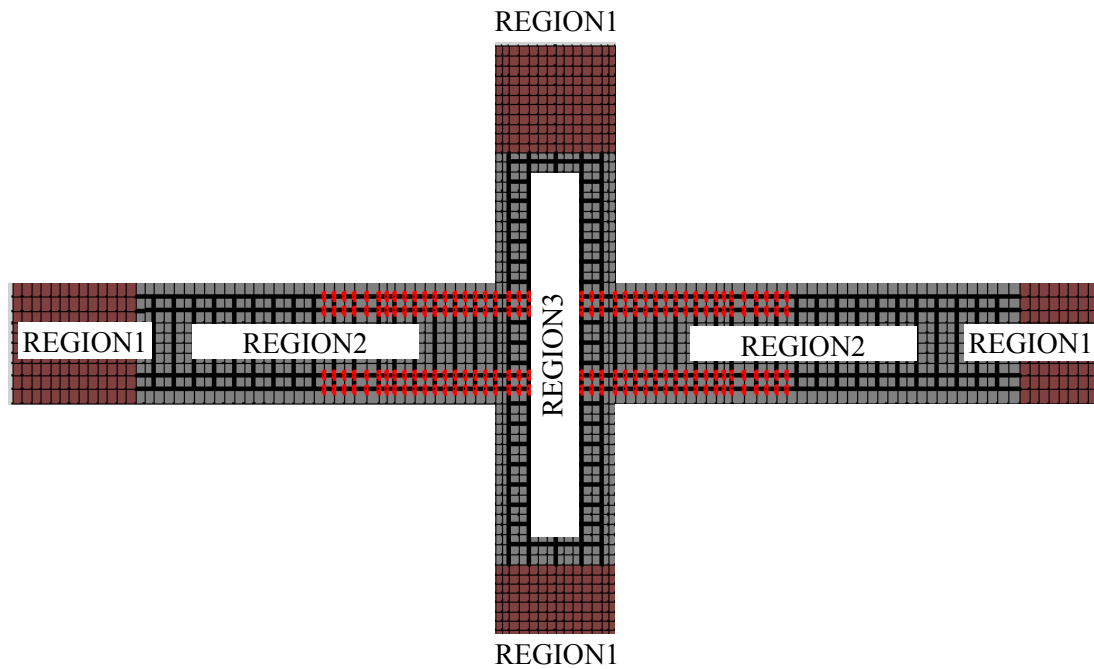


Fig. 3.40 Material Regions for Specimen ID1

Table 3.26 Concrete Regions for Specimen ID1

Concrete Regions	# 1	# 2	# 3
Thickness (mm)	300		
Mesh Size (mm)	25 x 25		
Purpose	Bearing	Beam and Joint	Column
ρ_z (%)	None	0.43	

A total of 1039 truss elements and 188 bond-link elements for Specimens A1, A2 and A3, and 891 truss elements and 196 bond-link elements for Specimen B1 were used for the reinforcement and bond representations in the models. The reinforcement was modelled using discrete truss bar elements. The reinforcement and bond element configuration is shown in Fig. 3.41, and detailed information about these properties is given in Table 3.27. The layout for the reinforcement and bond regions are only shown here for the Series A Specimens. As for Specimen B1, the beam reinforcement

configuration was similar to the exterior beam-column subassembly (i.e. Specimen ED2) that was presented earlier in this chapter.

Table 3.27 Reinforcement Elements for Specimen ID1

Reinforcement	Type	Location
Specimen A1, A2, A3		
# 1	4 D13 (Full Section)	Beam Longitudinal
# 2	4 D13 (25% Reduced Section)	
# 3	5 D13 (Full Section)	Column Longitudinal
# 4	2 D13 (Full Section)	
# 5	1 D6 (Full Section)	Transverse Reinforcement
Specimen B1		
# 1	5 D13 (Full Section)	Beam Longitudinal
# 2	5 D13 (25% Reduced Section)	
# 3	3 D13 (29% Reduced Section)	Column Longitudinal
# 4	3 D13 (Full Section)	
# 5	2 D13 (Full Section)	
# 6	1 D6 (Full Section)	Transverse Reinforcement

As the transverse reinforcement along the beam provided moderate confinement for member, bond elements were introduced into the model in confined and unconfined bond regions. The confined region was located in the beam-column joint, and was defined by Bond #2 in the model. The bond elements defined by Bond #1 were assigned to the longitudinal bars away from the joint. The configuration of the bond-link elements and confinement pressure index values selected for each bond-link element are given in Fig. 3.41 and Table 3.28.

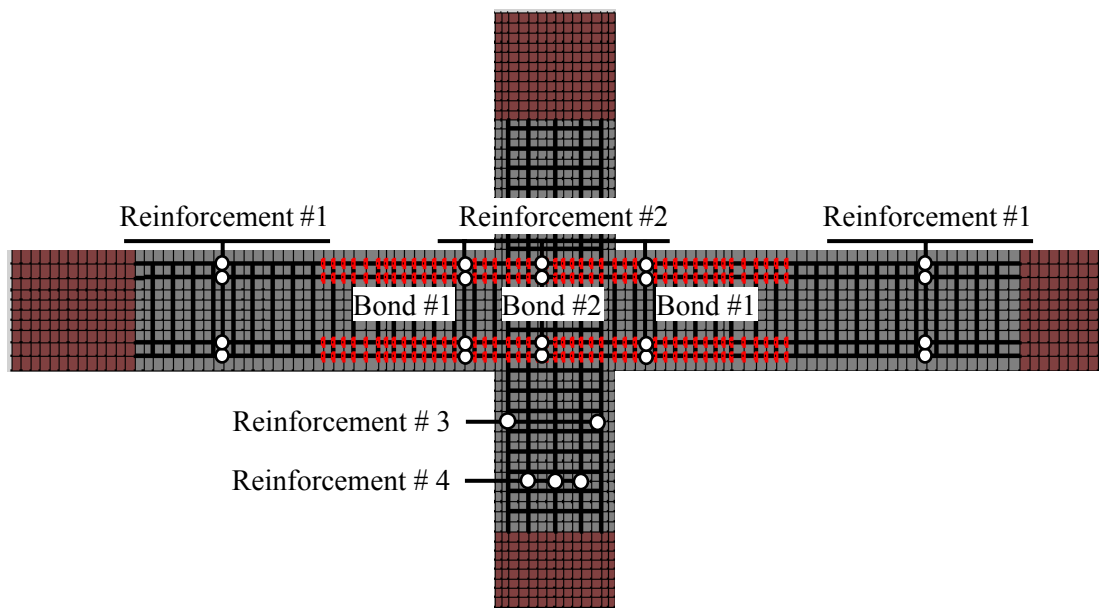


Fig. 3.41 Reinforcement Regions for Specimen ID1

Table 3.28 Bond Elements for Specimen ID1

Type	Bond # 1	Bond # 2
Reinforcement	Beam Top and Bottom Layer Longitudinal	
Confinement Pressure (MPa)	1.4	7.5

Loading and Restraint Conditions:

The loading protocol applied to the specimens during testing was followed in the analysis including the small cycle intervals. Load Case 1 was the horizontally applied displacement-based reversed cyclic loading, while Load Case 2 was the constant axial load applied to the top of upper column. A pinned support was applied to the end of lower column in all of the loading systems. The restraint conditions were changed according to the loading system applied to the specimen during testing. The south end pinned roller was removed in Specimens A2 and A3, and the horizontal displacement loading was applied to the beam instead of the column for Specimen A3. The test set-up used for Specimen A1 is shown in Fig. 3.42.

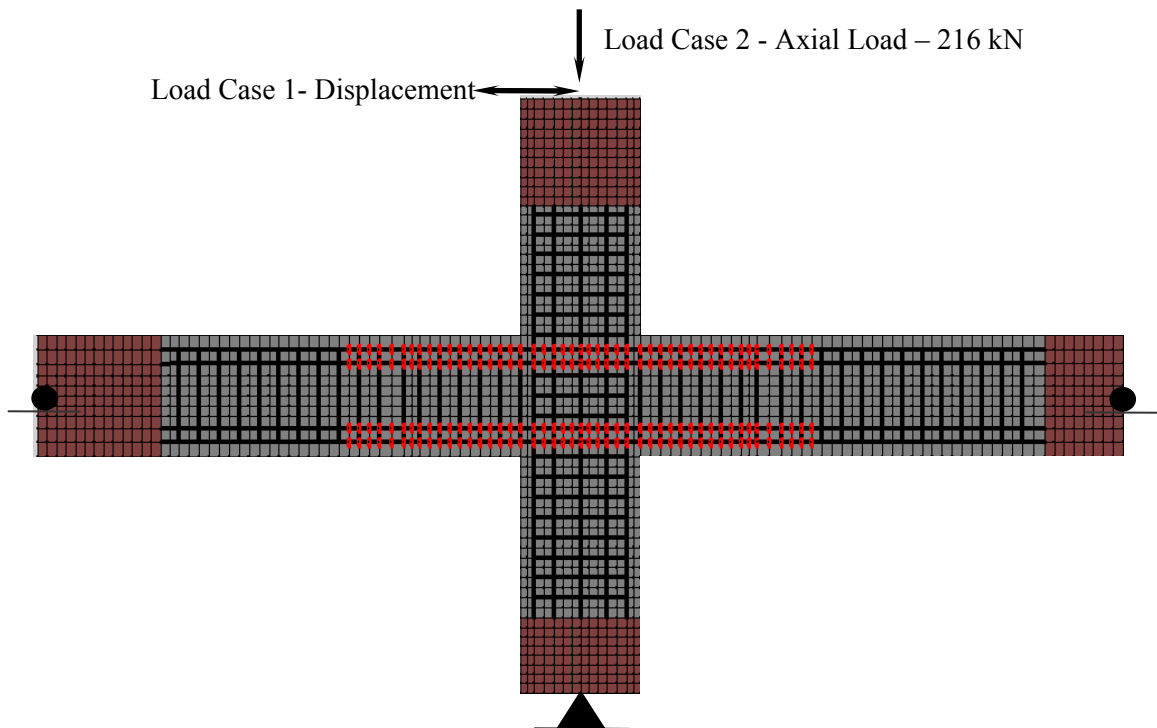


Fig. 3.42 Loading and Restraint Conditions for Specimen ID1

3.2.1.3. RESULTS OF EXPERIMENTAL AND ANALYTICAL STUDY

In this section, the analysis results are compared to the experimental results in terms of the hysteretic response, crack formation failure mechanisms, and sequence of events. The results of each specimen in this group were individually discussed in comparison to the predicted response by the VecTor2 analysis.

SPECIMEN A1

In the experiment, a pinched hysteresis response was observed in the story shear force versus story displacement behaviour. The observed behaviour was summarized from the Benchmark Test Report by Shiohara and Kusuhara (2006). This beam-column subassembly failed under high shear deformations with the concrete cover bulging and crushing at the beam end, near the joint, at the 2.0% story drift ratio. Later, concrete cover spalling occurred at the 3.0% story drift ratio and severe joint deformation was visible during the last cycle at the 4.0% story drift ratio. The beams remained elastic with no deformation throughout the loading, but extensive shear deformations were observed in the joint. No plastic hinging was observed in the beams. After the beam bars yielded, the beam-column joint face rotation and the expansion of the joint were significantly increased. (Shiohara and Kusuhara, 2006)

The predicted hysteretic response of this specimen shows a very close match to the experimental results (see Fig. 3.43). The sequence of events of the specimen are also given in comparison to the experimental results for both loading directions in Table 3.28 and Table 3.29. The predicted crack formations and the failure mechanisms at 1.0%, 2.0%, and 3.0% drift cycles were also compared to the observed behaviour, and are shown in Fig. 3.46, Fig. 3.47 and Fig. 3.48. The analysis results predicted this excessive shear cracking in the joint starting at the 1.0% drift cycle. At a drift ratio of 2.0%, these diagonal cracks were propagating in the joint. As a result, the joint region was highly disturbed, and the specimen started losing its strength at the end of this drift cycle. Later these cracks gradually increased, and the specimen lost nearly half of its strength. The difference in the energy dissipation capacity between the observed and predicted

response suggest that smaller bond-slip effects were experienced in the specimen during testing. This suggestion was also confirmed by the difference in the shape of hysteresis as it was more pinched compared to the observed behaviour.

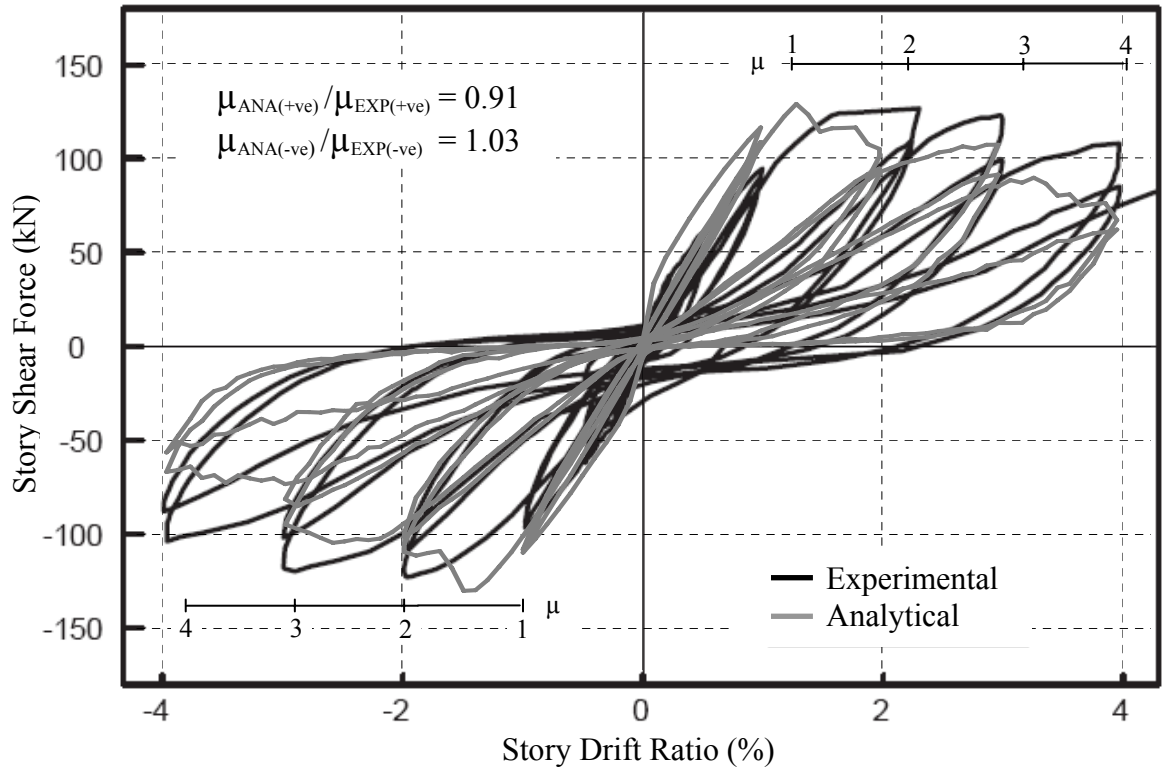


Fig. 3.43 Comparison of Story Shear vs. Story Drift Ratio of Specimen A1

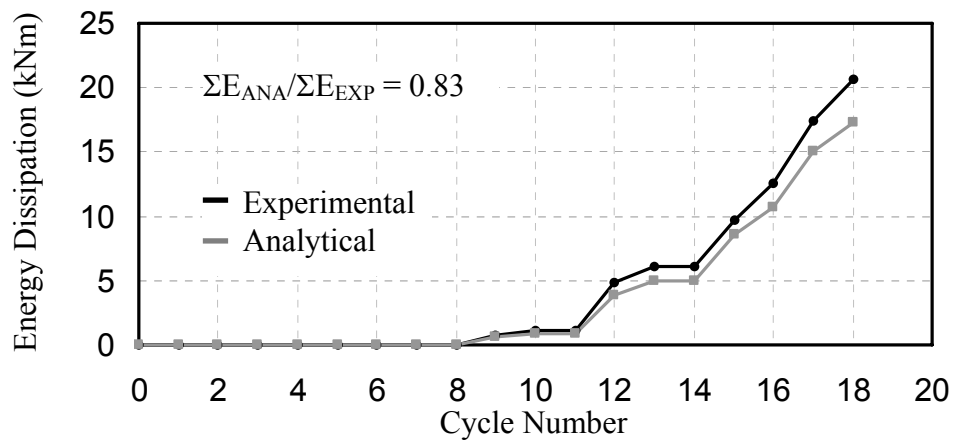


Fig. 3.44 Comparison of Energy Dissipation of Specimen A1

The ratio of the predicted and observed ductility ratios for this specimen was 0.91 in the positive loading direction, and 1.03 in the negative loading direction. The predicted energy dissipation capacity for this specimen was also compared to the observed value, and a ratio of 0.83 was obtained.

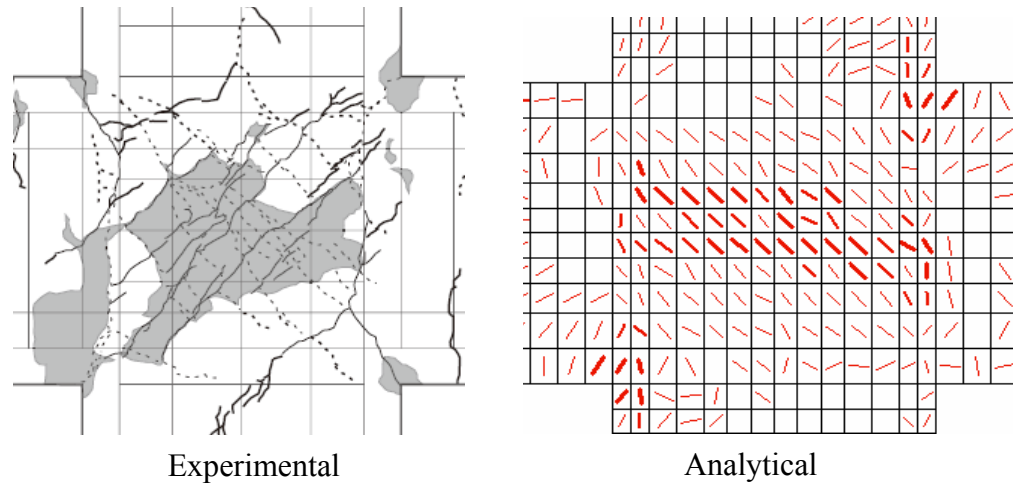


Fig. 3.45 Comparison of Final Failure of Specimen A1

Table 3.29 Sequence of Events at the Positive Loading Direction for Specimen A1

Event	Experimental		Analytical	
	Story Shear (kN)	Story Drift (%)	Story Shear (kN)	Story Drift (%)
Beam Reinforcement-1 st Layer Yielding	118.60	1.48	122.50	1.19
Beam Reinforcement-2 nd Layer Yielding	126.60	2.30	128.60	1.28
Column Reinforcement-Yielding	126.60	2.30	128.60	1.28
Max Story Shear	126.60	2.30	128.60	1.28

Table 3.30 Sequence of Events at the Negative Loading Direction for Specimen A1

Event	Experimental		Analytical	
	Story Shear (kN)	Story Drift (%)	Story Shear (kN)	Story Drift (%)
Beam Reinforcement-1 st Layer Yielding	113.90	1.58	117.30	1.18
Beam Reinforcement-2 nd Layer Yielding	121.10	1.86	124.00	1.28
Column Reinforcement-Yielding	119.70	1.79	129.30	1.39
Max Story Shear	122.80	1.96	130.00	1.48

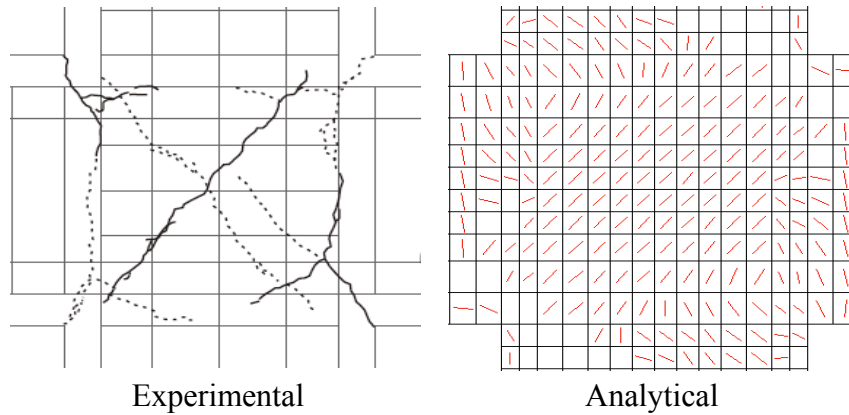


Fig. 3.46 Comparison of Failure Mechanisms at the 1% Drift Ratio

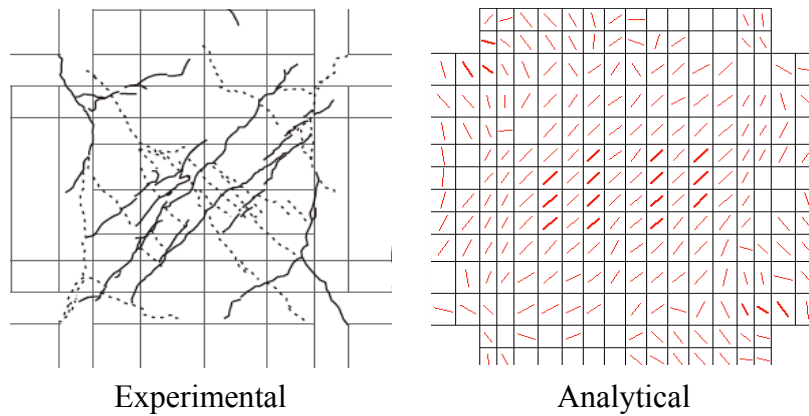


Fig. 3.47 Comparison of Failure Mechanisms at the 2% Drift Ratio

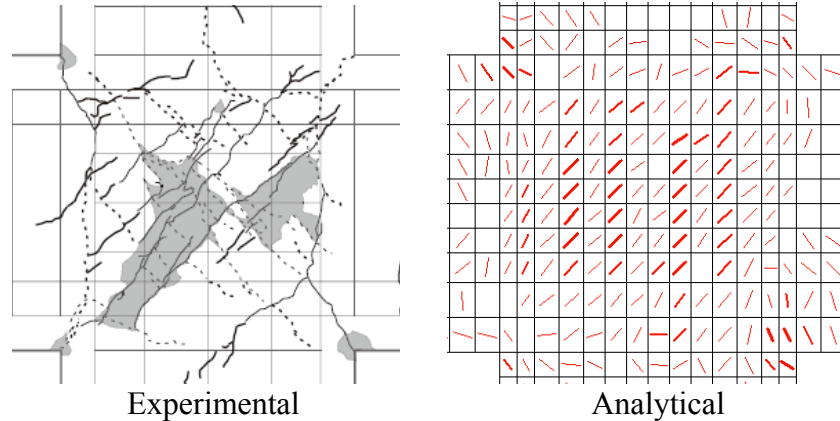


Fig. 3.48 Comparison of Failure Mechanisms at the 3% Drift Ratio

SPECIMEN A2

Specimen A2 was the interior beam-column subassembly tested under Loading Type II. The main crack formation was the flexural cracking at the beam column interface. Flexural cracks were first seen at the beam-column interface, and then diagonal shear cracks on the joint were observed. Later, the widths of the flexural cracks increased rapidly compared to the shear cracks at the joint. The hysteretic response of this specimen showed a symmetric and stable behaviour (Shiohara and Kusuhara, 2006).

The results of VecTor2 analysis are compared to the experimental results in Fig. 3.49, Fig. 3.50, Fig. 3.51, Table 3.31 and Table 3.32. In the VecTor2 analysis, the flexural crack at the beam-column interface was larger than the shear cracks at the joint. The right beam remained intact which was similar to the observed behaviour. The predicted response of load-deformation also showed a stable behaviour. In the analysis, the specimen started losing its strength after reaching the 1.0% drift ratio. A similar behaviour was observed during the testing. However the shear force capacity of the specimen increased even towards the end of loading, in the negative direction, during testing. This suggests a slight difference in the energy dissipation capacity of the predicted response of the specimen, and is possibly the result of the bond-slip model under cyclic conditions. Further explanation on this subject was given in Chapter 2.

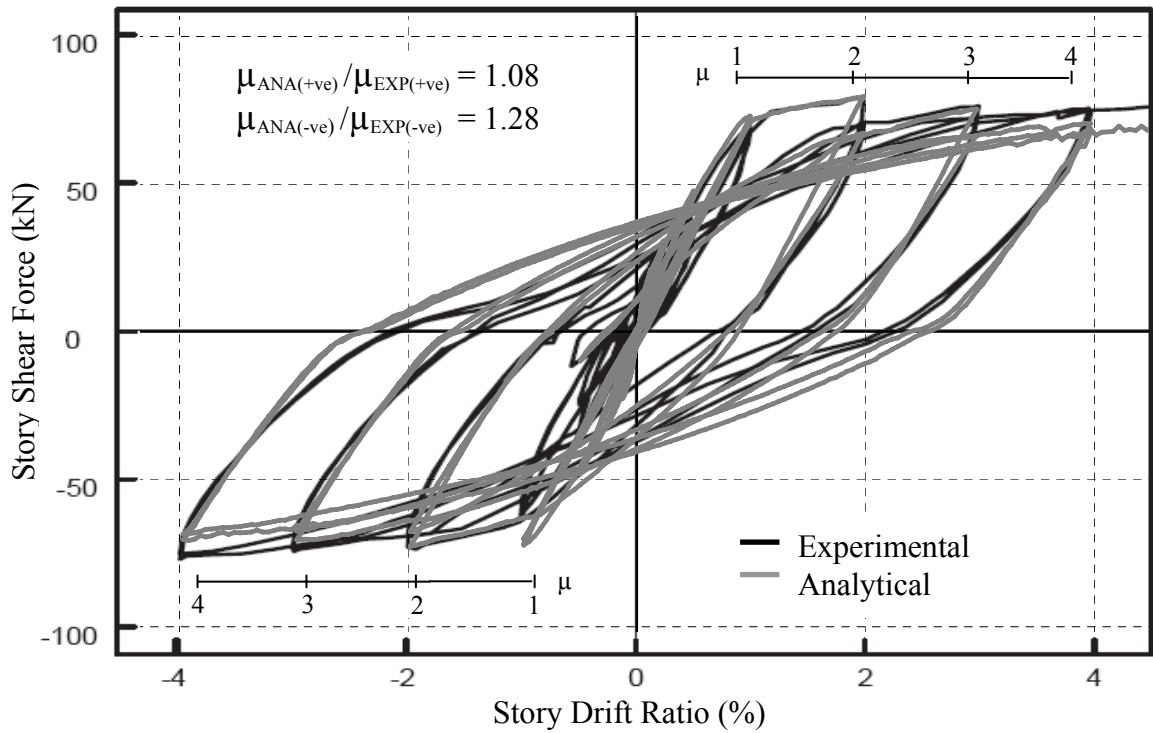


Fig. 3.49 Comparison of Story Shear vs. Story Drift Ratio for Specimen A2

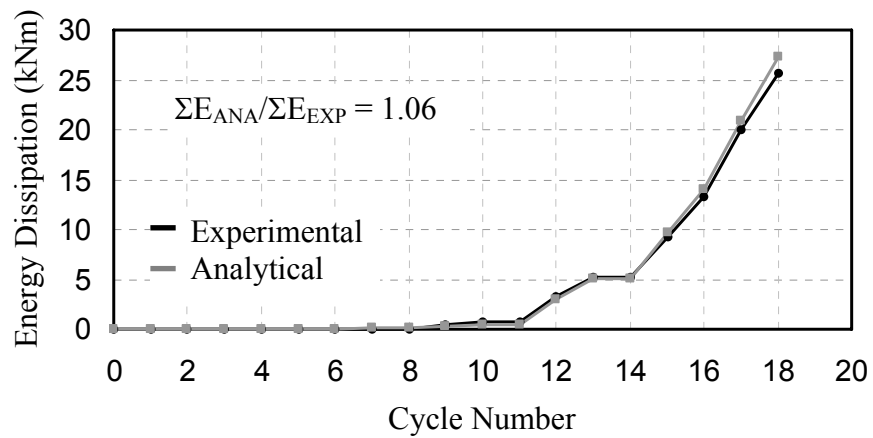


Fig. 3.50 Comparison of Energy Dissipation of Specimen A2

The ratio of the predicted and observed ductility ratios for this specimen was 1.08 in the positive loading direction, and 1.28 in the negative loading direction. The

predicted energy dissipation capacity for this specimen was also compared to the observed value, and a ratio of 1.06 was obtained.

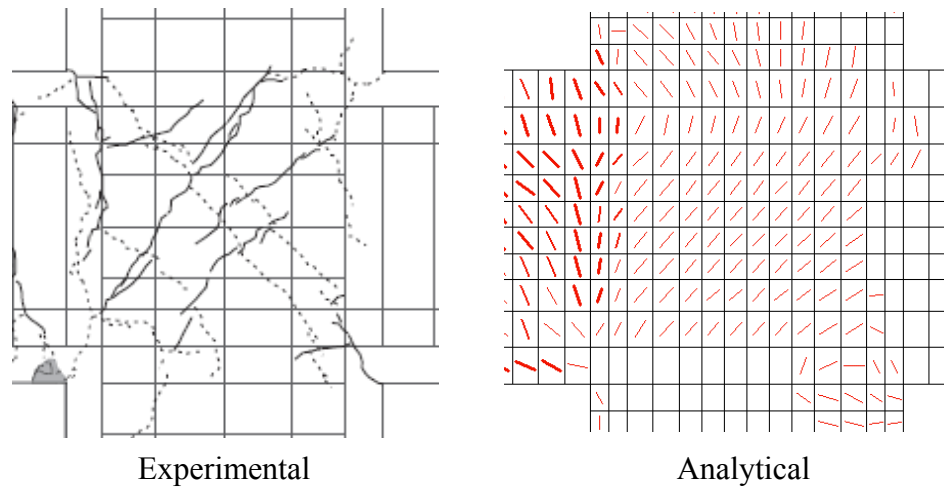


Fig. 3.51 Comparison of Final Failure for Specimen A2

Table 3.31 Sequence of Events at the Positive Loading Direction for Specimen A2

Event	Experimental		Analytical	
	Story Shear (kN)	Story Drift (%)	Story Shear (kN)	Story Drift (%)
Beam Reinforcement-1 st Layer Yielding	63.30	0.86	70.20	0.89
Beam Reinforcement-2 nd Layer Yielding	74.10	1.18	74.40	1.24
Column Reinforcement-Yielding	No yielding		No yielding	
Max Story Shear	77.90	1.99	79.60	1.98

Table 3.32 Sequence of Events at the Negative Loading Direction for Specimen A2

Event	Experimental		Analytical	
	Story Shear (kN)	Story Drift (%)	Story Shear (kN)	Story Drift (%)
Beam Reinforcement-1 st Layer Yielding	60.90	0.97	60.60	0.79
Beam Reinforcement-2 nd Layer Yielding	60.90	0.97	60.60	0.79
Column Reinforcement-Yielding	No yielding		No yielding	
Max Story Shear	77.10	3.98	70.60 (68.6)	0.99 (3.97)

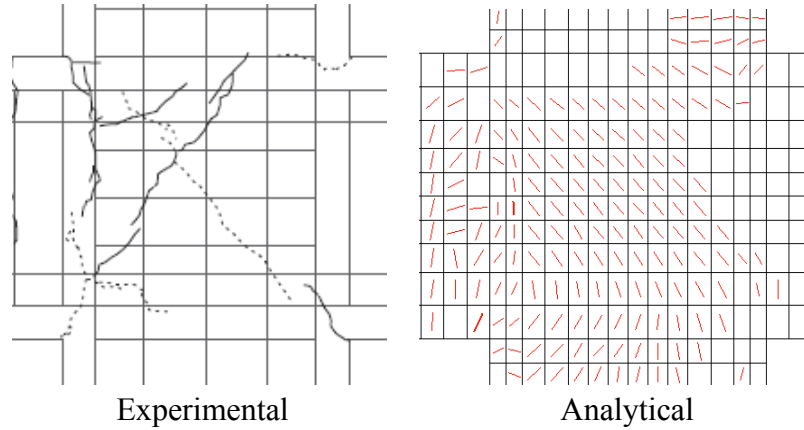


Fig. 3.52 Comparison of Failure Mechanisms at the 1% Drift Ratio

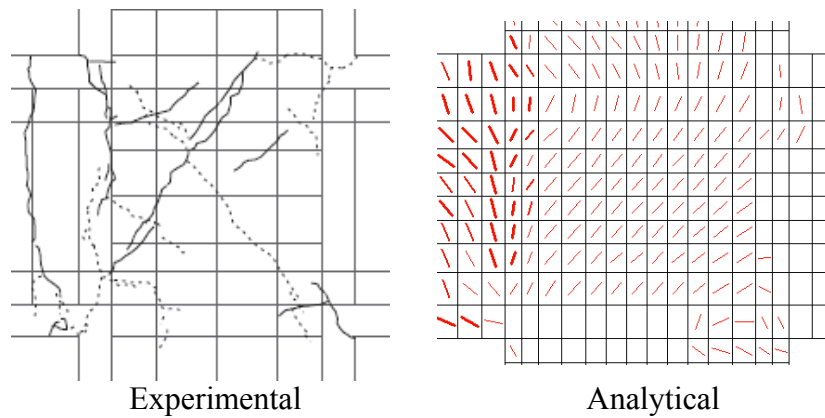


Fig. 3.53 Comparison of Failure Mechanisms at the 2% Drift Ratio

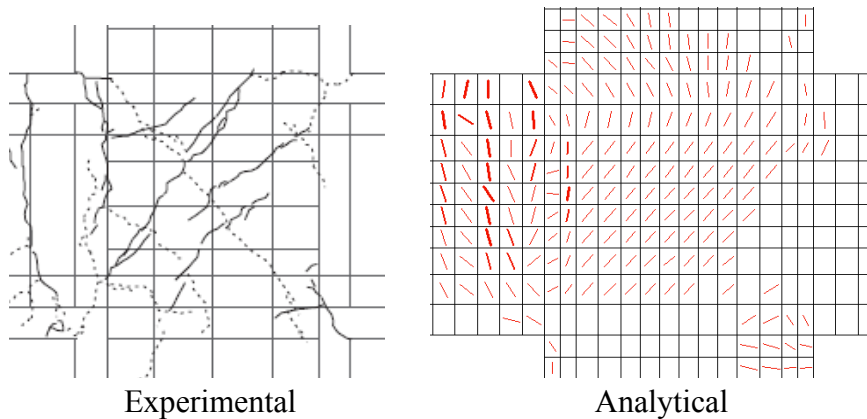


Fig. 3.54 Comparison of Failure Mechanisms at the 3% Drift Ratio

SPECIMEN A3

Specimen A3 was tested under Loading Type III. The observed hysteretic response was stable. Both flexural and shear cracking was observed, and these cracks gradually increased during testing. As a result of this flexural cracking, concrete spalling at the corner of the specimen was observed (Shiohara and Kusuhara, 2006).

The predicted seismic response is similar to the one observed in the test. The predicted and observed story shear force versus story drift behaviour is shown in Fig. 3.48. The sequence of events in the positive and negative loading directions, observed in the experimental and obtained from analytical results, are reported in Table 3.33 and Table 3.34. The flexural cracking at the beam-column face, and shear cracks at the joint were examined for different drift levels in Fig. 3.50, Fig. 3.51 and Fig. 3.52. Similar flexural cracking that caused the concrete spalling at the bottom corner of the left beam was also observed at the end of the 3.0% drift cycle. Under this applied loading condition, the right beam remained intact both in the test and in the predicted response.

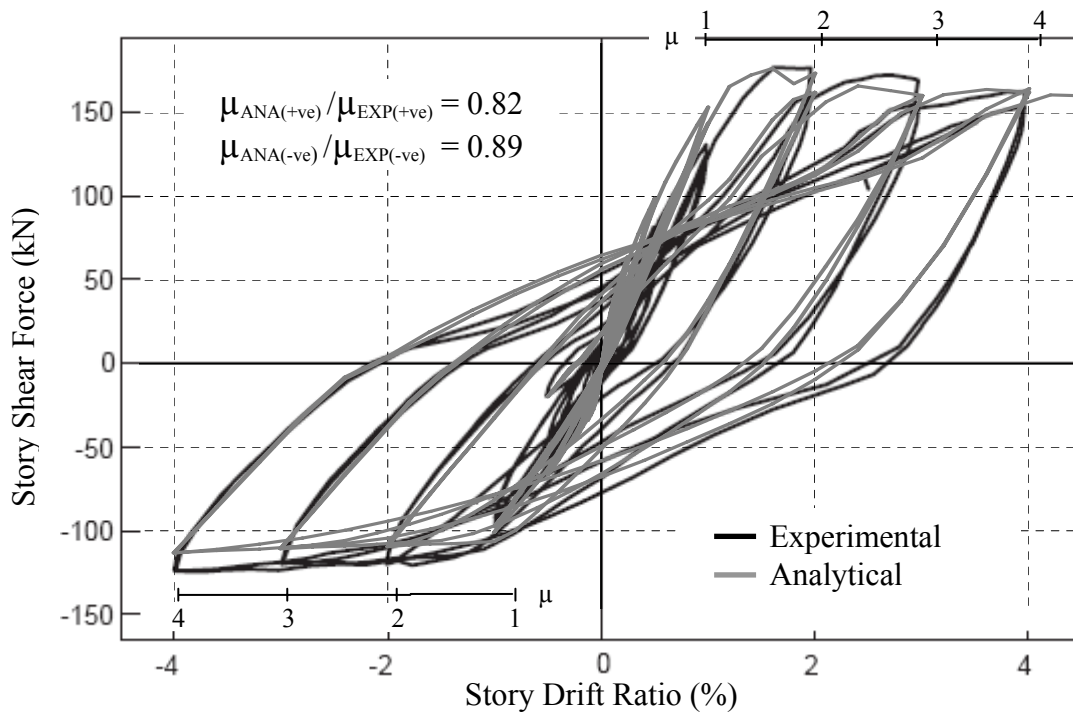


Fig. 3.55 Comparison of Story Shear vs. Story Drift Ratio for Specimen A3

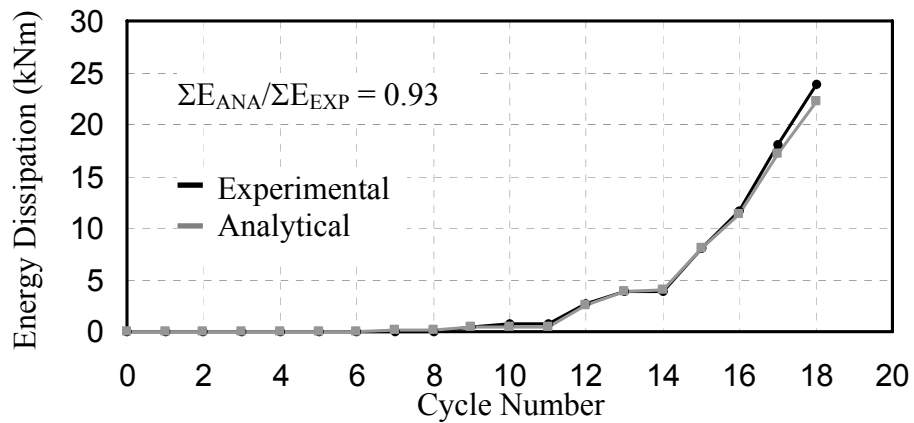


Fig. 3.56 Comparison of Energy Dissipation of Specimen A3

The ratio of the predicted and observed ductility ratios for this specimen was 0.82 in the positive loading direction, and 0.89 in the negative loading direction. The

predicted energy dissipation capacity for this specimen was also compared to the observed value, and a ratio of 0.93 was obtained.

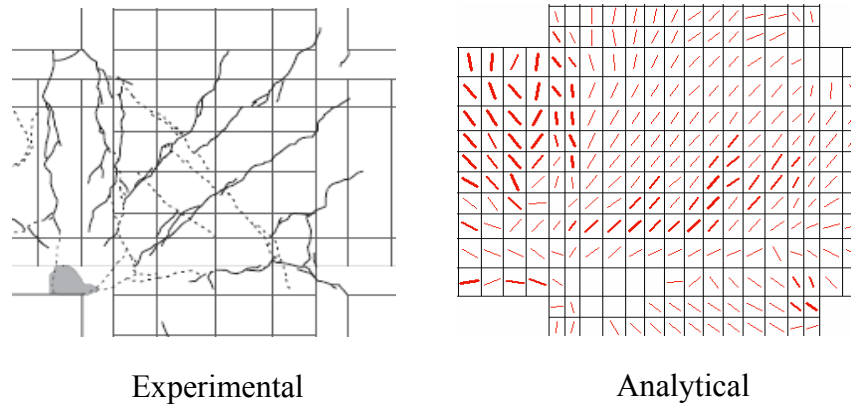


Fig. 3.57 Comparison of Final Failure for Specimen A3

Table 3.33 Sequence of Events at the Positive Loading Direction for Specimen A3

Event	Experimental		Analytical	
	Story Shear (kN)	Story Drift (%)	Story Shear (kN)	Story Drift (%)
Beam Reinforcement-1 st Layer Yielding	158.30	1.34	165.80	1.21
Beam Reinforcement-2 nd Layer Yielding	176.40	1.62	176.10	1.60
Column Reinforcement-Yielding	156.10	1.83	158.10	1.80
Max Story Shear	176.40	1.62	176.10	1.60

Table 3.34 Sequence of Events at the Negative Loading Direction for Specimen A3

Event	Experimental		Analytical	
	Story Shear (kN)	Story Drift (%)	Story Shear (kN)	Story Drift (%)
Beam Reinforcement-1 st Layer Yielding	93.40	0.85	99.60	0.80
Beam Reinforcement-2 nd Layer Yielding	100.90	0.97	106.40	1.00
Column Reinforcement-Yielding	123.60	3.03	110.30	3.00
Max Story Shear	124.50	3.84	113.30	4.00

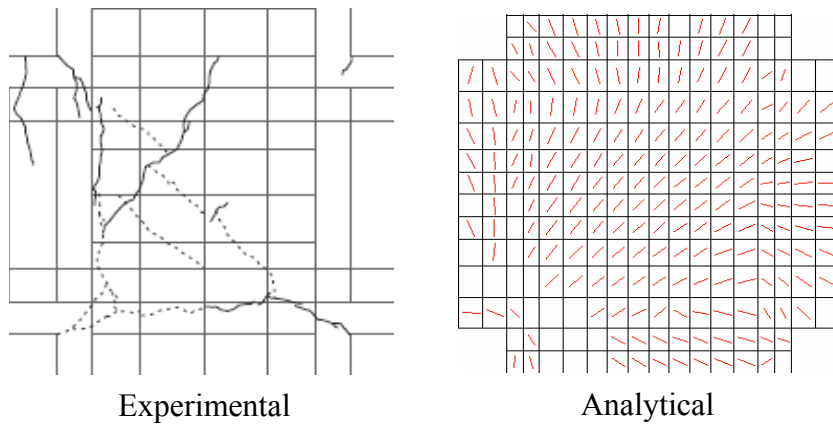


Fig. 3.58 Comparison of Failure Mechanisms at the % Drift Ratio

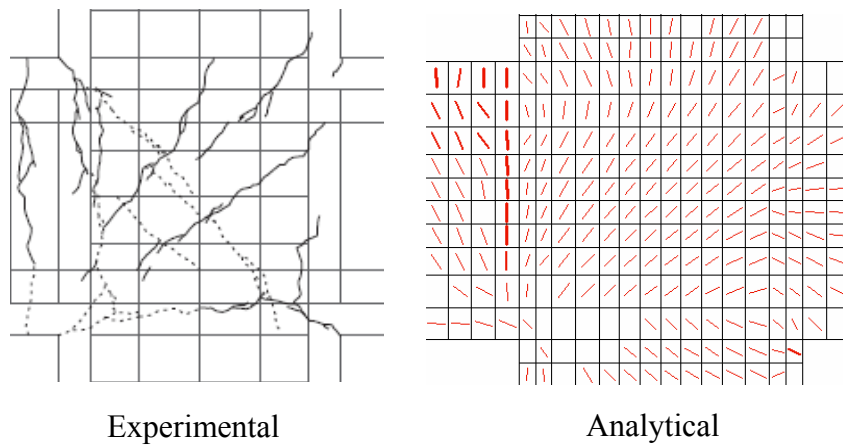


Fig. 3.59 Comparison of Failure Mechanisms at the 2% Drift Ratio

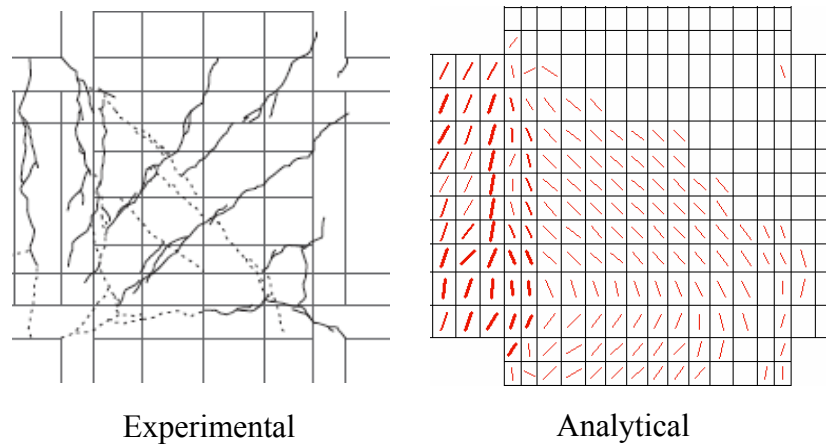


Fig. 3.60 Comparison of Failure Mechanisms at the 3% Drift Ratio

SPECIMEN B1

Specimen B1 was the other interior beam-column subassembly that was tested under Loading Type II conditions. The story shear force versus story drift ratio of this specimen showed a symmetric hysteretic behaviour. The right beam remained intact during testing. The first diagonal shear cracks were observed at the positive 0.5% drift loading cycle. The crack openings were significantly increased at 1.0 % drift ratio. The first flexural crack was seen at the end of the 1.0% drift cycle. Crushing of the concrete was severe at the beam-column joint and at the inner corners of the beam-column connection. The deformations and residual deflections were increased after yielding of the beam longitudinal reinforcement (Shiohara and Kusuhara, 2006).

The predicted crack formations included excessive flexural cracking at the beam end and shear cracking on the joint panel. The predicted and observed load-displacement responses are given in Fig. 3.53. The sequence of events of the analysis were also examined at the positive and negative loading directions, and compared to the observed behaviour as summarized in Table 3.35 and Table 3.36. The flexural cracking was predicted by the VecTor2 analysis, but the shear crack widths were smaller compared to the observed response. The right beam showed no signs of cracking and deformation.

Contrary to the other (right) beam, the loaded beam was gradually disturbed at the column face with extensive flexural cracking.

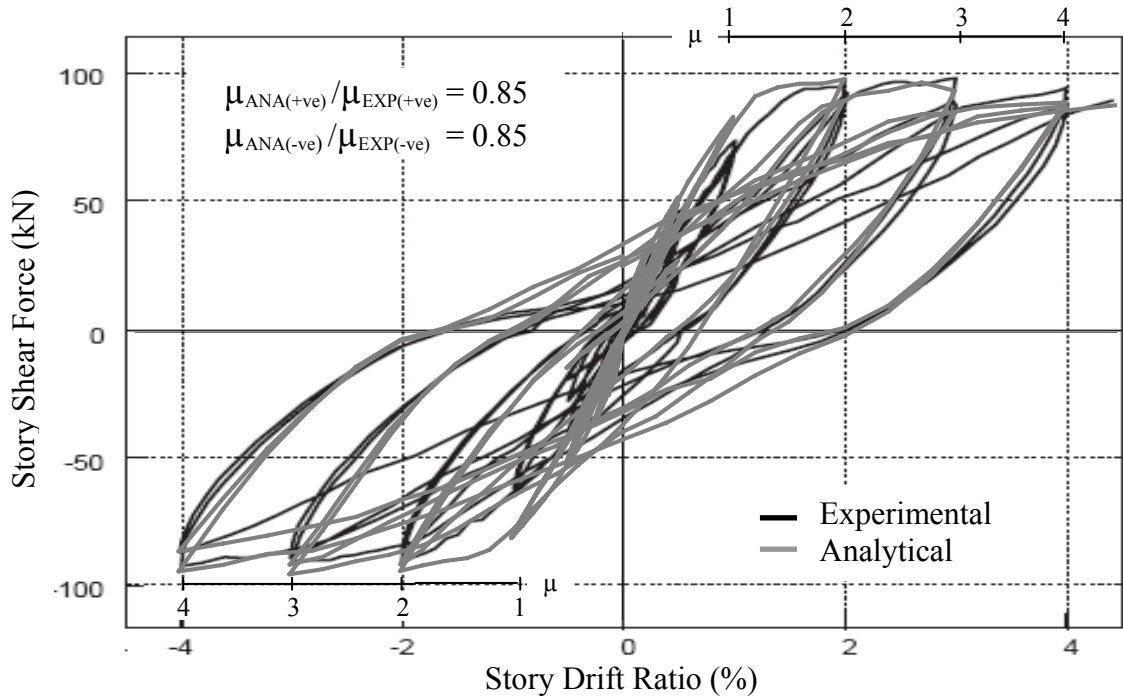


Fig. 3.61 Comparison of Story Shear vs. Story Drift Ratio for Specimen B1

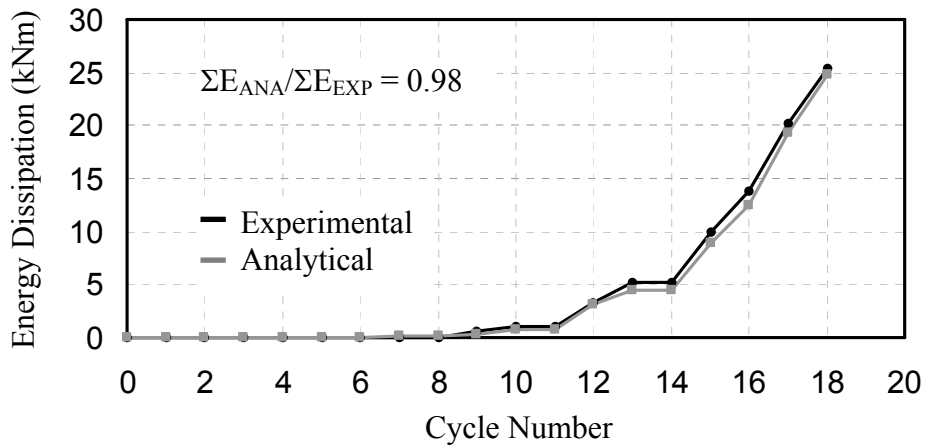


Fig. 3.62 Comparison of Energy Dissipation of Specimen B1

The ratio of the predicted and observed ductility ratios for this specimen was 0.85 in the positive and negative loading directions. The predicted energy dissipation

capacity for this specimen was also compared to the observed value, and a ratio of 0.98 was obtained.

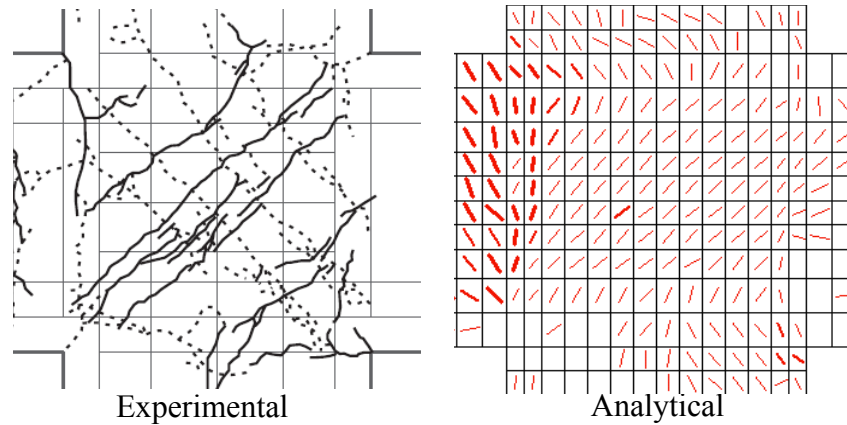


Fig. 3.63 Comparison of Final Failure for Specimen B1

Table 3.35 Sequence of Events at the Positive Loading Direction for Specimen B1

Event	Experimental		Analytical	
	Story Shear (kN)	Story Drift (%)	Story Shear (kN)	Story Drift (%)
Beam Reinforcement-1 st Layer Yielding	73.60	1.01	80.20	0.99
Beam Reinforcement-2 nd Layer Yielding	88.90	1.43	93.30	1.58
Column Reinforcement-Yielding	88.90	1.43	93.30	1.58
Max Story Shear	98.10	2.99	94.90	1.99

Table 3.36 Sequence of Events at the Negative Loading Direction for Specimen B1

Event	Experimental		Analytical	
	Story Shear (kN)	Story Drift (%)	Story Shear (kN)	Story Drift (%)
Beam Reinforcement-1 st Layer Yielding	68.90	1.14	74.70	0.99
Beam Reinforcement-2 nd Layer Yielding	89.10	1.90	87.60	1.78
Column Reinforcement-Yielding	85.40	1.70	86.00	1.58
Max Story Shear	92.60	4.00	89.90	3.97

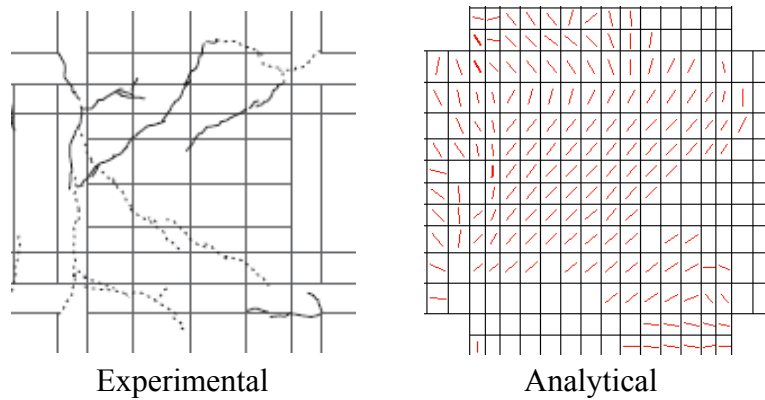


Fig. 3.64 Comparison of Failure Mechanisms at the 1% Drift Ratio

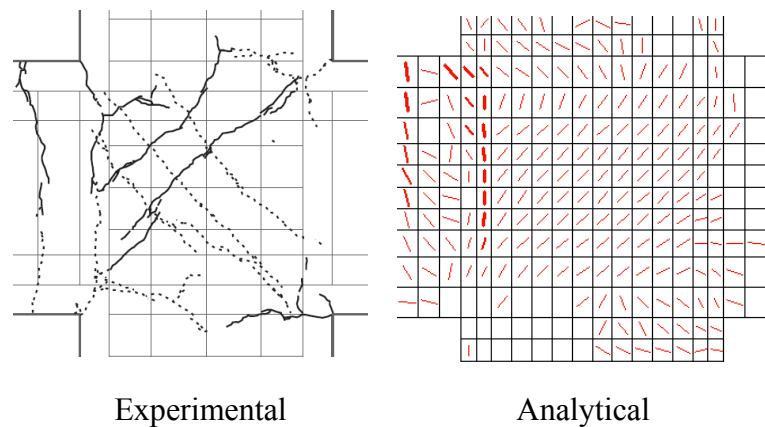


Fig. 3.65 Comparison of Failure Mechanisms at the 2% Drift Ratio

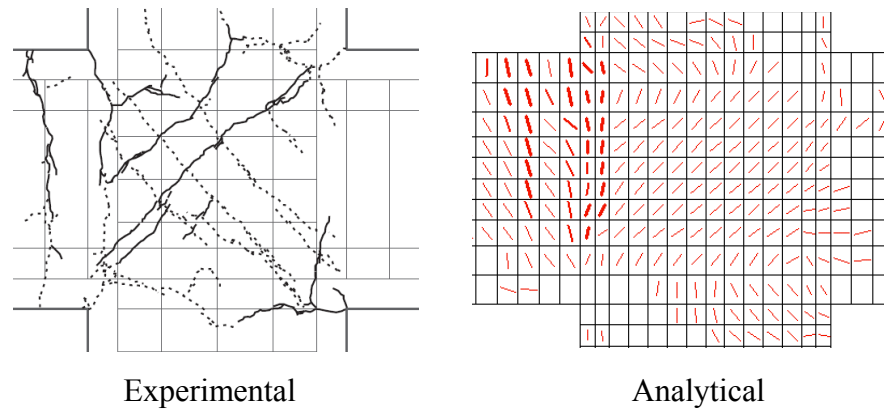


Fig. 3.66 Comparison of Failure Mechanisms at the 3% Drift Ratio

3.2.2. DISCUSSION OF INTERIOR BEAM-COLUMN SUBASSEMBLIES

A comparison of the interior beam-column subassemblies with deformed reinforcement is presented here. A total of four interior specimens tested under simulated seismic loadings were modelled in this portion of the study. The ratio of the predicted to the observed peak shear force results had a mean of 1.00 and a coefficient of variation of 2.11% in the positive loading direction. The mean value of the same ratio was 0.97, with a coefficient of variation of 6.27%, in the negative loading direction. The ratio of the predicted to the observed ultimate displacement results were better, and had a mean of 0.99 and a coefficient of variation of 1.09% in the positive loading direction. The mean value of the same ratio was 0.99, and had a coefficient of variation of 0.75% in the negative loading direction. A better correlation was observed in the positive loading direction for interior specimens due to reasons explained above related to cyclic bond-slip behaviour. The predicted peak shear force and ultimate displacement values for all interior specimens designed with deformed reinforcement are compared to the observed shear force values in the positive and negative loading directions, as reported in Table 3.37, 3.38, 3.39 and 3.40.

Table 3.37 Comparison of Peak Shear Force at the Positive Loading Direction

Specimen	V_{\max} (EXP) (kN)	V_{\max} (VT2) (kN)	V_{\max} (VT2)/ V_{\max} (EXP)
A1	126.6	128.6	1.02
A2	77.9	79.6	1.02
A3	176.4	176.1	1.00
B1	98.1	94.9	0.97
		Mean	1.00
		St. Dev	0.02
		COV (%)	2.11

Table 3.38 Comparison of Peak Shear Force at the Negative Loading Direction

Specimen	V_{\max} (EXP) (kN)	V_{\max} (VT2) (kN)	V_{\max} (VT2)/ V_{\max} (EXP)
A1	122.8	130.0	1.06
A2	77.1	70.6	0.92
A3	124.5	113.1	0.91
B1	92.6	91.0	0.98
		Mean	0.97
		St. Dev	0.06
		COV (%)	6.27

Table 3.39 Comparison of Ultimate Displacement at the Positive Loading Direction

Specimen	Δ_{\max} (EXP) (mm)	Δ_{\max} (VT2) (mm)	Δ_{\max} (VT2)/ Δ_{\max} (EXP)
A1	58.8	58.2	0.99
A2	73.5	72.2	0.98
A3	40.4	39.8	0.98
B1	80.8	81.6	1.01
		Mean	0.99
		St. Dev	0.01
		COV (%)	1.09

Table 3.40 Comparison of Ultimate Displacement at the Negative Loading Direction

Specimen	Δ_{\max} (EXP) (mm)	Δ_{\max} (VT2) (mm)	Δ_{\max} (VT2)/ Δ_{\max} (EXP)
A1	58.8	58.2	0.99
A2	58.8	57.6	0.98
A3	29.4	29.4	1.00
B1	58.8	58.5	1.00
		Mean	0.99
		St. Dev	0.01
		COV (%)	0.75

Overall, the VecTor2 analysis of beam-column subassemblies with deformed reinforcement for both exterior and interior and seismically and non-seismically designed members were successful in predicting the response with accurate estimates of the crack formations, ultimate strength, load-deformation response, energy dissipation capacity, and ductility ratios.

CHAPTER 4

Analysis of Smooth Reinforcement Beam-Column Subassemblies

Four specimens were examined for the analytical study on beam-column subassemblies designed with smooth (plain round) reinforcement. The experimental data was obtained from an extensive experimental and analytical research program performed on non-seismically designed beam-column subassemblies at the University of Pavia and University of Canterbury by Pampanin et al. (2003-2006). These specimens were exterior and interior beam-column subassemblies designed with no consideration of capacity design principles; they were mostly designed to resist gravity loads. This design approach was prevalent in pre-1970s reinforced concrete framed buildings, which were designed before current seismic regulations were introduced.

The first group of specimens consisted of two exterior beam-column subassemblies that were tested at the University of Canterbury by Chen (2006). The second specimen involved another non-seismically designed interior beam-column subassembly tested by Pampanin et al. (2002). The results of the study by Chen (2006) provided a base for a new retrofitting technique applicable to non-seismically designed beam-column subassemblies, which was examined as the last specimen in this study. This is a newly developed low-invasive retrofitting technique which successfully mitigates the shear failure mechanism from joint panel to the beam as a flexural failure mechanism (Pampanin et al., 2006). The sectional and material properties, test set-up and loading protocol are described for each beam-column subassembly. The results of the analytical study are also given in comparison to the experimental results in this chapter.

The finite element modelling of the specimens were similar to the ones described in Chapter 3. However the bond-slip modelling of smooth reinforcement was changed through the course of the research. The embedded smooth rebar option developed by Gan (2000) wasn't successful in capturing the seismic behaviour of non-seismically

designed members. Based on experimental research by Abrams (1913), Feldman and Bartlett (2005) and Fabbrocino et al. (2002), another approach for smooth-bar bond modelling was suggested and investigated in this study.

4.1. EXTERIOR BEAM-COLUMN SUBASSEMBLIES

4.1.1. SPECIMEN ES1

4.1.1.1. TEST SPECIMENS

Two non-seismically designed beam-column subassemblies tested by Chen (2006) were examined in this section. The specimens in this group were similar to the exterior beam-column subassemblies described in the previous chapter (i.e. Specimen ED3). While the design principles remained the same, the reinforcement used in these specimens was smooth (plain round) reinforcement to represent a typical design deficiency of these structures. There were also problems in reinforcement detailing such as inadequate anchorage detailing and poor confinement in the joints. The beam longitudinal bars were anchored into the joint with hooked ends, and an inadequate amount of shear reinforcement was included in the joint. These two exterior beam-column subassemblies were designed with identical sectional details, and tested under the same loading and support conditions.

Sectional and Material Properties:

The sectional and material details were similar to the Specimen ED3 examined in the previous chapter. The concrete compressive strength and Young's Modulus were 23 MPa and 28700 MPa, respectively. Detailed information on these specimens is shown in Fig. 4.1

The smooth reinforcing bars were used for both longitudinal reinforcement and transverse reinforcement. The transverse reinforcement had a 100 mm spacing in the columns, and a 133 mm spacing in the beams. The longitudinal reinforcement was anchored into the joint with hooked ends, and the joint was confined with only one tie

bar to represent the confinement problem that is present in these beam-column subassemblies. The reinforcement detailing and material properties of the reinforcement used in these specimens are given in Table 4.1 and Table 4.2.

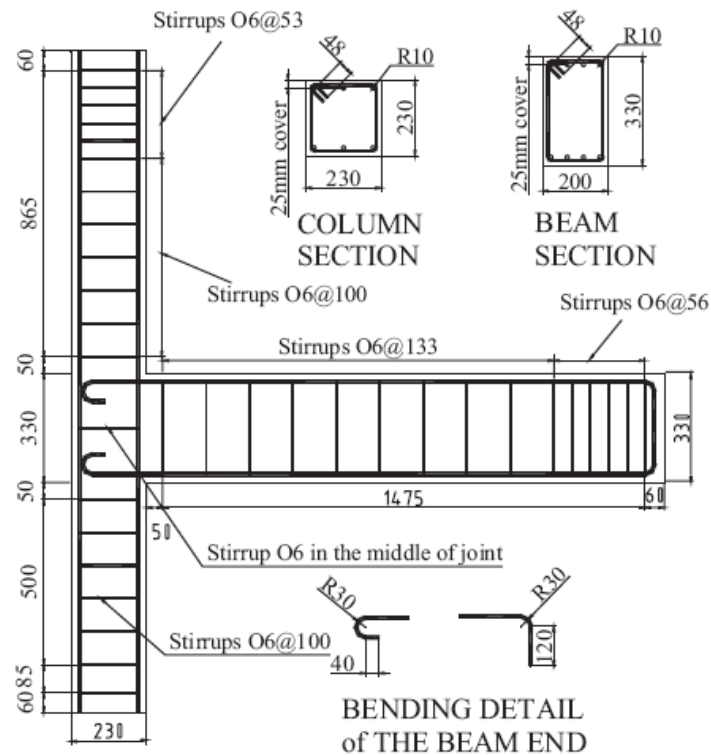


Fig. 4.1 Reinforcement Detailing for Specimen ES1 (Chen, 2006)

Table 4.1 Reinforcement Detailing for Specimen ES1 (Chen, 2006)

Specimen	Beam		Column		Joint
	Longitudinal	Transverse	Longitudinal	Transverse	
TDP1	4 R10 2 R10	R6 @ 133 mm	3 R10	R6 @ 100 mm	1- R6
TDP2	4 R10 4 R10		3 R10		

Table 4.2 Material Properties of Reinforcement Specimen ES1 (Chen, 2006)

Type	Grade	Diameter (mm)	Area (mm ²)	f _y (MPa)	E _s (MPa)	f _u (MPa)
R10	300	10	127	456	176000	582
R6	300	6	32	326	151300	488

Test Set-Up and Loading:

The specimens were tested under the same loading protocol that was applied to Specimen ED3, described in Chapter 3. Therefore, no additional information is given in this section for this purpose.

4.1.1.2. FINITE ELEMENT MODELLING

Material and Regional Properties:

Similar modelling techniques were applied to these specimens as the ones that were applied to the exterior beam-column subassemblies with deformed reinforcement. Seven concrete regions were defined and employed to model these specimens. A total of 1796 rectangular concrete elements with a 25 by 25 mm mesh configuration were used for the concrete regions. Detailed information about the concrete regions is given in Fig. 4.2 and Table 4.3.

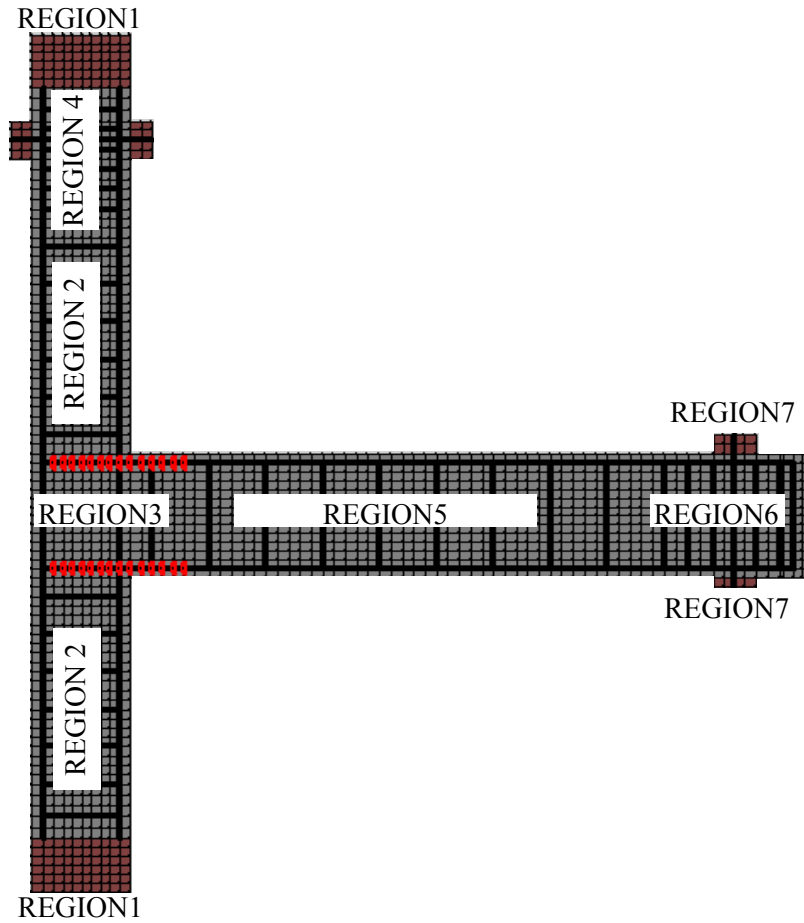


Fig. 4.2 Material Regions for Specimen ES1

Table 4.3 Concrete Regions for Specimen ES1

Concrete Regions	# 1 (#7)	#2	# 3	#4	#5	#6
Thickness (mm)	230 (200)	230		200		
Mesh Size (mm)	25 x 25					
Purpose	Bearing	Column	Joint	Column	Beam1	Beam2
ρ_z (%)	None	0.267	0.074	0.464	0.129	0.305

The reinforcement and bond regions were modelled with 678 truss elements and 28 bond-link elements respectively. The reinforcement and bond element configuration is shown in Fig. 4.3, and detailed information for the reinforcement regions is given in Table 4.4.

Table 4.4 Reinforcement Elements for Specimen ES1

Reinforcement	Type	Location
# 1	3 R10	Column Longitudinal
# 2	4 R10	Beam Top Layer Longitudinal
# 3	4 R10 (2 R10)	Beam Bottom Layer Longitudinal
# 4	2 R6	Transverse Reinforcement
# 5	D20	Strengthening Rebar for Test Set-Up

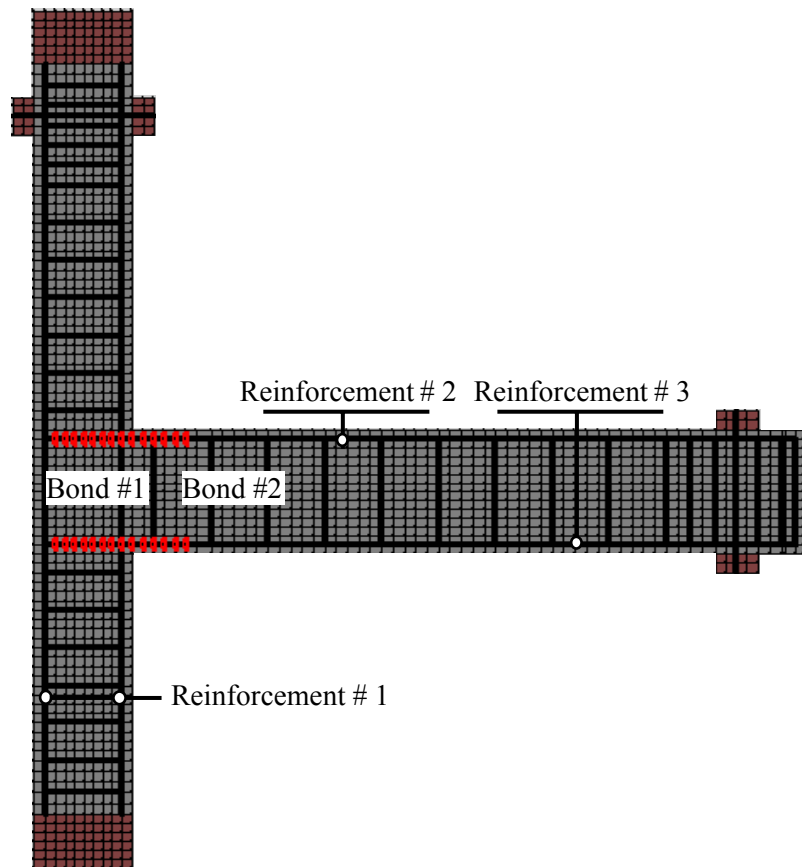


Fig. 4.3 Reinforcement and Bond Regions for Specimen ES1

The smooth-bar bond-slip effects were modelled based on the experimental results reported by Fabbrocino et al. (2002). The hooked ends of the beam longitudinal bars were modelled with the “Perfect Bond” model. The bond-slip properties for this model were constant and can’t be modified during the analysis. Information on these bond slip model was given in Chapter 2. This model was only assigned to the hooked section of the bar, and was defined by Bond #1. The rest of the beam longitudinal bars were modelled with the smooth-bar bond-slip model suggested by Fabbrocino et al. (2002), and implemented in VecTor2. The observed bond stress-slip relationships for 12 mm and 16 mm straight smooth bars were used to represent the straight section of these bars. The monotonic bond-slip behaviour that were obtained from tests by Fabbrocino et al. (2002) on concrete blocks embedded with straight shaped smooth bars were used to represent the bond-slip behaviour for the rest of the longitudinal bars. The straight section of the beam longitudinal bars was defined by Bond #2, and the bond-slip relation for a 12 mm smooth bar was used from the test results by Fabbrocino et al. (2002). The ‘Custom Input’ option for embedded bars was used to assign the second bond model. The bond stress-slip parameters used for modelling are given in Table 4.5.

Table 4.5 Bond Stress-Slip Parameters for Smooth Bars

Parameter	Bond # 1	Bond # 2
	Hooked End	Straight Section
τ_1 (MPa)	250	1.05
τ_2 (MPa)	250	0.3
τ_f (MPa)	250	0.3
Δ_1 (mm)	0.1	0.03
Δ_2 (mm)	3.0	1
Δ_3 (mm)	10.0	3

Loading and Restraint Conditions:

A pinned support was assigned to the lower column end, and pinned roller supports were assigned to the beam end. A displacement-based loading scheme was employed for Load Case 1, and the axial loads applied to the top of the column were described as the Load Case 2 and Load Case 3 (see Fig 4.4).

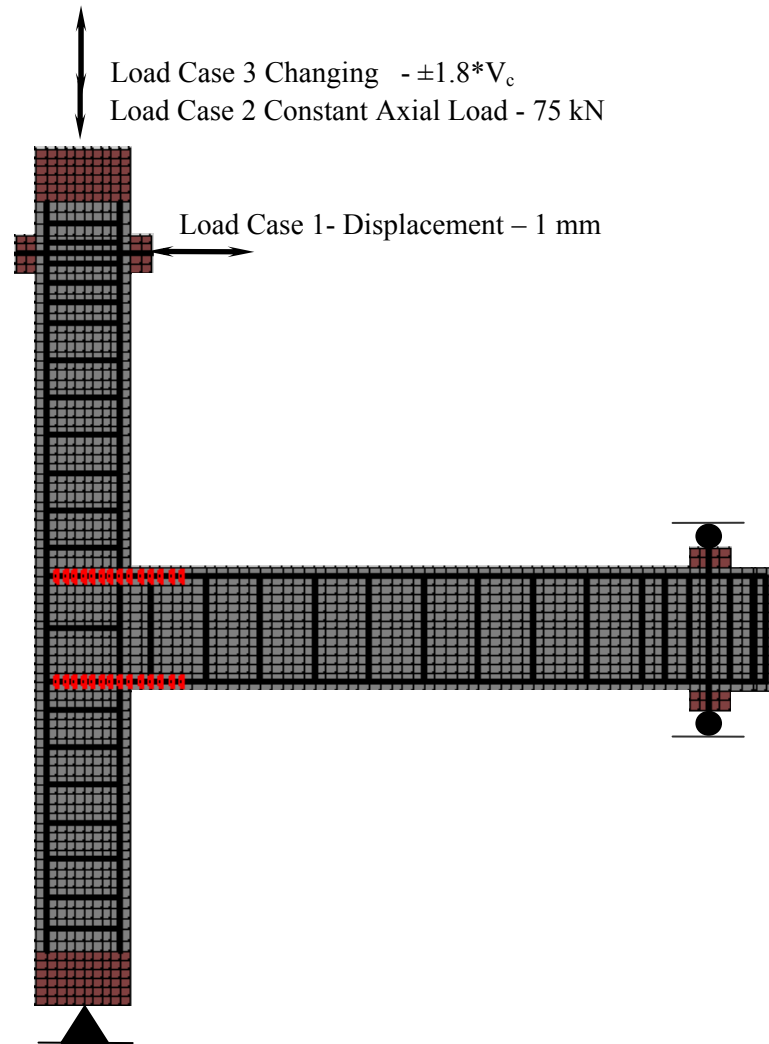


Fig. 4.4 Loading and Restraint Conditions for Specimen ES1

4.1.1.3. RESULTS OF EXPERIMENTAL AND ANALYTICAL STUDY

A comparison of the predicted and the observed response is given individually for Specimen TDP1 and TDP2 in the following sections.

Specimen TDP1

In the experiment by Chen (2006), a joint shear failure was observed in the positive loading direction, while a flexural failure at the beam-column interface was observed in the negative loading direction. In the positive loading direction, the first joint shear cracking was observed at a 1.33% story drift ratio, and the shear resistance of the member decreased after this cracking occurred. Later, the shear strength of the specimen recovered to its previous values, and started decreasing gradually with the opening of the diagonal cracks in the joint. The beam hinging was observed only in the negative loading direction. The hysteretic response showed a pinched behaviour which indicated slippage of the reinforcement (Chen, 2006).

The predicted response of this specimen was somewhat similar to the observed response. Similar crack formations were observed in the analytical results. Once the bond strength of the smooth bars was surpassed, these bars started to push the concrete cover at the end of the beam, and caused the spalling of the concrete cover at the back of the column. These cracks were gradually increased under the push-pull effects of the reversed cyclic loading conditions. Later these cracks joined to the diagonal joint cracks, and formed a concrete wedge in the joint. The flexural cracking at the beam-column face was observed both in the positive and the negative loading directions.

The predicted story shear force versus story drift behaviour for this specimen is compared to the observed behaviour of the test specimen in Fig. 4.5. The ductility ratios of the specimen was estimated in the positive and negative loading directions, and given in Fig. 4.24 for further comparison between the analytical and experimental results. The ratio of the predicted and observed ductility ratios for this specimen was 1.26 in the positive loading direction, and 1.15 in the negative loading direction.

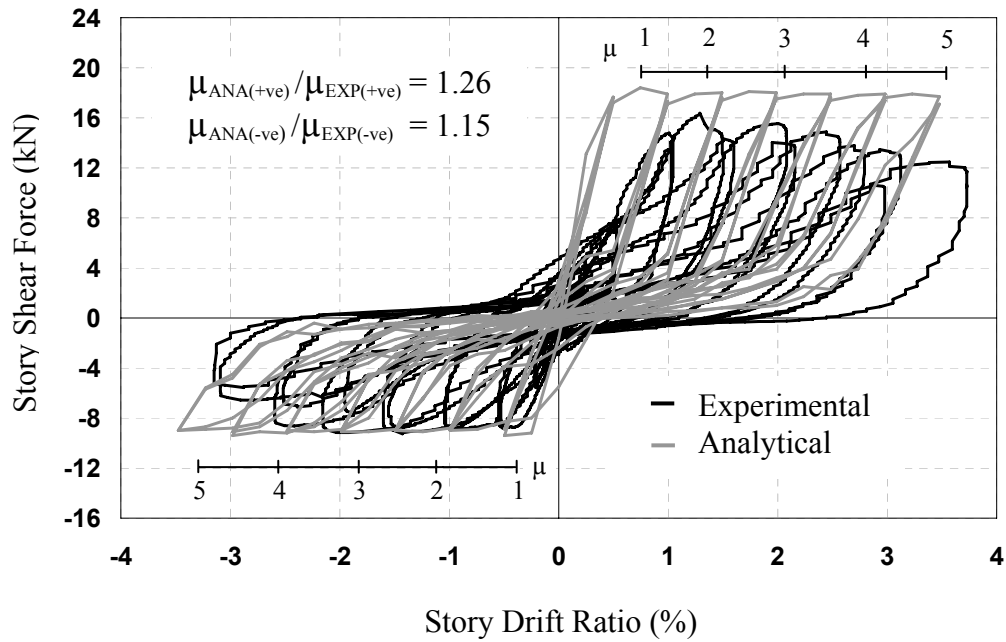


Fig. 4.5 Comparison of Story Shear vs. Story Drift Ratio for Specimen TDP1

The energy dissipation capacity obtained from the predicted and observed response of the specimen was also given in comparison in Fig. 4.6, and a ratio of 0.60 was obtained.

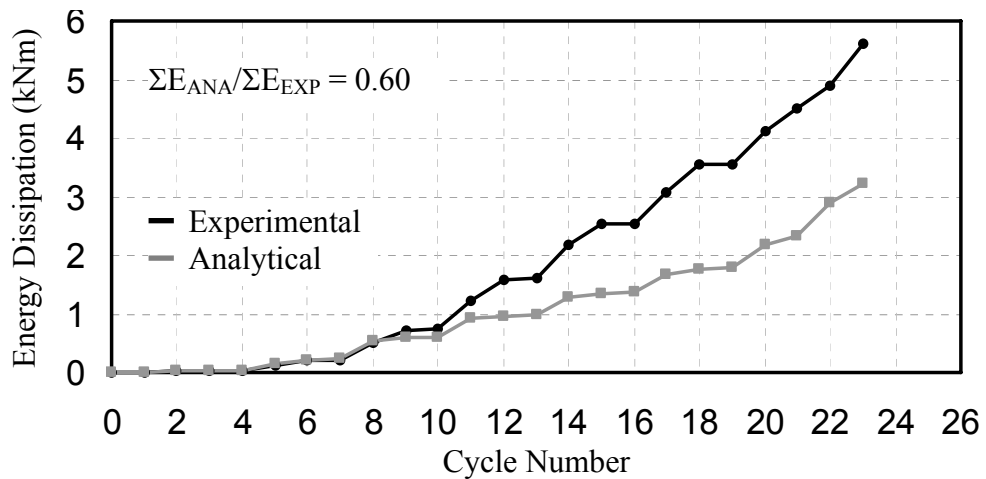


Fig. 4.6 Comparison of Energy Dissipation of Specimen TDP1

The crack formations and failure mechanism of the observed behaviour are also compared to the response predicted by the VecTor2 analysis in Fig. 4.7. The sequence of events occurred leading to the failure of the specimen is given in comparison to the analytical results in Table 4.6.

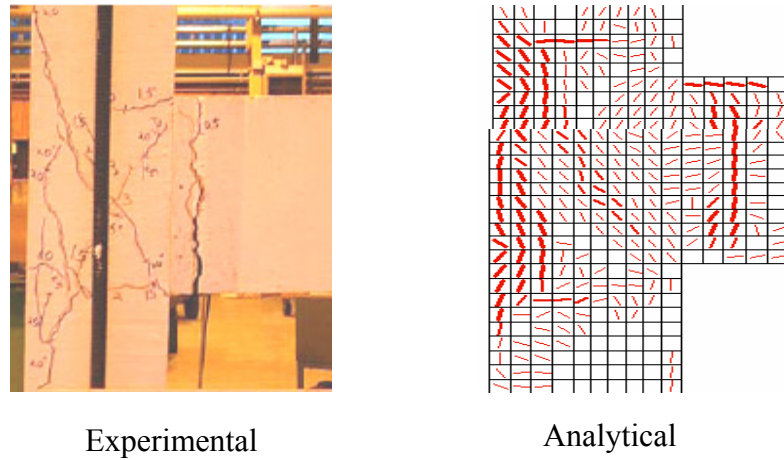


Fig. 4.7 Comparison of Failure Mechanisms for Specimen TDP1

Table 4.6 Sequence of Events for Specimen TDP1

Event	Experimental		Analytical	
	Story Shear (kN)	Story Drift (%)	Story Shear (kN)	Story Drift (%)
Positive Loading Direction				
First Shear Cracking	16.3	1.33	18.4	0.75
Beam Hinging	Not Observed		17.2	0.5
Max Story Shear	16.3	1.33	18.4	0.76
Negative Loading Direction				
First Shear Cracking	8.2	2.6	8.8	1.0
Beam Hinging	8.7	0.4	9.2	0.26
Max Story Shear	8.9	0.5	9.4	0.5

Specimen TDP2

A brittle joint shear failure was observed by Chen (2006) for this specimen. The first joint shear cracks occurred at the 1.0% drift cycles, and gradually increased in the positive and the negative loading directions. Similar to Specimen TDP1, the hysteretic response showed a pinched behaviour which indicated slippage of the reinforcement. The concrete wedge mechanism was observed in this specimen (Chen, 2006).

The ratio of the predicted and observed ductility ratios for this specimen was 1.09 in the positive loading direction, and 0.93 in the negative loading direction.

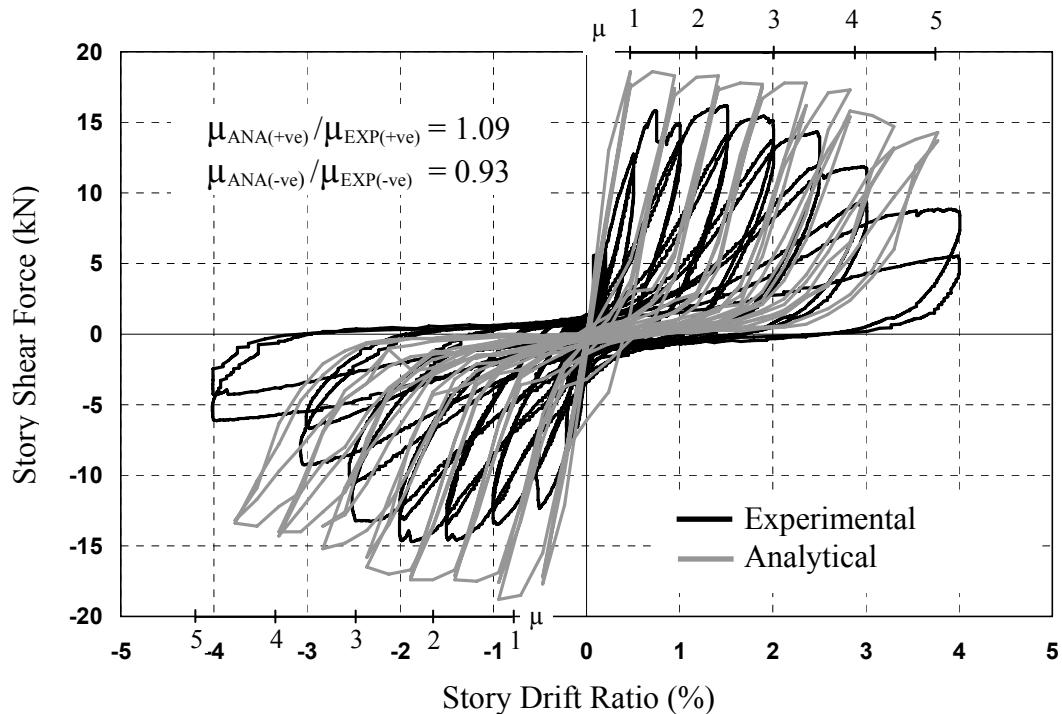


Fig. 4.8 Comparison of Story Shear vs. Story Drift Ratio for Specimen TDP2

The energy dissipation capacity obtained from the predicted and observed response of the specimen was also given in comparison in Fig. 4.9, and a ratio of 0.60 was obtained.

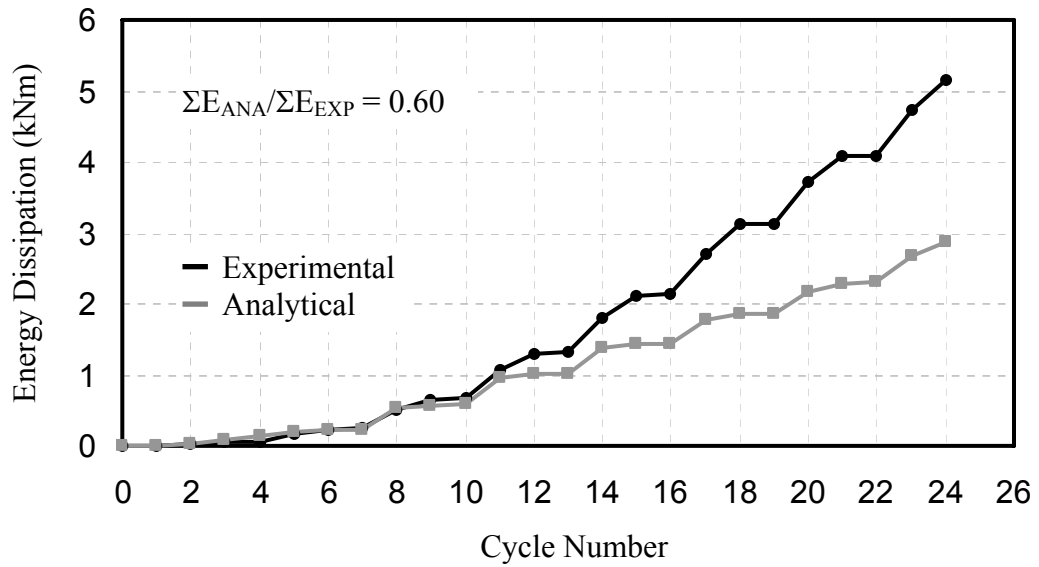


Fig. 4.9 Comparison of Energy Dissipation of Specimen TDP2

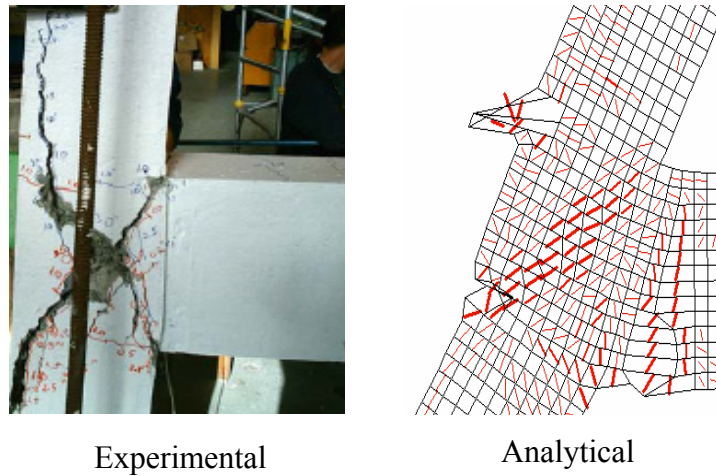


Fig. 4.10 Comparison of Failure Mechanisms of Specimen TDP2

The predicted response of this specimen was similar to the observed response. Similar crack formations, which resulted in a concrete wedge mechanism, were also observed in the analytical results. The predicted story shear force versus story drift behaviour, crack formations and the sequences of events are compared to the observed behaviour in Fig. 4.8, Fig. 4.10 and Table 4.7.

Table 4.7 Sequence of Events for Specimen TDP2

Event	Experimental		Analytical	
	Story Shear (kN)	Story Drift (%)	Story Shear (kN)	Story Drift (%)
Positive Loading Direction				
First Shear Cracking	16.0	0.7	18.4	0.8
Concrete Wedge Mechanism	14.0	2.5	17.2	2.2
Max Story Shear	16.2	1.5	18.6	0.8
Negative Loading Direction				
First Shear Cracking	12.4	0.5	18	0.8
Concrete Wedge Mechanism	12.5	0.4	16.8	2.3
Max Story Shear	14.0	2.0	18.8	1.0

4.1.1.4. DISCUSSION ON EXTERIOR BEAM-COLUMN SUBASSEMBLIES

Overall, the numerical analyses of the exterior specimens designed with smooth reinforcement were successful in estimating the crack formations, load-deformation response and energy dissipation observed experimentally. As there were two beam-column subassemblies examined in this section, no comparison of the predicted and observed response is given for these specimens.

4.2. INTERIOR BEAM-COLUMN SUBASSEMBLIES

4.2.1. SPECIMEN IS1

4.2.1.1. TEST SPECIMENS

An interior beam-column subassembly tested by Pampanin et al. (2002) was examined in this section. This specimen was designed with similar design deficiencies as the Specimen ES1. The sectional details, material properties, and loading system of this specimen were different than the other specimens examined previously in this chapter, and are explained in more detail in the following paragraph.

Sectional and Material Properties:

The columns were 200 by 200 mm, and beams were 200 by 330 mm. The compressive strength and Young's Modulus of the concrete used in this specimen were 23.9 and 22000 MPa, respectively. The longitudinal reinforcement used in this specimen was R8 and R12 smooth reinforcing bars, and R4 smooth reinforcing bar was used for the shear reinforcement. The transverse reinforcement was placed with a 115 mm spacing along the beam, and a 135 mm spacing along the column. Detailed information on the reinforcement layout is given in Fig. 4.11, Table 4.8, and Table 4.9.

Table 4.8 Reinforcement Detailing for Specimen IS1 (Pampanin et al, 2002)

Specimen	Beam		Column		Joint
	Longitudinal	Transverse	Longitudinal	Transverse	
C2	2 R8 + 1 R12 2 R8 + 1 R12	R4 @ 115 mm	3 R8 3 R8	R4 @ 135 mm	None

Table 4.9 Material Properties of Reinforcement for Specimen IS1

(Pampanin et al, 2002)

Type	Grade	Diameter (mm)	Area (mm ²)	f _y (MPa)	E _s (MPa)	f _u (MPa)
R12	300	10	127	456	176000	582
R8	300	10	127	357	176300	493
R4	300	6	32	326	151300	488

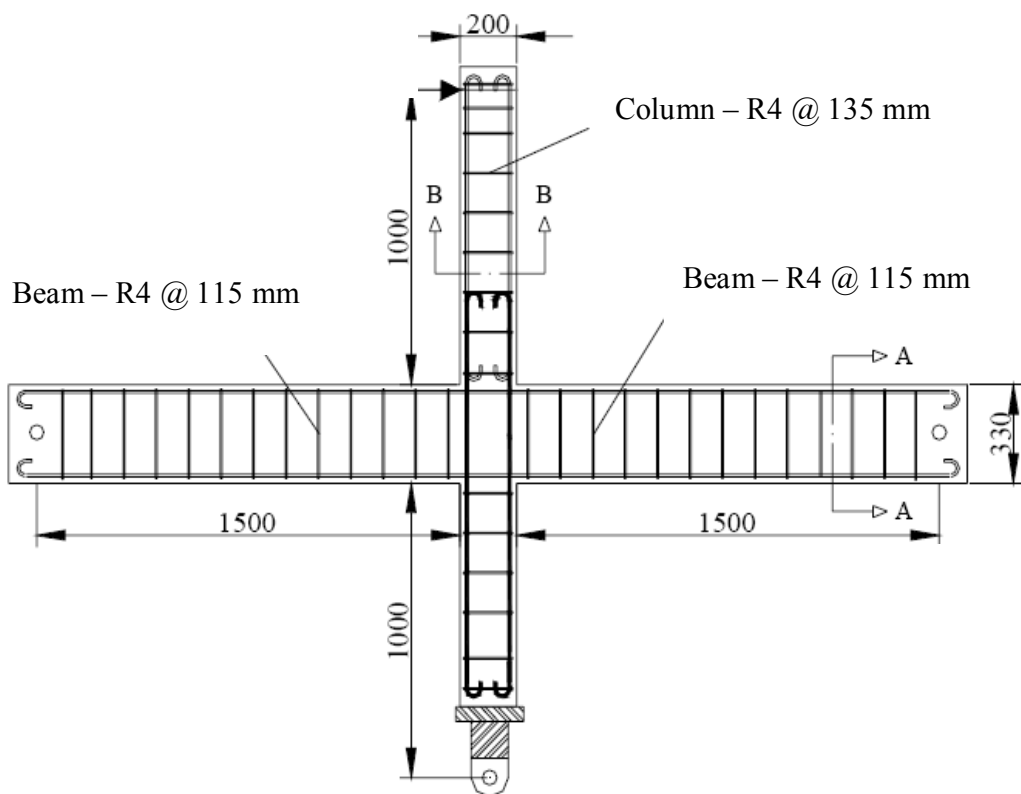


Fig. 4.11 Reinforcement Detailing for Specimen IS1 (Pampanin et al., 2005)

Test Set-Up and Loading:

The test set-up used for this specimen is shown in Fig. 4.12. A displacement-controlled loading system was used to apply the horizontal force at the top of the column. A constant axial load of 120 kN was applied to the top of the column with the

varying axial load equal to 1.4 times the shear force. The direction of this second axial load applied was changed according to the loading direction. The loading protocol followed for this specimen is given in Fig. 4.13. The specimen was subjected to three consecutive cycles of drift ratios from 0.2% to 3.5%.

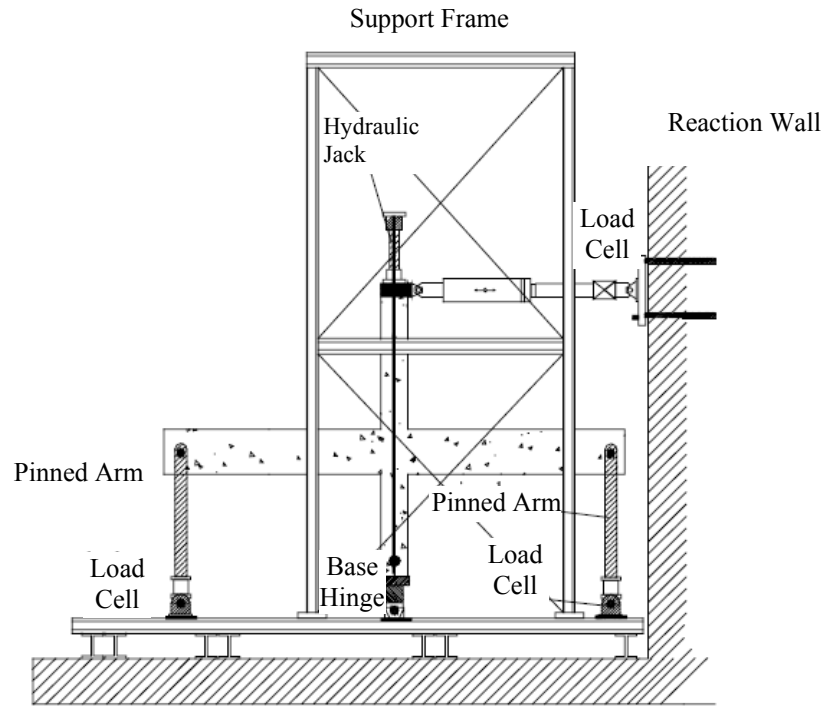


Fig. 4.12 Test Set-up for Specimen IS1 (Pampanin et al, 2005)

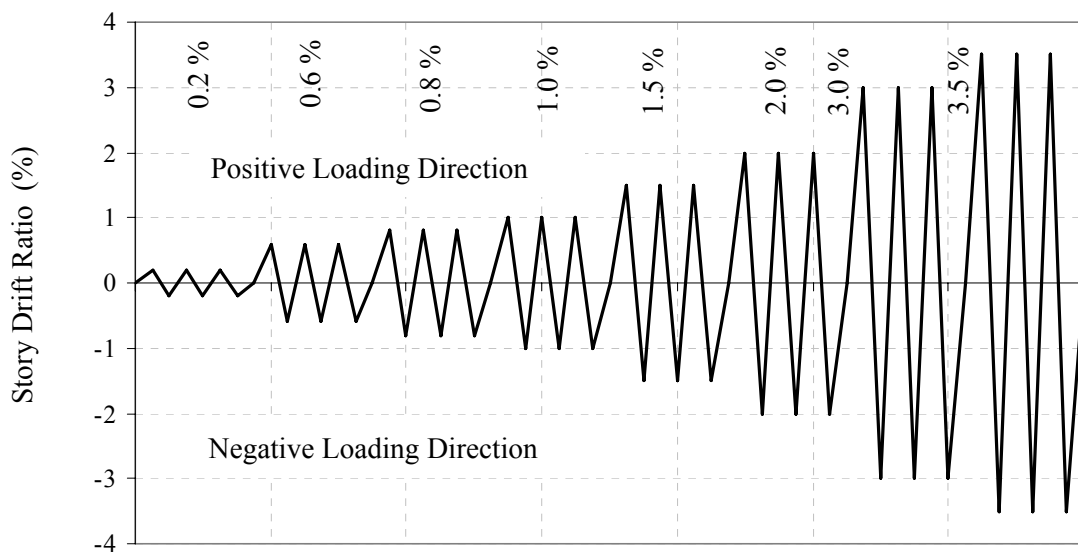


Fig. 4.13 Loading Protocol for Specimen IS1

4.1.2.2. FINITE ELEMENT MODELLING

Material and Regional Properties:

Four concrete regions were utilized in modelling this specimen. A total of 4670 rectangular concrete elements, with a 20 by 20 mm mesh configuration, were used to represent the interior beam-column subassembly. Detailed information about the concrete regions is given in Fig. 4.14 and in Table 4.10.

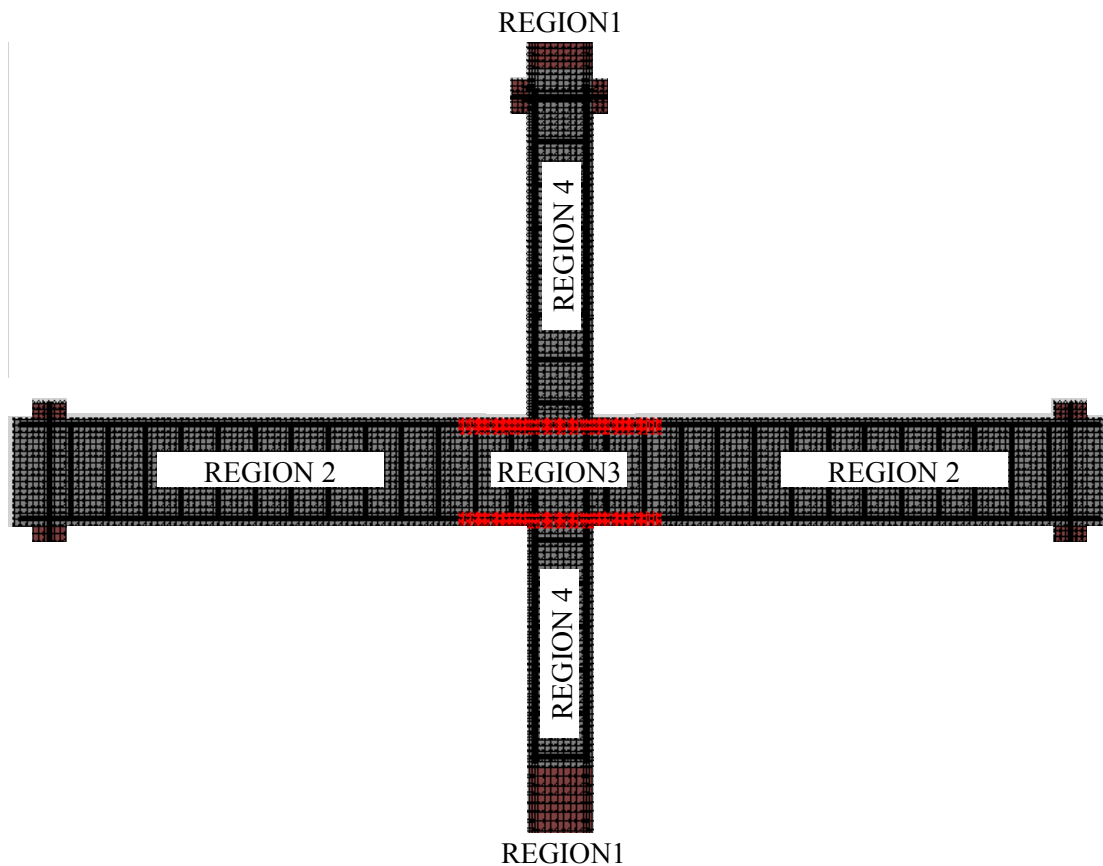


Fig. 4.14 Material Regions for Specimen IS1

Table 4.10 Concrete Regions for Specimen IS1

Concrete Region	# 1	#2	# 3	#4
Thickness (mm)	200	200	200	200
Mesh Size (mm)	20 x 40	20 x 20	20 x 20	20 x 20
Purpose	Bearing	Beam	Joint	Column
ρ_z (%)	None	0.28	None	0.24

The reinforcement and bond regions were modelled with 1196 truss elements and 78 bond-link elements. A representation of the reinforcement and the bond element configuration is shown in Fig. 4.15, and detailed information on the reinforcement regions is given in Table 4.11.

Table 4.11 Reinforcement Elements for Specimen IS1

Reinforcement	Type	Location
# 1	3 R8	Column Reinforcement
# 2	2 R8 + 1 R12	Beam Reinforcement
# 3	2 R4	Transverse Reinforcement
# 4	D20	Strengthening Rebar for Test Set-Up

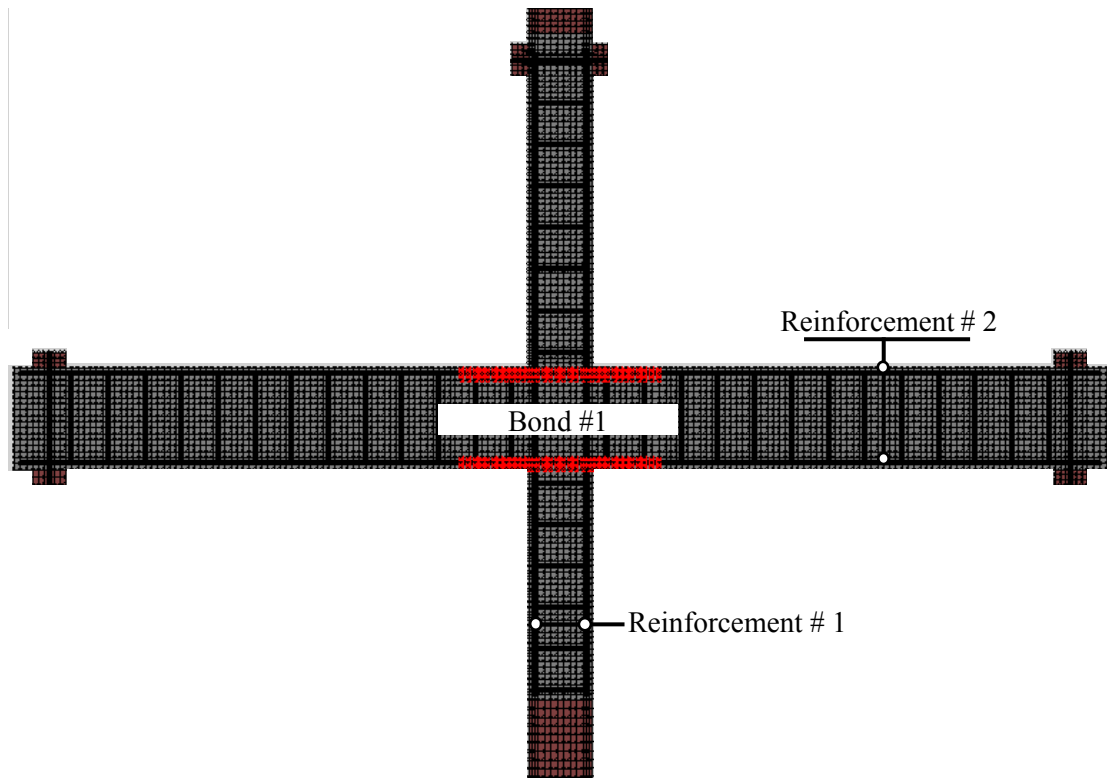


Fig. 4.15 Reinforcement and Bond Elements for Specimen IS1

The bond-slip effects were modelled with one bond-slip model. The joint of this specimen had no shear ties for confinement, and the connecting beam was a deep beam compared to the column. The bond-slip effects along the beam longitudinal bar were modelled with a smooth-bar bond behaviour. The smooth-bar bond-slip behaviour was adapted from the study by Fabbrocino et al. (2002). The bond stress-slip parameters used for modelling are suggested by and are given in Table 4.12.

Table 4.12 Bond Stress-Slip Parameters for Bond #1

τ_1 (MPa)	τ_2, τ_f (MPa)	Δ_1 (mm)	Δ_2 (mm)	Δ_3 (mm)
1.05	0.30	0.03	1.00	3.00

Loading and Restraint Conditions:

The loading protocol was modelled as described previously. Load Case 1 was the horizontally applied displacement-based reversed cyclic loading, Load Case 2 was the constant axial load applied to the top of the column, and Load Case 3 was the varying axial loading vertically applied to the top of the column. The restraints included a pinned support at the end of lower column, and two pinned rollers at the end of the beams.

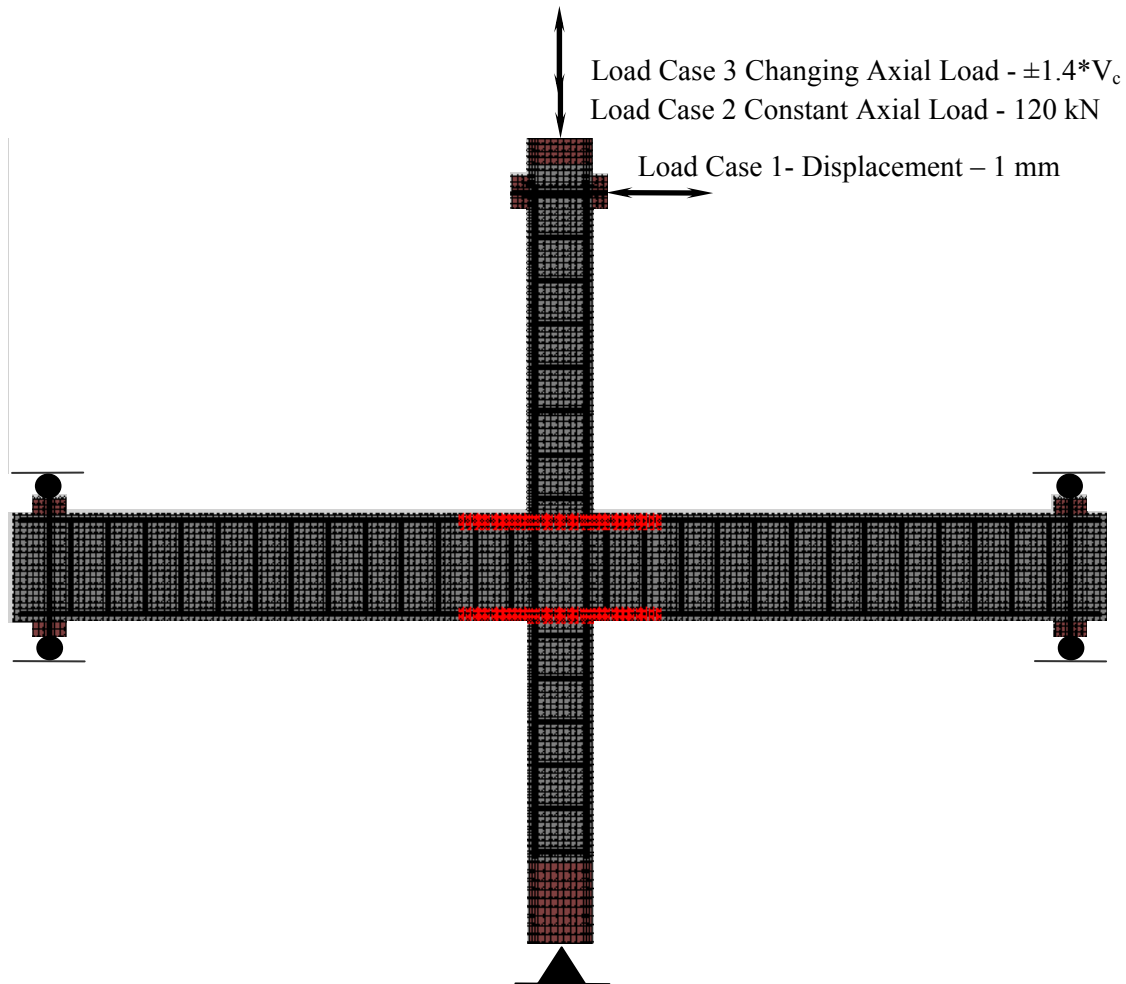


Fig. 4.16 Loading and Restraint Conditions for Specimen IS1

4.2.2.3. RESULTS OF EXPERIMENTAL AND ANALYTICAL STUDY

The interior beam-column subassembly showed a pinched hysteretic response and failed with shear cracking at the joint. Firstly, the shear cracking was observed in the joint, and then a drop in stiffness was observed at the 0.8% drift ratio both in the analytical and the experimental results. After reaching the ultimate shear force value at 3.5% drift, a softening in the hysteretic response was observed. However the specimen continued to carry a significant portion of the peak load up to the end of the experiment.

The information on the experimental results was limited compared to the other specimens examined in this study. The observed story shear force versus story drift behaviour and report of some events were the only experimental data that were available for this specimen. The predicted and observed load-deformation response is shown in Fig. 4.17. The failure mechanism and the sequences of events observed during the experiment were also compared to the VecTor2 analysis, and are given in Fig. 4.19 and in Table 4.13.

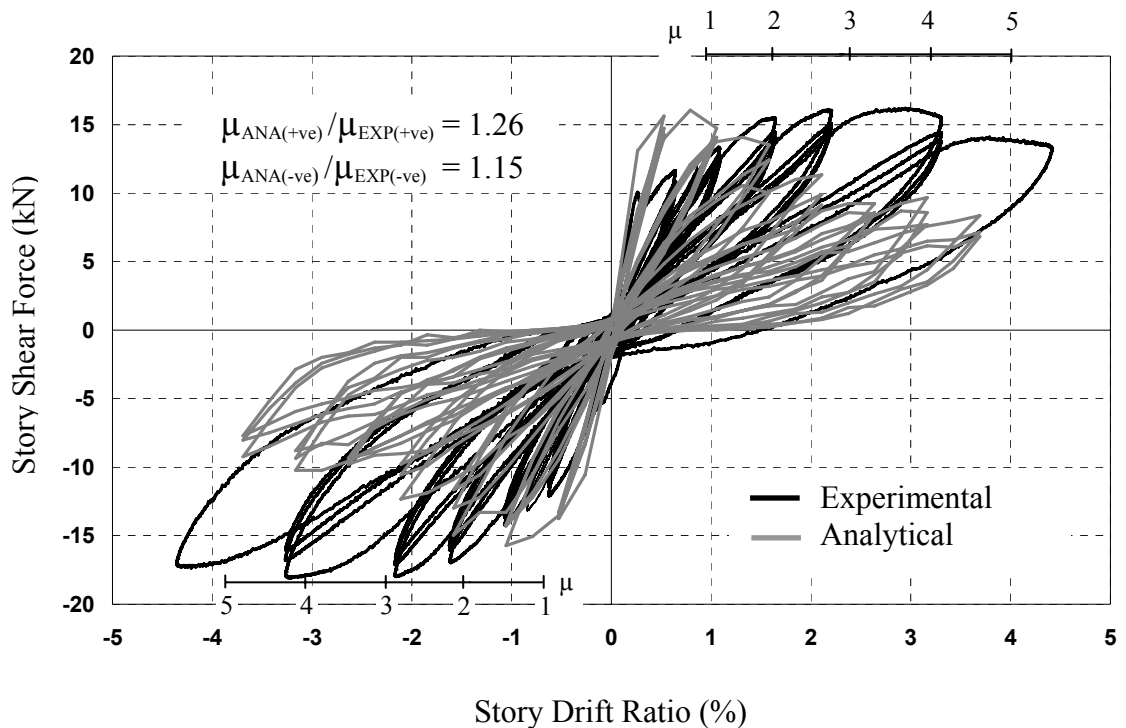


Fig. 4.17 Comparison of Story Shear vs. Story Drift Ratio for Specimen IS1

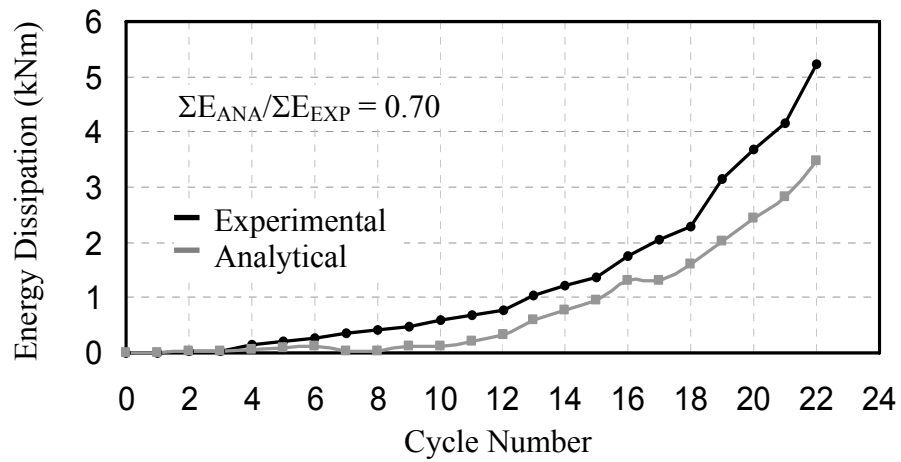
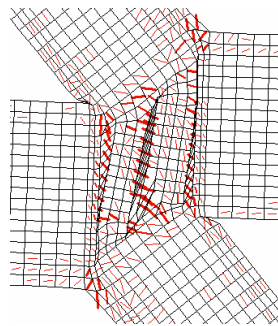


Fig. 4.18 Comparison of Energy Dissipation Capacity for Specimen IS1



Analytical

Fig. 4.19 Failure Mechanisms for Specimen IS1

The ratio of the predicted and observed ductility ratios for this specimen was 1.26 in the positive loading direction, and 1.15 in the negative loading direction. The energy dissipation capacity obtained from the predicted and observed response of the specimen was also given in comparison, and a ratio of 0.70 was obtained.

Table 4.13 Sequence of Events for Specimen IS1

Event	Experimental		Analytical	
	Story Shear (kN)	Story Drift (%)	Story Shear (kN)	Story Drift (%)
Positive Loading Direction				
First Shear Cracking	10.00	0.25	13.00	0.25
Max Story Shear	16.00	3.00	16.00	0.75
Negative Loading Direction				
First Shear Cracking	Not reported		10.00	0.25
Max Story Shear	17.00	3.25	15.00	1.62

4.3. RETROFITTED EXTERIOR BEAM-COLUMN SUBASSEMBLY

The last beam-column subassembly in this section was also a specimen tested by Pampanin et al., (2006). The specimen was retrofitted using a new technique which is effective in transforming the unwanted brittle failure mechanism to a seismically desirable ductile mechanism for non-seismically designed beam-column subassemblies. A specimen that is very similar to the previously examined specimen in this chapter (i.e. Specimen TDP2) was retrofitted and tested by Chen (2006).

4.3.1. RETROFITTING TECHNIQUE

Due to the poor quality of the concrete, reinforcement detailing and the absence of a seismic design philosophy, brittle failure mechanisms are usually observed in non-seismically designed beam-column subassemblies. As observed by earthquake reconnaissance teams over the years, this local failure leads to severe global failure mechanisms which endangers the lives of building occupants. Therefore, there is an urgent need to find efficient and economic solutions to this problem. Retrofitting of these existing buildings is the most expedient and practical solution since reconstruction in most cases is not possible.

The proposed scheme is a low-invasive and practical retrofitting technique when compared to other more evolved alternatives such as FRP wrapping (Pampanin et al., 2006). The focus in retrofitting the beam-column subassemblies is set on protecting the global integrity of the structure. The hierarchy of strength between the different components comprising the beam-column-joint assembly need to be altered. In this retrofitting technique, haunch bars are applied to the joint panel region of the structure. The stress flow around the joint is redirected to the beam, and a designated plastic hinge region in the beam is developed (Christopoulos et al., 2000; Pampanin et al., 2003). The brittle failure mechanisms around the joint panel regions can be prevented with the proper selection of the geometry and stiffness of the haunch elements, but capacity design considerations must be followed properly in order not to have shear failures in

the structural elements. The proposed haunch configuration and the modifications experienced in the internal force path are given in Fig. 4.20 and Fig. 4.21.

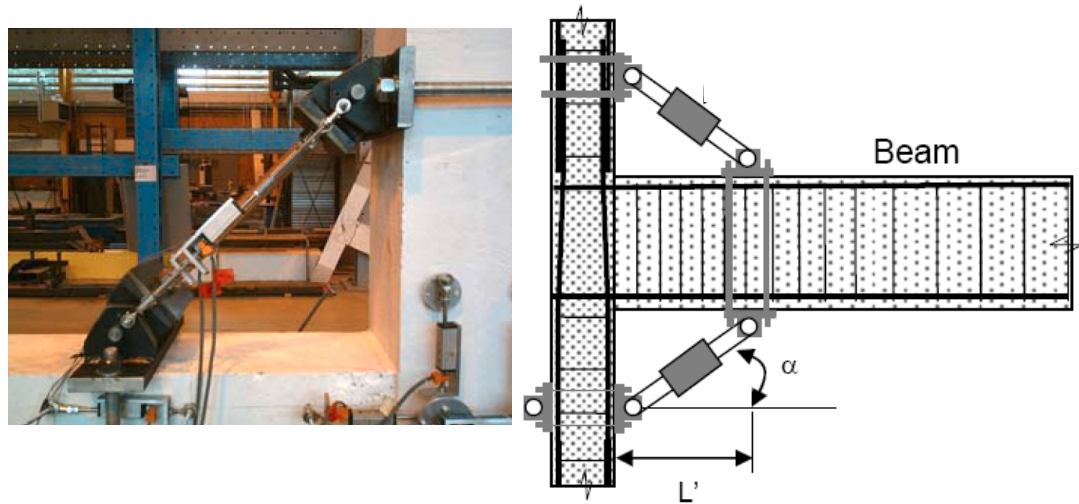


Fig. 4.20 Proposed Haunch Configuration (Pampanin et al., 2006)

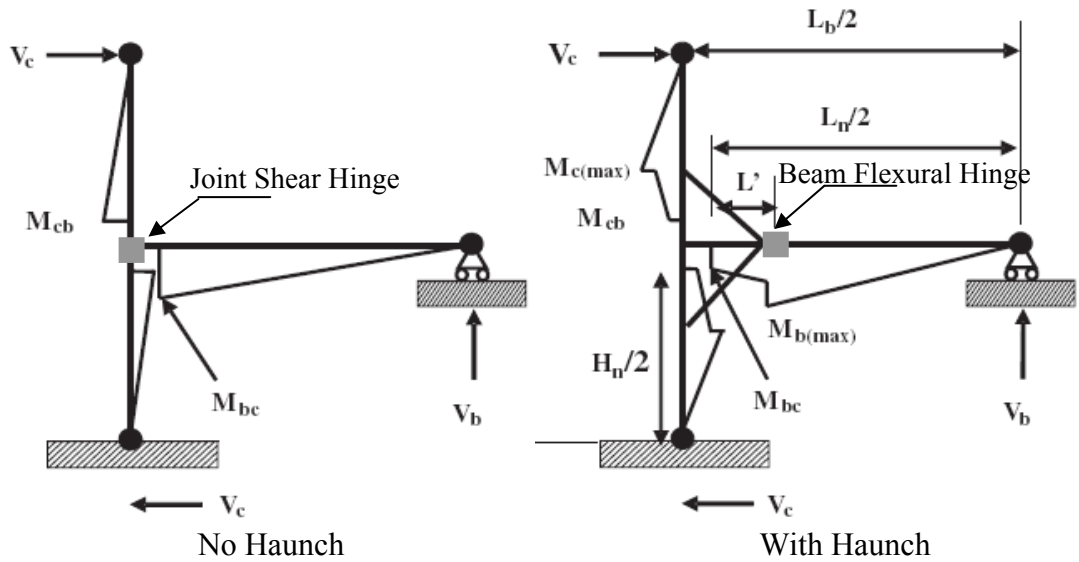


Fig. 4.21 Moment Diagrams of Exterior Beam-Column Subassemblies
(Pampanin et al., 2006)

An experimental study was conducted by Chen (2006) at the University of Canterbury, in New Zealand, to investigate the effectiveness of this technique on non-seismically designed exterior beam-column subassemblies. The seismic performance of these structures was substantially increased by using this technique to retrofit the exterior beam-column subassemblies. The strength and ductility of these structures were increased and plastic hinges were formed in the beam away from the joint panel region as desired. It was shown that this retrofitting technique is capable of protecting the joint panel region from extensive damage and brittle failure.

4.3.2. TEST SPECIMENS

Sectional and Material Properties:

In order to see the effects of this retrofitting technique, an exterior specimen similar to the Specimen TDP2 was tested by Chen (2006). Therefore, the sectional and material properties of this specimen were the same as those of Specimen TDP2. The concrete compressive strength and Young's Modulus was 25.9 MPa, and 28700 MPa, respectively. The reinforcement mechanical properties are given in Table 3.14. A detailed drawing of the retrofitted specimen is given in Fig. 4.22.

Table 4.14 Reinforcement Mechanical Properties

Type	Grade	Diameter (mm)	Area (mm ²)	f _y (MPa)	E _s (MPa)	f _u (MPa)
R10	300	10	78.5	344	228000	478
R6		6	32	396	198000	485

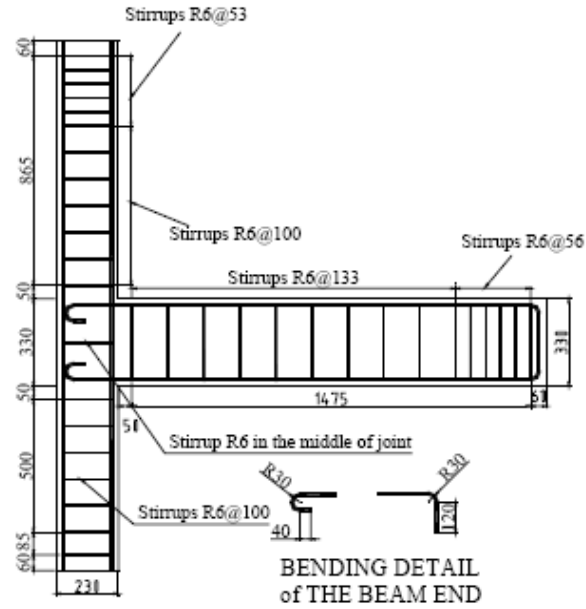


Fig. 4.22 Sectional Details for Specimen THR (Chen, 2006)

Test Set-Up and Loading:

A similar test set-up and loading protocol was followed during testing of this retrofitted beam-column subassembly to the Specimen ED3 and ES1 which was previously discussed.

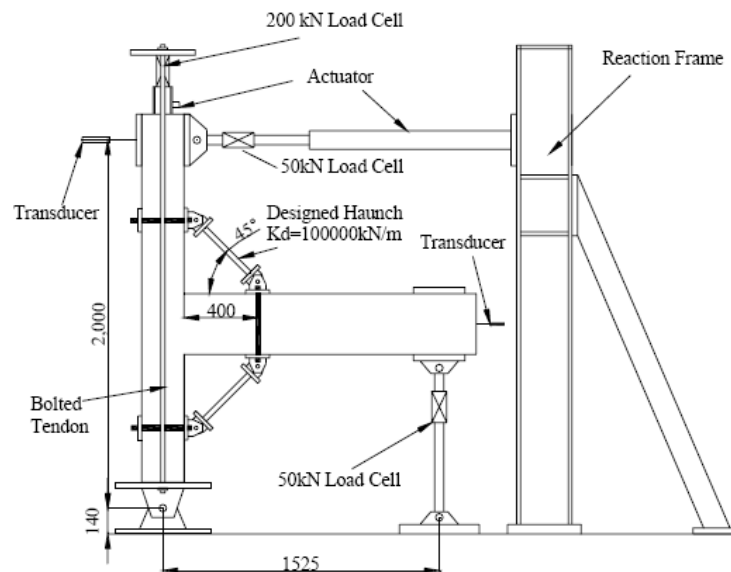


Fig. 4.23 Test Set-up for Specimen THR (Pampanin et al., 2006)

4.3.3. FINITE ELEMENT MODELLING

Sectional and Material Properties:

The retrofitted beam-column subassembly was modelled with seven concrete regions similar to the Specimen TDP2. A total of 1808 rectangular concrete elements, with a 25 by 25 mm mesh configuration, were used to represent the exterior beam-column subassembly. Detailed information about the concrete regions is given in Fig. 4.24 and Table 4.15.

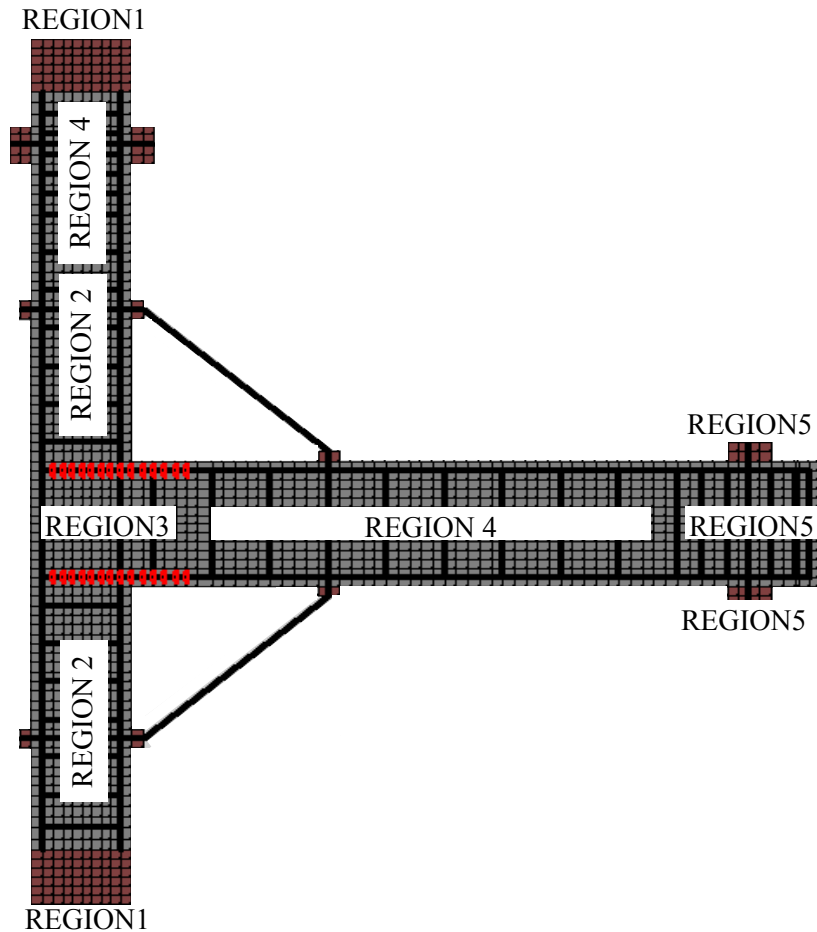


Fig. 4.24 Material Regions for Specimen THR

Table 4.15 Concrete Regions for Specimen THR

Concrete Regions	# 1 (#7)	#2	# 3	#4	#5	#6
Thickness (mm)	230 (200)	230		200		
Mesh Size (mm)	25 x 25					
Purpose	Bearing	Column	Joint	Column	Beam1	Beam2
ρ_z (%)	None	0.267	0.074	0.464	0.129	0.305

A total of 720 truss elements and 28 bond-link elements were used to represent the reinforcement and the bond regions. The reinforcement and the haunch bars were modelled with discrete truss elements. The strengthening for those regions was obtained by increasing the material properties of the concrete, and strengthening with reinforcement in these regions. Similar bond-slip behaviour was assigned to the bond-link elements as it was for the Specimen TDP1 and TDP2.

A representation of the reinforcement and the bond element configuration is shown in Fig. 4.25, and detailed information about the reinforcement regions is given in Table 4.16.

Table 4.16 Reinforcement Elements for Specimen THR

Reinforcement	Type	Location
# 1	3 R10	Column Longitudinal Reinforcement
# 2	4 R10	Beam Longitudinal Reinforcement
# 3	D14	Haunch Bars
# 4	2 R6	Transverse Reinforcement
# 5	D20	Strengthening Rebar for Test Set-Up

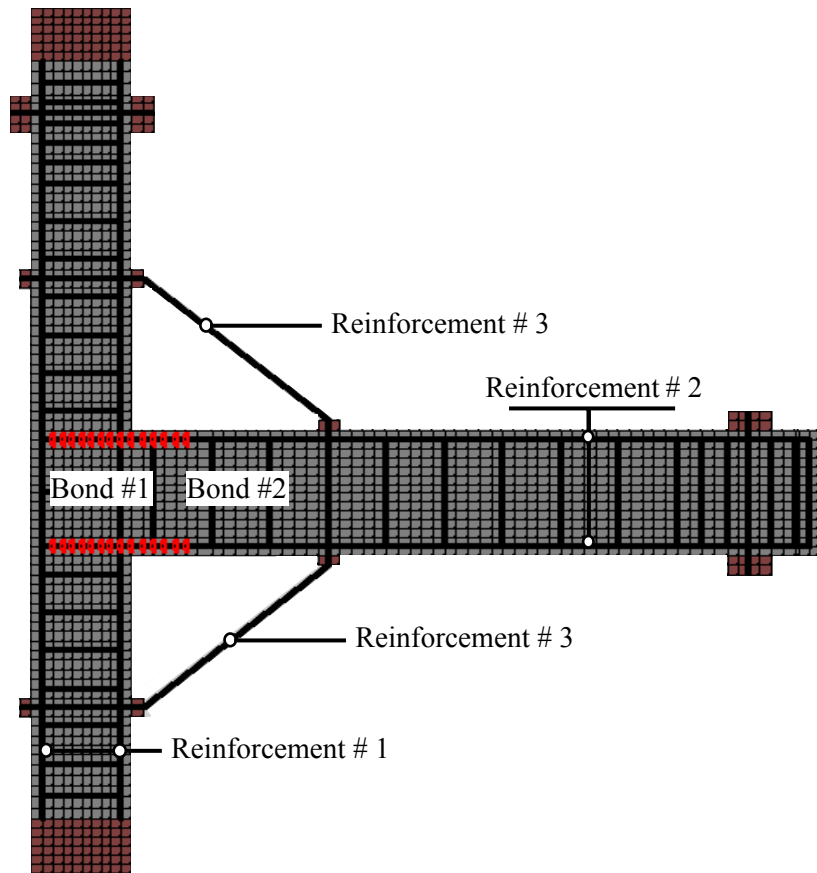


Fig. 4.25 Reinforcement and Bond Elements for Specimen THR

Loading and Restraint Conditions:

The restraint conditions consisted of a pinned support at the bottom of the lower column, and pinned roller supports at the end of the beam. The same loading protocol and loading system was followed for the analysis of this specimen as it was for the Specimen TDP1 and TDP2 (see Fig. 4.23).

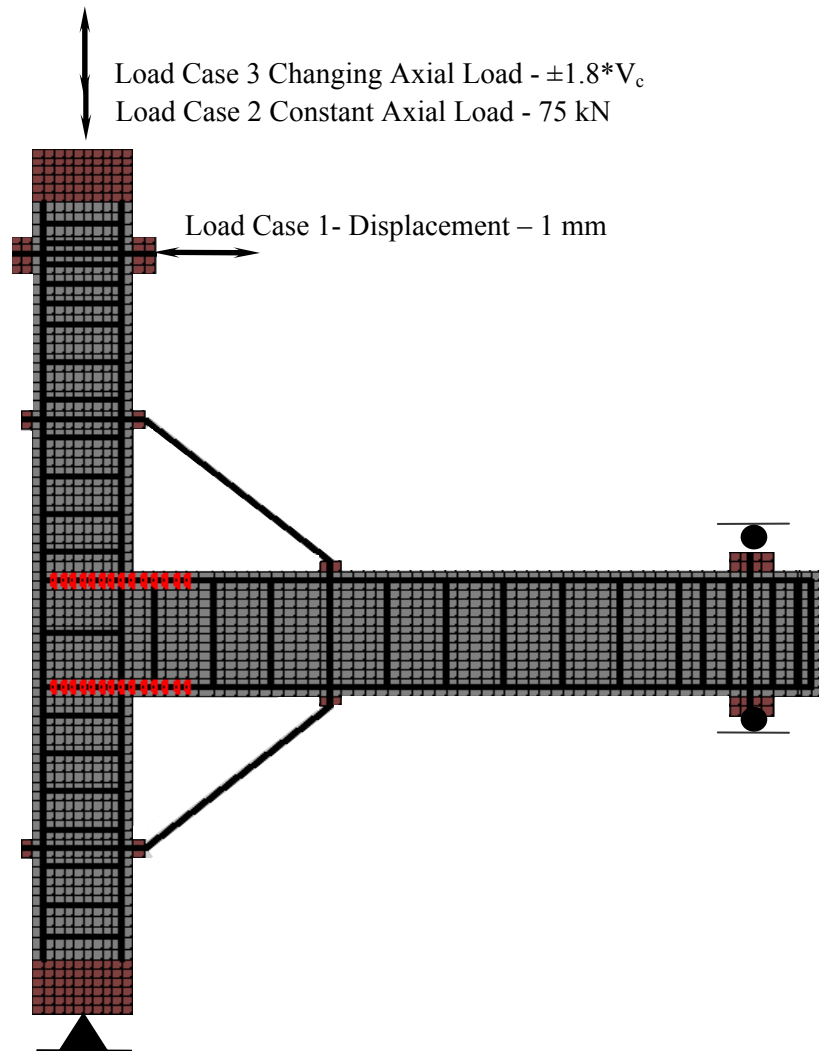


Fig. 4.26 Loading and Restraint Conditions for Specimen THR

4.3.4. RESULTS OF ANALYTICAL AND EXPERIMENTAL STUDY

In the experiment, the plastic hinge was successfully diverted to the beam. Minor cracks were reported around the joint by Chen (2006), but the flexural crack on the beam outside the haunched area dominated the failure mechanism. As previously explained in this chapter, Specimen TDP2 (the as-built configuration) had sustained a brittle failure mechanism with severe shear cracking in the joint panel zone. The hysteretic response of the member was changed from a pinched behaviour to a ductile and stable response. The excessive flexural cracking resulted in concrete spalling at this section of the beam. This retrofitting technique changed the brittle failure mechanism of a non-seismically

designed beam-column subassembly to a ductile one. The test was stopped due to the extensive cracking on the beam (Chen, 2006). The hysteretic response behaviour is compared to the VecTor2 analysis in Fig. 4.27.

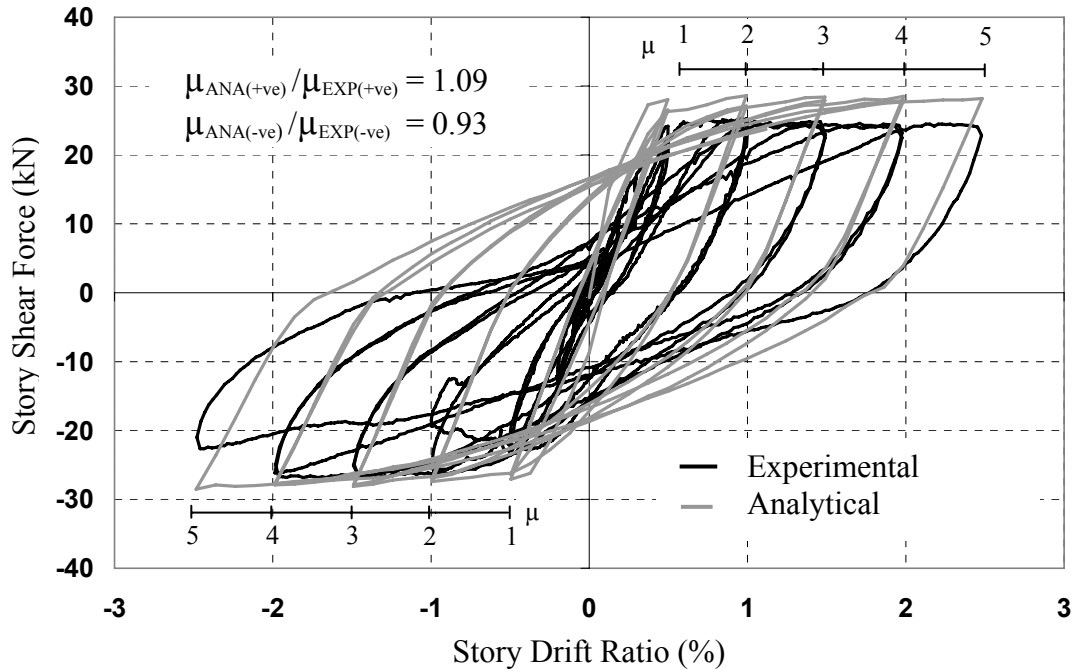


Fig. 4.27 Comparison of Story Shear vs. Story Drift Ratio for Specimen THR

The ductility ratios of the specimen was estimated in the positive and negative loading directions, and given in Fig. 4.27 for further comparison between the analytical and experimental results. The ratio of the predicted and observed ductility ratios for this specimen was 1.09 in the positive loading direction, and 0.93 in the negative loading direction.

The VecTor2 analysis captured the failure mechanism with a reasonably accurate load-deformation response. The flexural crack in the beam caused some stability problems during the analysis with the default concrete crack width options. The analysis was stopped at 1.0% drift cycle. After careful investigation of the problem, a successful analysis with the ‘Stability Check Omitted’ option for the ‘Crack Width Check’ was accomplished. The predicted response of the retrofitted specimen was in good

correlation with the observed response. The final failure mechanism and the sequences of events are also given in Fig. 4.29 and Table 4.17 for further comparison of the predicted and the observed response.

The energy dissipation capacity obtained from the predicted and observed response of the specimen was also given in comparison in Fig. 4.28, and a ratio of 1.42 was obtained.

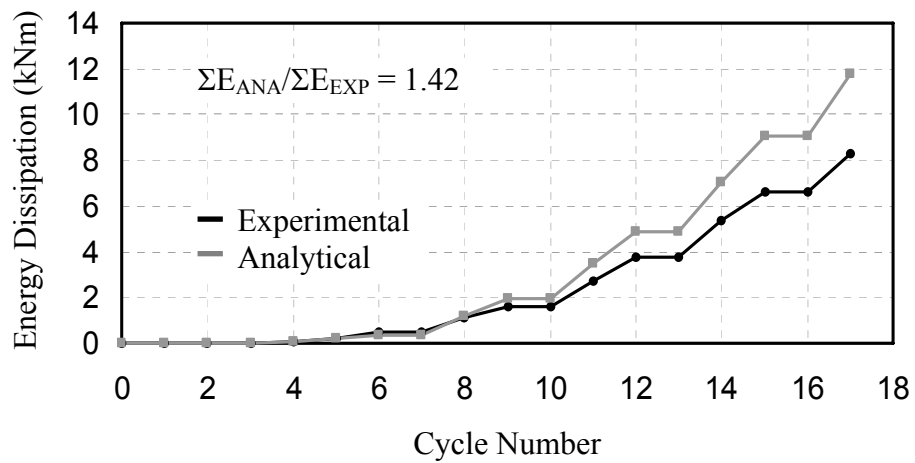


Fig. 4.28 Comparison of Energy Dissipation of Specimen THR

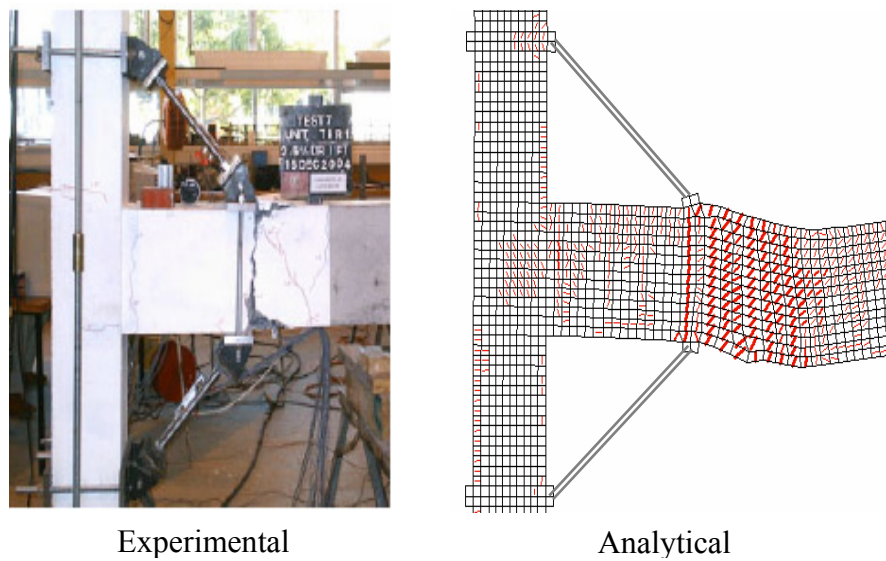


Fig. 4.29 Comparison of Failure Mechanisms for Specimen THR

Table 4.17 Sequence of Events for Specimen THR

Event	Experimental		Analytical	
	Story Shear (kN)	Story Drift (%)	Story Shear (kN)	Story Drift (%)
Positive Loading Direction				
Beam Hinging	25.0	0.5	28.0	0.5
Max Story Shear	25.5	1.0	28.6	1.0
Negative Loading Direction				
Beam Hinging	22.0	0.5	27.1	0.5
Max Story Shear	26.2	2.0	28.7	2.5

4.4. DISCUSSION ON RESULTS

This analytical study indicates that the VecTor2 analysis of beam-column subassemblies with the suggested modifications were reasonably accurate in modelling both seismically and non-seismically designed specimens. A retrofitted beam-column subassembly was also examined during this study, and the analytical results were in good agreement with the experimental results and captured the improved response and failure mechanism of this retrofitted specimen. Considering an analytical study by Wong and Vecchio (2003) on FRP retrofitted beams, it is very likely that VecTor2 can be used as an assessment tool for future retrofitting applications.

The differences in energy dissipation capacity or strength degradations in analytical results can only be explained through the behaviour of the bond-slip model. The bond-slip models applied to smooth reinforced specimens were adapted from an experimental study on concrete blocks embedded with straight and hooked end smooth bars (Fabbrocino et al., 2002; Fabbrocino et al., 2004). Due to limited experimental data

on smooth bar bond behaviour, a bond model wasn't developed. The material bond-slip behaviour results were directly taken and used on the smooth bars without any modification. The current smooth bond model was able to capture the peak story shear force and ultimate ductility, but further studies are needed with the availability of new data on smooth bars.

CHAPTER 5

Guidelines for Modelling Beam-Column Subassemblies

An important goal of every research endeavour should be to assimilate and convey the knowledge gained through the process of the research. Not only should the results of the research be provided, but also the solutions developed to problems encountered during this research. These conclusions can be valuable for future studies in the research area. Therefore, detailed information on the modelling of beam-column subassemblies is provided in this chapter.

There were four different types of beam-column subassemblies that were encountered, and modelled, in this study. Three of these were exterior beam-column subassemblies. The first two were non-seismically designed beam-column subassemblies designed with either 180° hooked end deformed bars or smooth bars. The third specimen was also an exterior specimen. The beam longitudinal bars were connected to steel plates at the end of the beam. The last specimen was a typical interior beam-column subassembly with either smooth or deformed bars where the beam longitudinal reinforcement passes along the beam and joint continuously.

5.1. CONCRETE

VecTor2 has three element options for concrete regions. Rectangular plane stress elements were used for modelling the concrete regions in this study. The beam-column subassemblies were also modelled using the quadrilateral elements for the concrete regions. A comparison of these models showed no significant difference in the analysis results. Therefore, the concrete regions of the specimens examined in this study were all modelled with the rectangular elements.

Accurate meshing of concrete regions is an important parameter in any finite element modelling study. It is always advised to start modelling with a relatively coarse mesh. This approach will lower the computation time, and will also ease the

interpretation of the results. After careful examination of the results, the number of elements can gradually be increased by using a finer mesh. The concrete meshing was carefully studied with different options on beam-column subassemblies, and it was found that assigning 10-15 elements in horizontal direction in the joint panel region is an adequate rule in defining mesh parameter. The joint panel region is where all the deformation and bond-slip action occurred; therefore it's very important to assign an accurate mesh to this region. In order to avoid a large number of elements and long computation time, a finer meshing can be assigned to this region while maintaining the aspect ratios of the types of elements that are selected.

The analysis of the beam-column subassemblies were performed using the default behavioural models for the material properties. The reason for this approach was to be able to examine these specimens in the simplest way that is available in VecTor2. The material models are assigned by the user, unless the default values are found to be adequate. All the model options should carefully be examined by the user before assigning an option different than the default model. The detailed information on the behavioural models are given in the "VecTor2 and FormWorks Manual" by Wong and Vecchio (2002). The behavioural and constitutive models in VecTor2 consisted of well known and accepted models, some of which developed through extensive experimental research at the University of Toronto. The results of this study also provided an understanding of these behavioural models. The capabilities of some of the model options were also examined in this thesis. Currently, the default behavioural and constitutive models that are suggested for starting a preliminary study, are given in Table 5.1, and the models that best suited the specimens examined in this study are shown on the "Definition of Models" window (see Fig. 5.1).

The “Hysteretic Response” feature for the concrete material models were investigated on different specimens tested under reversed cyclic loading conditions. The default hysteretic model option for the concrete is “Nonlinear w/ Plastic Offsets”. The applications of this model to the beam-column subassemblies under reversed cyclic loading conditions proved that “Palermo 2002 (w/Decay)” is a better option. The analysis results of load-deformation behaviour with the default option resulted in higher stiffness values compared to the experimental results. The effects of previous loading conditions which might result in plastic deformations were successfully captured with the “Palermo 2002 (w/Decay)” option.

Table 5.1 Default Material Models in VecTor2

Material Property	Model
Concrete Compression Pre-Peak Response	Hognestad Parabola
Concrete Compression Post-Peak Response	Modified Park-Kent
Concrete Compression Softening	Vecchio 1992-A (e1/e2-Form)
Concrete Tension Stiffening	Modified Bentz 2003
Concrete Tension Softening	Linear
Concrete Tension Splitting	Not Considered
Concrete Confined Strength	Kupfer/Richard Model
Concrete Dilation	Variable Kupfer
Concrete Cracking Criterion	Mohr-Coulomb (Stress)
Concrete Crack Slip Check	Vecchio-Collins 1986
Concrete Crack Width Check	Agg/5 Max Crack Width
Concrete Hysteretic Response	Nonlinear w/ Plastic Offsets

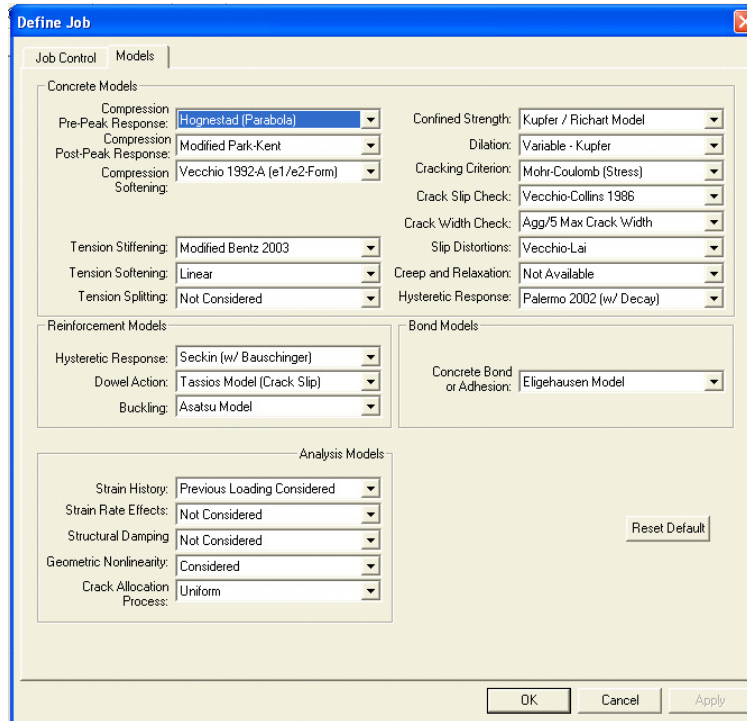


Fig. 5.1 Definition of Material Behaviour Models

The “Crack Width Check” was another feature that was investigated in this study. The default option for this feature usually did not interfere with the analysis results. However, the beam-column subassemblies designed with no or very little shear reinforcement and/or members that were experiencing excessive flexural cracks, needed further attention with this model. In some cases, the analysis suddenly stopped due to numerical stability problems. If any type of stability problem occurred during the analysis, the iteration stopped and the message “Stiffness matrix is not positive definite” error was displayed. Neither the predicted load-deformation behaviour of the specimens, nor the experimental results of the same specimen, showed any signs of failure at that stage. This was experienced in modelling the non-seismically designed members. It is advised to increase the crack width limits, if any of these kinds of stability problems are encountered during the VecTor2 analysis.

Changes in the behavioural or constitutive models of VecTor2 should be done to reflect the differences in the applied loading or the material properties that are specific to

the structure that is analyzed. The modifications without a firm understanding of each models' applicability area might lead to unrealistic and erroneous results. The modifications made to match the experimental research results are never encouraged, since there is no scientific study or physical reason to make such changes.

5.2. REINFORCEMENT

Reinforcement elements can be modelled with either smeared or discrete reinforcement options. The initial models of the beam-column subassemblies were constructed using smeared reinforcement elements to represent the reinforcement regions. After a detailed investigation on the bond-slip effects of reinforcement to the seismic performance of these structures, the selection of the discrete truss elements for representing the reinforcement was unavoidable. Both the longitudinal and transverse reinforcement in the specimens were modelled as discrete truss bar elements. The application of the bond elements was only made possible by using the discrete reinforcement elements. The use of these elements allows the local stress-strain values on the reinforcement to be examined.

When assigning the reinforcement elements, the confinement effect of the shear reinforcement in the beams and columns was also considered. The smeared reinforcement was used to represent this out-of-plane confinement effect. This modelling approach was very important for the well-confined sections of the specimens, where the loading system or restraint conditions were introduced to the system.

Another warning that might be useful in modelling beam-column subassemblies was a stability problem related to the reinforcement models. A stability error occurred during the analysis of some specimens due to excessive cracking and reinforcement shearing. This incident was related to the specimens experiencing excessive flexural cracking at the beam-column face. The focus was given on one of the reinforcement model options to avoid this problem. The "Dowel Action" feature has the default "Tassios (Slip)" option available in VecTor2. If a certain stability problem during the

analysis was encountered the “Tassios (Strength)” option would be a solution to this problem.

Table 5.2 Material Behaviour Models

Material Property	Model
Reinforcement Hysteretic Response	Seckin Model (Bauschinger)
Reinforcement Dowel Action	Tassios Model (Crack Slip)
Reinforcement Buckling	Asatsu Model

5.3. BOND

Beam-column subassemblies are subjected to severe reversed cyclic loading conditions under seismic effects. The integrity of these structures is crucial for the survival of the whole structure in a moment resisting framed building. The concrete and the reinforcement interaction play an important role in the load transfer mechanisms. Previous research on bond-slip effects and on the seismic performance of the beam-column subassemblies proved that ‘perfect bond’ conditions weren’t present, especially for non-seismically designed structures. Therefore, an additional element at the interface between the concrete and the reinforcement elements was needed for the accurate estimation of this imperfect bonding condition. The distinction between confined and unconfined regions, and confinement pressure values selected were done according to the recommendations by Eligehausen et al. (1983) and the CEB-FIB MC90 (1993).

5.3.1. DEFORMED REINFORCEMENT BOND MODELLING

The bond modelling of two different types of beam-column subassemblies were described in this section. The first one was an exterior beam-column subassembly with an unconfined joint panel. The beam longitudinal reinforcement was not extended into the joint, and had 90° hooked ends in Specimen ED3. Bond-slip elements were introduced to the model similar to the suggestions made by Soroushian et al. (1988) on modelling beam-column subassemblies. The specimen was modelled in two regions with

two bond material models, but the analysis results showed a problem at the connection of the imperfectly bonded nodes to the reinforcement nodes. The specimens failed due to flexural cracks at the nodes where imperfectly bonded elements introduced to an element with a different bond material property. It was understood that the connection of the perfectly bonded and imperfectly bonded elements was the main problem. Therefore, the bond material properties were changed accordingly, and one bond material with a perfectly bonded node was assigned to the bond-link elements. As can be seen below in Fig. 5.2, the “Imperfect Bond” box when selected, assigns the bond and reinforcement material property to the member that has been selected for the element. The first and last connection nodes of the imperfectly bonded reinforcement were assigned as a perfect node. This approach helped to avoid the unrealistic local failures between different bond materials. The “Hooked Bar” option, which was developed based on the findings of Eligehausen et al. (1983) and Soroushian et al. (1988), was selected with the proper confinement pressure values as shown in Table 5.3.

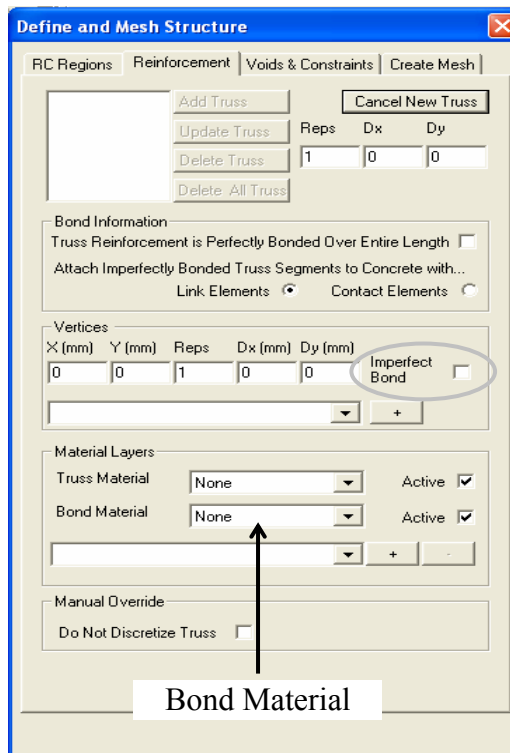


Fig. 5.2 Reinforcement and Bond Region Window for Automatic Mesh Option

The configuration of bond-link elements and confinement pressure index values that were selected for these specimens are given in Fig. 5.3 and Table 5.3.

Table 5.3 Bond Elements

Type	Bond # 1
Confinement Pressure (MPa)	$\rho_v * f_{yv} * 7.5$
Hooked Bar	Selected

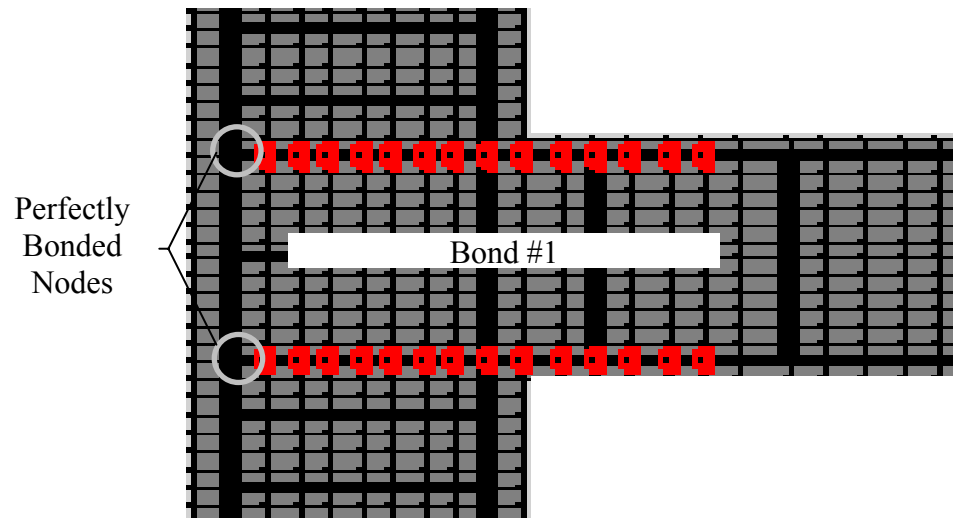


Fig. 5.3 Bond Element Configuration for Specimen ED3

The second beam-column subassembly that required a different bond modelling approach can either be a seismically designed exterior or an interior specimen. In the first case, the beam longitudinal reinforcement was extended beyond the joint region horizontally and connected to a steel plate at the back of the column. As shown in Fig 5.4, the beam longitudinal bars were welded to the steel plates, which were connected to the column.

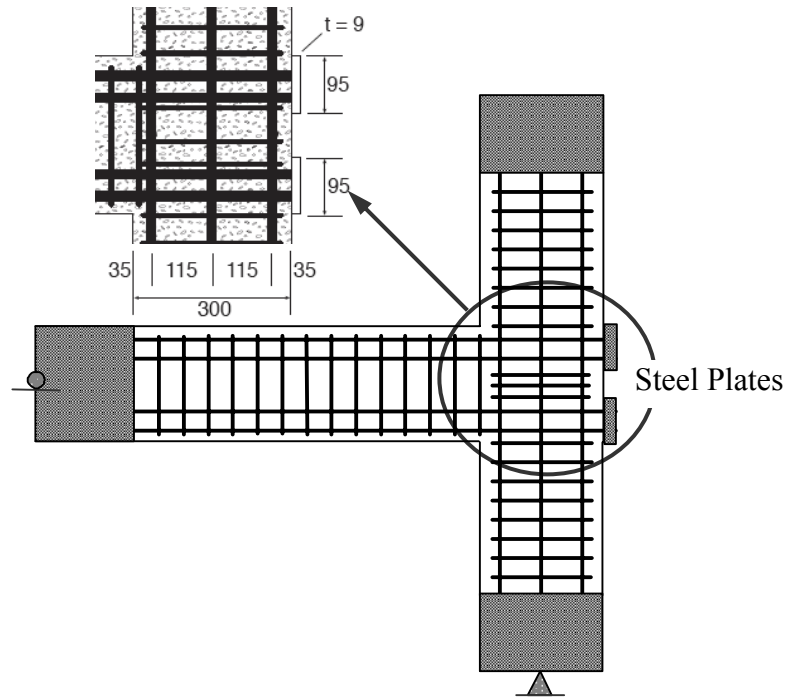


Fig. 5.4 Exterior Beam-Column Subassembly

The bond elements were modelled with two different bond material models. The transverse reinforcement along the beam provided a well-confined concrete region in the joint. This region within the joint was defined as a confined region, and a 7.5 MPa confinement pressure value was assigned to these elements (Eligehausen et al., 1983; CEB-FIB MC90, 1993). The rest of the longitudinal bars were modelled by assigning the unconfined region properties to the elements. The shear reinforcement provided in the beam was used to estimate the confinement pressure value for this region. The configuration of bond-link elements and confinement pressure index values selected for each bond-link element is given in Fig. 5.5 and Table 5.4.

Table 5.4 Bond Elements

Type	Bond # 1	Bond # 2
Reinforcement	Beam Top and Bottom Layer Longitudinal	
Confinement Pressure (MPa)	$\rho_v * f_{yv} * 7.5$	7.5

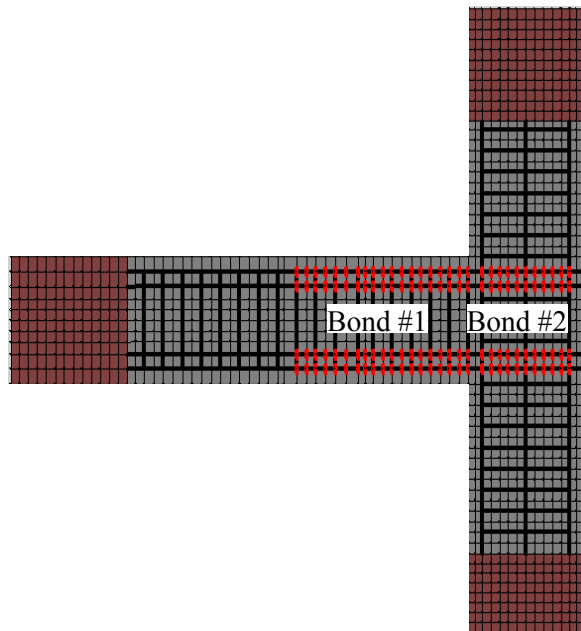


Fig. 5.5 FE Model of Exterior Beam-Column Subassembly

The bond elements should start, and end with a perfectly bonded node. This can only be accomplished at the member sectional configuration step by activating or deactivating ‘Imperfect Bond’ option as illustrated in Fig. 5.6.

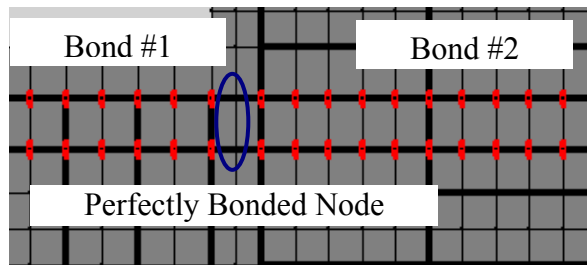


Fig. 5.6 Bond Material Connection Details

The interior beam-column subassemblies can be modelled with the same approach. The confined bond regions within the joint panel and unconfined bond regions at each side of the joint are shown in Fig. 5.7.

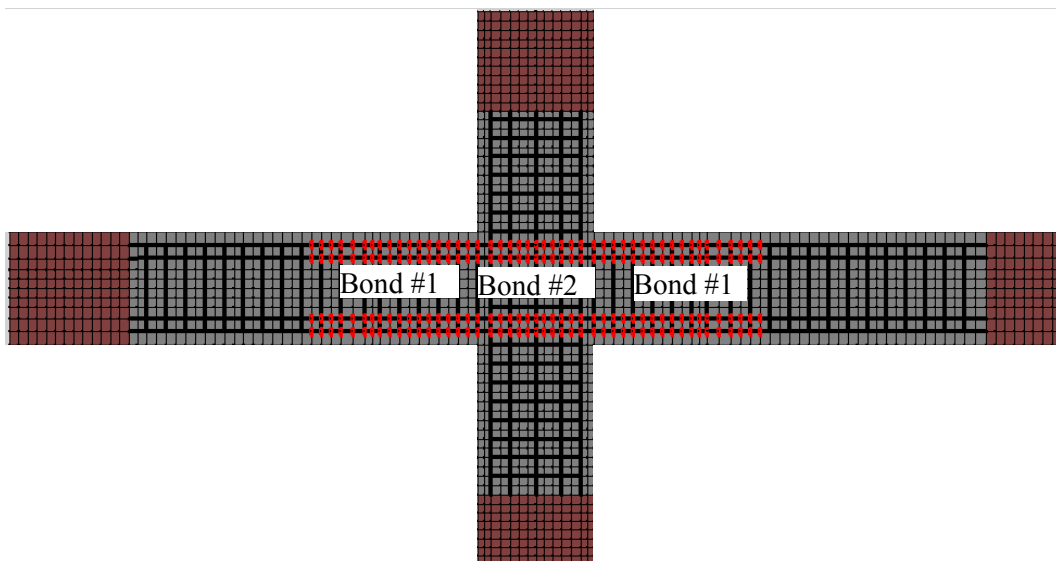


Fig. 5.7 Interior Beam-Column Subassembly

5.3.2. SMOOTH REINFORCEMENT BOND MODELLING

The specimen was an exterior beam-column subassembly designed with hooked end smooth reinforcement at the joint. The reinforcement detailing of this specimen was modelled in two regions. As shown in Fig. 5.8, the perfect bond model was used to represent the hooked end section, and the straight smooth bar section was modelled by using the user defined bond-slip behaviour option. This option was recently added to the program to be able to assign a bond-slip curve for the embedded bars (see Fig. 5.9).

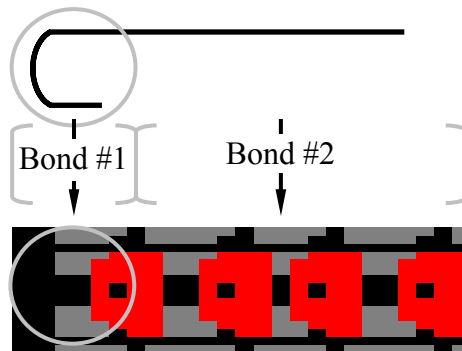


Fig. 5.8 Bond Element Configuration for Hooked End Bars

As described in Chapter 4 for the smooth-bar bond behaviour models, these beam longitudinal bars were modelled based on the experimental study results by Fabbrocino et al. (2002). These values are given in Table 5.5.

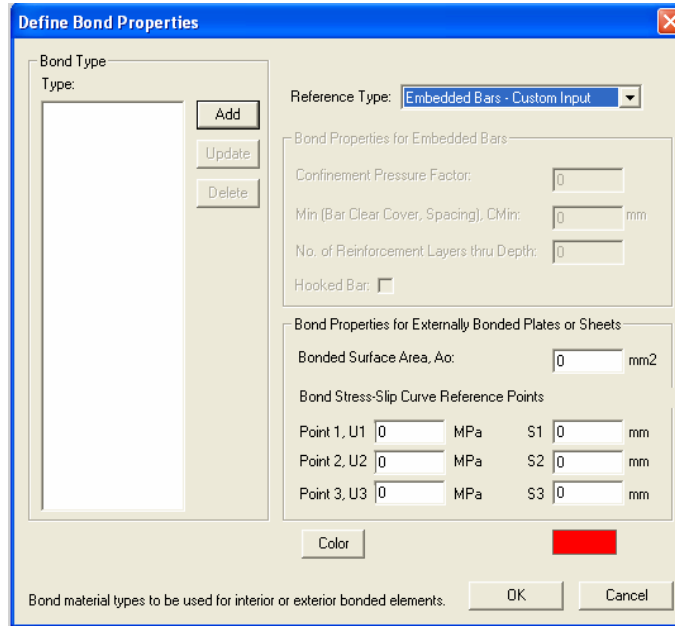


Fig. 5.9 Custom Input Option for Embedded Bars

Table 5.5 Bond Stress-Slip Parameters for Smooth-Bar

Parameter	Bond # 1	Bond # 2
	Hooked End	Straight Section
τ_1 (MPa)	250	1.05
τ_2 (MPa)	250	0.3
τ_f (MPa)	250	0.3
Δ_1 (mm)	0.1	0.03
Δ_2 (mm)	3.0	1
Δ_3 (mm)	10.0	3

5.4. SIMULATION OF LOADING SYSTEM

The simulation of the loading system for the beam-column subassemblies was achieved with a firm understanding of the possible failure mechanisms and of the capabilities of VecTor2.

The seismic loading conditions were simulated with a displacement-based loading, and constant axial load applied to the top of the column. The restraint conditions allowed the movement of the columns in the horizontal direction, but limited the vertical movement of the beams. The specimens were fixed to the reaction floor by steel threaded bars to limit the movement in certain directions. Steel bearing plates were also used for accurate load transfer and prevention of local failures at the support regions.

The displacement-based loading was applied by a similar system in order to ensure that the load transfer from the actuator to the structure was accomplished. The simulation of this loading and support system was accomplished by strengthening these sections. The beam ends were restrained with pinned rollers, and steel plates connected with 20 mm steel bars were placed to the top and bottom of the beam as illustrated in Fig. 5.10a. A similar support system used during testing was applied to displacement-based load applied to the node as shown in Fig.5.10b. In the regions where a support or loading system was introduced, strong and stiff concrete regions were assigned at the section between the structure and the loading or support system. These sections were prevented from sustaining any possible local failure with this approach.

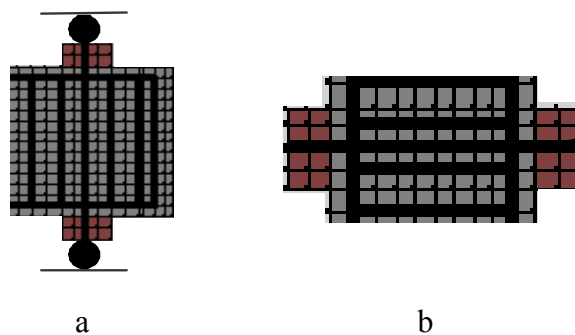


Fig. 5.10 Support Conditions Parameter

5.5. ANALYSIS OPTIONS

The definition of the ‘Job data’ is one of the important steps in defining the analysis options and the loading protocol to be followed during the analysis. The ‘Job data’ window is shown in Fig. 5.11. VecTor2 uses an iterative process during the analysis, and the maximum number of iterations that will be computed before proceeding to the next load stage is determined by the “Max. No. of Iterations’ option. The default parameter is 100 for the maximum number of iterations, and this value can be changed to lower the computation time after careful investigation of the analysis results. The default value for ‘Dynamic averaging factor’, which is used to update the material stiffness coefficients between the iterations, is assigned to 1.0. However, for an accurate analysis of the non-seismically designed structures a value not higher than 0.5 for the averaging factor was required. The bond-slip behaviour under reversed cyclic loading was accurately computed by using this value.

The loading protocols followed for the beam-column subassemblies were not consistent for all tests. The loading might be stopped for stability reasons or the loads were applied in different amplitudes to better simulate the seismic loading effects. This type of loading can be accomplished with the SEED file option of VecTor2. It is important to select the “ASCII and Binary Files” option for the result files. The default option for this feature is “ASCII Files Only”, and this creates the results of each iteration step in a text file format with a *.A2E extension. The “ASCII and Binary Files” option so that an additional file with a *.A2R extension, which is essential for the combination of separate analysis results, is created for each load increment. The “Seed File Name” is the box where the last step of the previous analysis is stored, and the “Starting Load Stage No.” is the first load step for the current analysis.

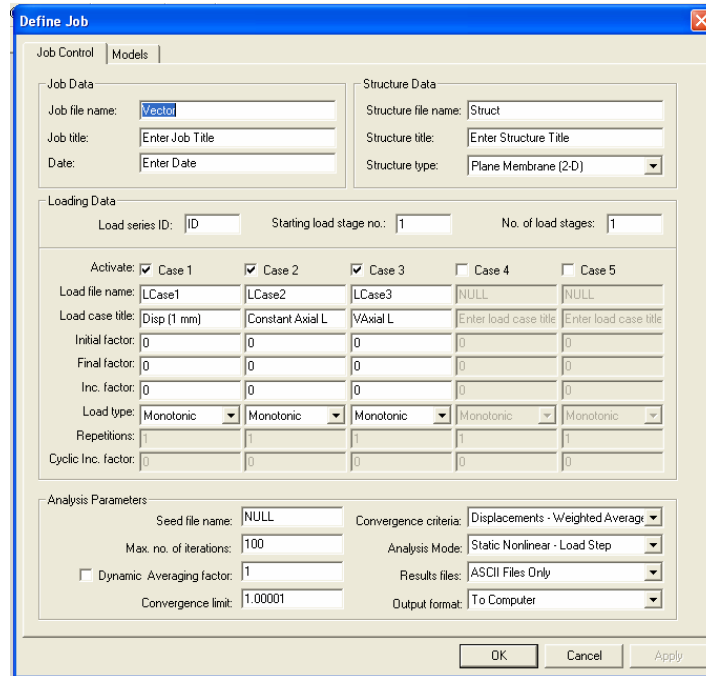


Fig. 5.11 Definition of Job Data

When cyclic and reversed cyclic loading type is selected, “Repetition” and “Cyclic Inc. Factor” option are activated for data entry. Five different loading systems can be applied to the program, separate from each other at the same time. However, the increments of each load type have to be consistent with the iteration number created. Otherwise, when one loading type is applied properly, the other one isn’t.

The displacement-based loading was applied using the “Support Displacement” option, and the “Nodal Load” option was used to represent the axial loading applied to the top of the columns.

5.6. INTERPRETATION OF RESULTS

After series of iterations, the analysis results can be extracted by examining the result text files or by using the post-processor, Augustus.

Augustus (©Bentz, 1996-2007) provides a user friendly output program for VecTor2. The general load-displacement results, average and crack stress-strains for

both concrete and reinforcement elements, visual crack formation and deformation of the structure, and various other result options are available for the user. The figures, and result data can easily be transferred to the computation software for more extensive graphical representations.

The analysis results can also be examined using the*.A2E text files. These files are created at the end of each load step. All the analysis results that aren't available in Augustus can be seen in further detail in these files. One parameter that was very important in this study, the bond-slip behaviour, can not be observed in the Augustus program. The stress-slip behaviour of each bond element is provided to the user for further investigation of the interaction between the reinforcement and the concrete.

Whether the program Augustus or the result text files are selected for the interpretation of the results, a wide range of data that might be crucial for the structure modelled is available to the user.

CHAPTER 6

Discussion and Conclusions

6.1. SUMMARY

An analytical investigation was carried out to investigate the effectiveness of the finite element modelling capabilities of VecTor2 in capturing the nonlinear cyclic response of beam-column subassemblies. The specimens considered covered a wide range of conditions, and included interior and exterior and seismically and non-seismically designed beam-column subassemblies.

The specimens were examined with particular attention to the effects of shear deformations in the joint regions and bond-slip effects of the beam longitudinal reinforcement. The hysteretic response under seismic loading conditions, failure mechanisms at selected story drift levels, and crack formations for each specimen were carefully examined, and compared to the experimental results. The sequence of events for each specimen also provided for further comparison of the predicted and the observed behaviour of the specimens, as did the energy dissipation characteristics.

6.2. CONCLUSIONS

The analysis results for each specimen were carefully examined, and compared to the experimentally observed behaviour, and the following conclusions can be drawn regarding the modelling capabilities of VecTor2:

- The finite element analysis program, VecTor2 was successful in estimating the hysteretic load-deformation response of beam-column subassemblies including load capacity, energy dissipation, ultimate ductility and failure mode
- For the 6 exterior specimens examined, the ratio of predicted and observed shear force capacity had a mean of 1.08, and coefficient of variation of 5 %

- For the 5 interior specimens, the shear force capacity had a mean of 1.00, and a coefficient of variation of 2 %
- The ratio of predicted and observed displacement capacity for exterior specimens had a mean of 1.01, and coefficient of variation of 4.62 %
- The ratio of predicted and observed displacement capacity for interior specimens had a mean of 0.96, and a coefficient of variation of 6.5 %
- The predicted failure mechanisms and crack patterns for the specimens examined also showed good correlation with the experimental results
- The current model for bond-slip in smooth reinforcement wasn't sufficiently accurate in simulating the behaviour of non-seismically designed beam-column subassemblies
- The "Custom Input" option for embedded bars, introduced into the program, provided improved simulations for specimens with smooth reinforcement,
- The bond-slip effects in non-seismically designed specimens were accurately captured in the analyses using this "Custom Input" option for smooth reinforcement
- The ductility ratios of predicted and observed ultimate displacement for interior specimens had a mean of 1.03, and a coefficient of variation of 13.4%,
- Similar comparison in the energy dissipation capacity calculations had a mean of 0.89, and a coefficient of variation of 22.5%,
- The correlation in the analysis and experimental behaviour of a retrofitted exterior beam-column subassembly suggests another potential finite element modelling area for VecTor2.

Overall, the finite element analysis program VecTor2 was able to model both seismically and non-seismically designed beam-column subassemblies. It was observed that VecTor2 analysis results showed better accuracy in estimating the seismic performance of seismically designed beam-column subassemblies opposed to non-seismically designed ones. Overall, however, the program exhibited good accuracy in predicting the strength, deformation response, energy dissipation, and failure mode of beam-column subassemblies.

6.3. RECOMMENDATIONS - VecTor2 MODELLING

The primary objective of this research was to investigate the modelling capabilities of VecTor2 on beam-column subassemblies. Some parametric studies were done on the specimens that were modelled, and certain conclusions were made in the process. Ensuing recommendations for VecTor2 modelling are briefly described as follows:

- The concrete hysteretic response under reversed cyclic conditions are best captured by the “Palermo – Nonlinear with Cyclic Decay” option, which accounts for damage to the concrete due to load cycling. It is recommended to perform VecTor2 analysis on specimens that were tested under reversed cyclic loading conditions
- Some of the lightly reinforced concrete members that were modelled under the default material model conditions showed stability problems. A decision to change the material model options is suggested if the cause of instability is determined
- A well known approach in finite element analysis on defining the mesh is also applicable when modelling beam-column subassemblies using VecTor2. It is always recommended to begin with a relatively coarse mesh. After careful examination of the results, the number of elements can gradually be increased by using a finer mesh. This approach will decrease the amount of time spent on modelling, since too fine a mesh will result in longer computation time. Limiting the joint area to 10 to 15

elements was found appropriate as a result of the finite element analysis that has been carried out on beam-column subassemblies tested under different loading conditions

- Bond-slip elements must be included in the modelling using the approach suggested in Chapter 5, but it is recommended that the bond-slip behaviour in one or two cycles in the final analysis be examined to confirm the accuracy of the analysis using the out-put text files.

6.4. RECOMMENDATIONS FOR FUTURE RESEARCH

The study presented here included an analytical investigation of the behaviour of beam-column subassemblies that were tested by various research groups. Some of the specimens analyzed had limited information regarding their experimental behaviour. A comparison of experimental and analytical response regarding bond-slip behaviour under reversed cyclic loading conditions would be useful for seismic assessment of beam-column subassemblies.

Additional experimental research on non-seismically designed interior beam-column subassemblies is needed to better test the capabilities of VecTor2 in modelling these structures. The experimental data available on smooth reinforcement behaviour was also found to be inadequate to develop a bond model. Most of the tests involving smooth reinforcement were limited to monotonic loading conditions, and therefore a detailed experimental research program on straight and end-hooked smooth bars subjected to cyclic loading is needed. While some such studies were described in this thesis, they were limited to certain sizes of smooth bars. Thus, there is insufficient experimental data to make revisions on the current smooth embedded bar bond model in VecTor2.

The cyclic behaviour of the bond-slip model that is currently used in VecTor2 needs to be further studied due to reasons described in Chapter 2. The energy dissipation capacity captured will likely be much improved if the necessary revisions are made.

A retrofitted beam-column subassembly was also modelled using VecTor2, and showed reasonably accurate results in the predicted hysteretic response, failure mode, and crack formations. The results of this research confirmed that VecTor2 is also capable of modelling members with retrofitting applications.

REFERENCES

Abrams, D.A., 1913. "Tests of Bond between Concrete and Steel", *University of Illinois, Bulletin No. 71*, 240 pp.

Bentz, E., 1996-2007. "Augustus-Finite Element Analysis of Reinforced Concrete Post-Processor for VecTor2 and TRIX", <http://www.civ.utoronto.ca/vector>, Last Accessed Sep. 17, 2007.

Bentz, E.C., 2000 "Sectional Analysis of Reinforced Concrete Members," *PhD Thesis*, Department of Civil Engineering, University of Toronto, 310 pp.

Bertero, V.V., and Popov, E.P., 1977. "Seismic Behaviour of Ductile Moment-Resisting Reinforced Concrete Frames", *Reinforced Concrete Structures in Seismic Zones, ACI Special Publication, SP-53*, American Concrete Institute, Detroit, Michigan.

CEB-FIB Model Code 90, 1993. Bulletin d' Information No. 213-214

Chen, Te-Hsui, 2006. "Retrofit Strategy of Non-Seismically Designed Frame Systems", *Masters Thesis*. Civil Engineering Department, University of Canterbury, New Zealand.

Dhakal, R.D., Pan, T., Irawan, P., Tsai, K., Lin, K., and Chen, C., 2005. "Experimental Study on the Dynamic Response of Gravity-Load Designed Reinforced Concrete Connections", *Engineering Structures*, Vol. 27, pp.75-87.

Eligehausen, R., Popov, E.P., and Bertero, V.V., 1983. "Local Bond Stress-Slip Relationship of Deformed Bars under Generalized Excitations", *EERC Report 83-23*, Earthquake Engineering Research Center, University of California, Berkeley, California.

Elmorsi, M., Kianoush, R. M., and Tso, W.K., 2000. "Modelling Bond-Slip Deformations in Reinforced Concrete Beam-Column Joints", *Canadian Journal of Civil Engineering*, Vol. 27, pp. 490-505.

Fabbrocino, G., Verderame, G.M., and Manfredi, G., 2002. "Experimental Behaviour of Straight and Hooked Smooth Bars in Existing R.C. Buildings", *12th European Conference on Earthquake Engineering*, PN.393, London.

Fabbrocino, G., Verderame, G.M., and Manfredi, G., and Edoardo, C., 2004. "Structural Models of Critical Regions in Old-Type RC Frames with Smooth Rebars", *Engineering Structures*, Vol. 26, Iss.4, pp. 2137-2148.

Feldman, L.R., and Barlett, F.M., 2005. "Bond Strength Variability in Pullout Specimens with Plain Reinforcement", *ACI Structural Journal*, Vol. 102, Iss.6, pp. 860-867.

Filippou, F.C., Popov, E.P., and Bertero V.V., 1983. "Effect of Bond Deterioration on Hysteretic Behaviour of Reinforced Concrete Joints", EERC Report 83-19, Earthquake Engineering Research Center, University of California, Berkeley, California.

Fleury, F., Reynouard, J.-M., and Merabet, O., 2000. "Multicomponent Model of Reinforced Concrete Joints for Cyclic Loading", *ASCE Journal of Engineering Mechanics*, Vol. 126, No.8, pp. 804-811.

Gan, Y., 2000. "Bond Stress and Slip Modeling in Nonlinear Finite Element Analysis of Reinforced Concrete Structures", *Masters Thesis*, Department of Civil Engineering, University of Toronto, 251 pp.

Hakuto, S., Park, R., and Tanaka, H., 1999. "Effect of Deterioration of Bond of Beam Bars Passing through Interior Beam-Column Joints on Flexural Strength and Ductility", *ACI Structural Journal*, Vol. 96, Iss.5, pp. 858-864.

Kankam, C.K., 1997. "Relationship of Bond Stress, Steel Stress, and Slip in Reinforced Concrete", *ASCE Journal of Structural Engineering*, Vol. 123, No.1, pp. 79-85.

Kupfer, H., Hilsdorf, H.K., and Rusch, H., 1969. "Behavior of Concrete under Biaxial Stress", *ACI Journal*, Vol. 87, Iss. 2, pp. 656-666.

Limkatanyu and Spacone, 2003. "Effect of Reinforcement Slippage on Non-linear Response under Cyclic Loadings of RC Frame Structures", *Earthquake Engineering and Structural Dynamics*, Vol. 32, pp. 2407-2424.

Lowes, N.L., and Altoontash, A., 2003. "Modelling Reinforced-Concrete Beam-Column Joints Subjected to Cyclic Loading", *ASCE Journal of Structural Engineering*, Vol. 129, No.12, pp. 1686-1697.

Menegotto, M., and Pinto, P., 1973. "Method of Analysis for Cyclically Loaded Reinforced Concrete Plane Frames Including Changes in Geometry and Non-Elastic Behavior of Elements under Combined Normal Force and Bending." *Proc., IABSE Symp. on Resistance and Ultimate Deformability of Structures Acted on by Well Defined Repeated Loads*, Lisbon, 15-22.

Mitra, N., and Lowes, N.L., 2004. "Evaluation and Advancement of a Reinforced Concrete Beam-Column Joint Model", *13th World Conference on Earthquake Engineering*, PN 1001, Vancouver, Canada.

Ngo, D., and Scordelis, A.C., 1967. "Finite Element Analysis of Reinforced Concrete Beams", *ACI Journal*, Vol. 64, Iss. 3, pp. 152-163.

Shiohara, H., 2001. "New Model for Shear Failure of RC Interior Beam-Column Connections", *ASCE Journal of Structural Engineering*, Vol. 127, No. 2, pp. 152-160.

Shiohara, H., 2004. "Quadruple Flexural Resistance in R/C Beam-Column Joints", *13th World Conference on Earthquake Engineering*, PN 491, Vancouver, Canada.

Palermo, D., and Vecchio, F.J., 2002. "Behaviour and Analysis of Reinforced Concrete Walls Subjected to Reversed Cyclic Loading", Publication No. 2002-01, Department of Civil Engineering, University of Toronto, 351 pp.

Park, R., 2002. "A Summary of Results of Simulated Seismic Load Tests on Reinforced Concrete Beam-Column Joints, Beams and Columns with Substandard Reinforcing Details", *Journal of Earthquake Engineering*, Vol. 6, No. 2, pp. 147-174.

Park, Y.J., and Ang, A.H.S., 1985. "Mechanistic seismic Damage Model for Reinforced Concrete", *ASCE Journal of Structural Engineering*, Vol. 111, No. 4, pp. 722-739.

Park, R., and Paulay, T., 1975. "Reinforced Concrete Structures", Wiley Publishing, New York, 769 p.

Paulay, T., 1994. "The Fourth Mallet-Milne Lecture: Simplicity and Confidence in Seismic Design", Wiley, Chichester.

Pampanin, S., Calvi, G.M., and Moratti, M., 2002. "Seismic Behaviour of RC Beam-Column Joints Designed for Gravity Loads", *12th European Conference on Earthquake Engineering*, PN.727, London.

Pampanin, S., Magenes, G., and Carr, A., 2003. "Modelling of Shear Hinge Mechanism in Poorly Detailed RC Beam-Column Joints", *fib2003 Symp. Concrete Struct. in Seismic Regions*, Athens.

Pampanin, S., and Christopoulos, C, 2003. "Non-Invasive Retrofit of Existing RC Frames Designed for Gravity Loads Only". *fib2003 Symp. Concrete Struct. in Seismic Regions*, Athens.

Pampanin, S., 2005. "Vulnerability Assessment and Retrofitting Strategies for Existing Under-Designed R.C. Frame Buildings", *2005 Annual Conference of the New Zealand Society of Earthquake Engineering*, Wairakei.

Pampanin, S., and Christopoulos, C, and Chen, T.-H, 2006. "Development and Validation of a Metallic Haunch Seismic Retrofit Solution for Existing Under-Designed RC Frame Buildings", *Earthquake Engineering and Structural Dynamics*, Vol. 35, pp. 1739-1766.

Pochanart, S., and Harmon, T., 1989. "Bond-Slip Model for Generalized Excitations Including Fatigue", *ACI Materials Journal*, Vol. 86, Iss. 5, pp. 465-474.

Richart, F.E., Brandtzaeg, A., and Brown, R.L., 1928. "A Study of the Failure of Concrete under Combined Compressive Stresses", Bulletin No.185, University of Illinois Engineering Experimental Station, Urbana, Illinois, 104 pp.

Seckin, M., 1981. "Hysteretic Behaviour of Cast-in-Place Exterior Beam-Column-Slab Subassemblies", *Ph.D. Thesis*, Department of Civil Engineering, University of Toronto, 266 pp.

Soroushian, P., Obasaki, K., Nagi, M., and Rojas, M.C., 1988. "Pullout Behavior of Hooked Bars in Exterior Beam-Column Connections", *ACI Structural Journal*, Vol. 85, Iss.3, pp.269-276.

Soroushian, P., and Choi, K.B., 1989. "Local Bond of Deformed Bars with Different Diameters in Confined Concrete", *ACI Structural Journal*, Vol. 86, Iss.2, pp.217-222.

Soroushian, P., Obasaki, K, and Marikunte, S., 1991. "Analytical Modeling of Bonded Bars under Cyclic Loads", *ASCE Journal of Structural Engineering*, Vol. 117, No.1, pp.48-60.

Vecchio, F.J. and Collins, M.P., 1982. "Response of Reinforced Concrete to In-Plane Shear and Normal Stresses", Publication No. 82-03, Department of Civil Engineering, University of Toronto, 332 pp.

Vecchio, F.J., and Collins, M.P., 1986. “The Modified Compression Field Theory for Reinforced Concrete Elements Subject to Shear”, *ACI Structural Journal*, Vol. 83, Iss.2, pp. 219-231.

Vecchio, F.J., 2000. “The Disturbed Stress Field Model for Reinforced Concrete: Formulation”, *ASCE Journal of Structural Engineering*, Vol. 126, No.9, pp. 1070-1077.

Vecchio, F.J., Bentz, E.C. and Collins, M.P., 2004. “Tools for Forensic Analysis of Reinforced Concrete Structures”, *Computers and Concrete*, Vol. 1, No.1, pp. 1-14.

Viwanatepa, S., Popov, E.P., and Bertero, V.V., 1979. “Effects of Generalized Loadings on Bond of Reinforcing Bars Embedded in Confined Concrete Blocks”, *UBC/EERC Report 79/22*, Earthquake Engineering Research Center, University of California, Berkeley, California.

Walraven, J.C., and Reinhardt, H.W., 1981. “Theory and Experiments on the Mechanical Behaviour of Cracks in Plain and Reinforced Concrete Subjected to Shear Loading”, *Concrete Mechanics – Part A, Heron*, Vol. 26, No. 4, 65 pp.

Wong, P.S., and Vecchio, F.J., 2002. “VecTor2 and FormWorks User’s Manual”, *Technical Report*, Department of Civil Engineering, University of Toronto, 217 p.